THE ROLE OF HEME REGULATORY ENZYMES IN MYOCYTES UNDER STRESS

by

Ashley Lynn Eadie

Submitted in partial fulfilment of the requirements
for the degree of Master of Science

at

Dalhousie University
Halifax, Nova Scotia
August 2016

A smooth sea
never made a good sailor.

TABLE OF CONTENTS

LIST OF TABLES

LIST OF FIGURES

ABSTRACT

The heme metabolism pathway remains a novel therapeutic target for heart failure treatment. However, how heme is regulated in the failing heart remains to be understood. To investigate the molecular mechanisms underlying heme regulation and its potential modulation by hypoxia inducible transcription factors, we investigated the expression of heme regulatory enzymes and hypoxia inducible factors in clinical heart failure and experimental heart failure rodent models. Here we show that heme regulatory enzymes - delta-aminolevulinic acid synthases (ALAS) and heme oxygenases (HMOX) - and heme bioavailability changed significantly in clinical and experimental rodent models of heart failure over time, that (HMOX1) protein levels remained relatively unchanged or decreased in experimental heart failure, and that HMOX1 expression is induced synergistically in heme-replete hypoxia, likely by hypoxia inducible factor 2α (HIF2α).

LIST OF ABBREVIATIONS USED

5-ALA	5-aminolevulinic acid
ABCB10	ATP-binding cassette subfamily B member 10
ACE	Angiotensin converting enzymes
ACTB	β-actin
ALAD	5-aminolevulinic acid dehydratase
ALAS	Delta-aminolevulinic acid synthase
AMI	Acute myocardial infarction
ANOVA	Analysis of variance
ARB	Angiotensin II receptor blocker
ARNT	Aryl hydrocarbon receptor nuclear transporter
ATCC	American Type Culture Collection
ATP	Adenosine triphosphate
BCA	Bicinchonic acid
BLAST	Basic Local Alignment Search Tool
BSA	Bovine serum albumin
BVR	Biliverdin reductase
cDNA	Complementary DNA
cGMP	Cyclic guanosine monophosphate
CM-H_2DCFDA	Chloromethyl dichlorodihydrofluorescein diacetate, acetyl ester
CMV	Cytomegalovirus
CO	Carbon monoxide
CPO	Coproporphyrinogen III oxidase
CPP	Coproporphyrinogen III
CT	Cycle threshold
DcytB	Duodenal cytochrome B
DMEM-HG	Dulbecco's Modified Eagle Medium-High Glucose
DMSO	Dimethyl sulfoxide
DMT-1	Divalent metal transporter-1
DNA	Deoxyribonucleic acid
dsDNA	Double stranded DNA
DTT	Dithiothreitol
ECM	Extracellular matrix
EDTA	Ethylenediaminetetraacetic acid
EPAS1	Endothelial PAS domain-containing protein 1
EPO	Erythropoietin
FACS	Fluorescence-activated cell sorting
FBS	Fetal bovine serum
FDA	Food and Drug Administration
Fech1	Ferrochelatase-1
GEO	Gene Expression Omnibus
GFP	Green fluorescent protein
HIF	Hypoxia inducible factor
HMOX	Heme oxygenase
HPRT1	Hypoxanthine phosphoribosyltransferase 1

HRE	Hypoxia response element
HRP	Horseradish peroxidase
HMB	Hydroxymethylbilane
IR	Ischemia reperfusion
IRE	Iron response element
IREBP	IRE-binding protein
IRES	Intermediate ribosomal entry site
kDa	KiloDalton
LAD	Left anterior descending
LV	Left ventricle
Mfrn-1	Mitoferrin-1
MI	Myocardial infarct
MIAME	Minimum Information About a Microarray Experiment
MOI	Multiplicity of Infection
mRNA	Messenger RNA
NAC	N-Acetyl-L-Cysteine
NADPH	Nicotinamide adenine dinucleotide phosphate oxidase
NCBI	National Center for Biotechnology Information
ND	Not detected
NF-kB	Nuclear factor-kappa B
NM	Not measured
Nrf2	Nuclear factor (erythroid-derived 2)-like 2
NTC	No-template control
OD	Optical density
ODD	Oxygen-dependent degradation
PBS	Phospho-buffered saline
PBG	Porphobilonogen
PBGD	Porphobilonogen deaminase
PCR	Polymerase chain reaction
PFU	Plaque-forming units
PHD	Prolyl hydroxylase
PP	Protoporphyrin IX
PPG	Protoporphyrinogen IX
PPO	Protoporphyrin oxidase
qPCR	Quantitative polymerase chain reaction
RAAS	Renin-angiotensin-aldosterone system
RFP	Red fluorescent protein
RNA	Ribonucleic acid
ROS	Reactive oxygen species
RPL32	Ribosomal protein L32
SD	Standard deviation
SDS-PAGE	Sodium dodecyl sulfate-polyacrylamide gel electrophoresis
SEM	Standard error of the mean
sGC	Soluble guanalyl cyclase
shRNA	Short hairpin loop RNA
SLC25A38	Solute carrier family 25 member 38

TAC	Transverse aortic constriction
TBS-T	Tris-buffered saline-Tween 20
TIC	Transcription initiation complex
TFR1	Transferrin receptor 1
UPB	Uroporphyrinogen III
UROD	Uroporphyrinogen III decarboxylase
UROS	Uroporphyrinogen III synthase
VAD	Ventricular assist device
VEGF	Vascular endothelial growth factor
VHL	Von Hippel Lindau
VSMC	Vascular smooth muscle cell

ACKNOWLEDGEMENTS

To my parents, David and Caroline, for their love and continued support. I could never thank you enough for providing me the opportunities that I had growing up. I love you more.

To my extended family, Dr. Alli Murugesan and Dasse Nadaradjan, for providing a home away from home. To Dasse, who never gave a second thought about going out of his way to ensure we were taken care of. To Alli, for keeping me spiritually grounded when it seemed like nothing would ever go right. Thank you for always looking out for me.

To Purvi Trivedi – the only expectation that was set when I joined DMNB was "you have to work as hard as Purvi." I'm still working on it. Thank you for your collegiality, friendship and company- especially during those late nights in the lab. I'm thankful that I had you to stumble through this process with.

To Amna Rasul, a genuinely kind and compassionate friend who never failed to discipline me when I put my work too often ahead of my other needs, and brought me food when I didn't listen anyway. Thank you for keeping a smile on my face.

To Malav Madhu, someone whose stubbornness rivals my own, but a good colleague and a great friend. Thank you for always keeping me sharp and on my toes. I'm made better for it.

To Andrew Cowie, a skilled scientist and a loyal friend and mentor. Somebody who could always find the time in his day to lend a helping hand. Thank you for your support – I wouldn't be where I am now without your selflessness.

To the Faculty who have supported my candidacy, many thanks for your counsel. Thank you to Dr. Christopher Sinal and Dr. Susan Howlett for keeping me on the right track.

Most importantly, thank you to Dr. Keith R. Brunt – words can never express my gratitude. You are both the quality of researcher and the quality of person that I aspire towards being. I've got my work cut out for me yet. I hope that I can make you proud.

The ideas conceived, experimental directions/protocols and hypotheses presented in the current work are the result of a collaboration between Ashley L. Eadie and Dr. Keith R. Brunt. Unless otherwise stated, Ashley L. Eadie designed and performed all experiments and analyzed results. Jason Huber and Mathew Platt performed rodent surgeries at the University of Guelph. Ashley L. Eadie received, processed and analyzed tissue samples (Figures 3.3-3.7). Dr. Melissa Allwood and Dr. Nadya Romanova designed primers for and performed qPCR for mouse tissues (Figure 3.2). Ashley L. Eadie performed qPCR analyses of the resulting *in vivo* data, and designed primers and performed qPCR for *in vitro* studies. Neonatal rat cardiomyocytes were isolated collaboratively with Purvi Trivedi (Figure 3.34). Bicistronic adenoviral vectors were developed by Dr. Keith R. Brunt in collaboration with Vector Biolabs.

CHAPTER 1
Introduction

Heart failure is the complex end result of one or more cardiovascular diseases that reduce the ability of the heart to meet the metabolic demands of the body. More than 26 million [1] individuals are currently living with heart failure, with a prevalence projected to exceed 1 in every 3 individuals by 2030 [2] as more patients survive acute adverse cardiac events (ex. myocardial infarction). The outcomes for heart failure patients are poor — <50% survive more than five years after diagnosis [3]. Targeting the heme metabolism pathway could be a novel approach to manage heart failure. Upregulation of the stress-inducible enzyme heme oxygenase-1 (HMOX1) in the heart exerts cytoprotection by catabolising pro-oxidant free-heme into the antioxidant biliverdin. Heme catabolism additionally releases the anti-inflammatory and vasodilatory gasotransmitter carbon monoxide (CO), and essential iron (Fe^{2+}). CO contributes indirectly to the reduction of oxidative stress and apoptosis through the soluble guanylyl cyclase pathway [4], whereas Fe^{2+} release coincides with increased production of cytoprotective ferritin [5]. Induction of HMOX1 in experimental models of heart failure has repeatedly demonstrated significant improvements in cardiac function and overall survival, such as after acute myocardial infarction (AMI) [6-8]. Although pro-oxidant when not encapsulated by hemoproteins, heme is otherwise an essential molecular oxygen carrier required for oxygen-dependent metabolic processes. Understanding the basic molecular mechanisms underpinning heme homeostasis in healthy cells and in heart failure is critical to clinical translation of therapeutics designed to target the cytoprotective benefits derived from altered heme metabolism. Here, we investigated heme metabolism in clinical and experimental heart failure during the progression of an AMI and in an experimental model of hypertension-induced heart failure. Given the inter-dependency of heme and oxygen-dependent metabolism within the heart, we further sought to elucidate the role of hypoxia inducible transcription factors (HIFs) in regulating heme metabolism in the progression to heart failure.

1.1 Clinical Characteristics and Management of Heart Failure

Heart failure is the inability of the myocardium to meet the metabolic requirements of the body. In a healthy patient, the volume of blood ejected from the

ventricle compared to the ventricle's end diastolic volume (ejection fraction) typically ranges from 60-80%. In heart failure, ejection fraction is reduced to 50% or less, resulting in significantly impaired delivery of oxygenated blood to the rest of the body and an inability to maintain the body's essential functions. Heart failure stems from an inability to contract (systolic dysfunction), to relax and fill with blood (diastolic dysfunction), or a combination thereof.

Heart failure results in a number of physical limitations and symptoms. Depending upon the degree of failure, heart failure patients can present with mild to severe fatigue, dyspnea, coughing, edema, or irregular heart rate, even while at rest [9], contributing to an inability to conduct basic physical activity. Frequently, patients will appear asymptomatic as a result of initial cardiopulmonary adaptation (compensation) [9, 10]. Symptoms differ depending upon whether heart failure occurs in the left or right ventricle. In left-sided heart failure, the left ventricle's ability to eject blood is impaired, which can result in pulmonary congestion characterized by an accumulation of pressure through the pulmonary veins and lungs [11-13]. Congestion results in pulmonary dysfunction by increasing fibrotic remodeling and pulmonary edema [13, 14], which impairs gas exchange [15, 16]. Although left ventricular dysfunction is regularly considered the most prominent cause of heart failure, there is significant overlap between left and right-sided failure. Accumulation of blood and increased pressure through the pulmonary vasculature as a result of left ventricular dysfunction can cause further dysfunction through the pulmonary arteries. Consequently, an increased hemodynamic load is placed on the right ventricle [11]. Right ventricular heart failure, whether the result of left ventricular dysfunction, valvular dysfunction or of idiopathic origin, compromises blood delivery to the lungs (causing shortness of breath and further pulmonary edema and fibrosis); this results in congestion of blood within the peripheral veins, and edema in the legs and abdomen [17]. If left untreated, edema can impair mobility and cause severe pain by restricting peripheral circulation as it imposes external pressure on the vasculature [13].

Treatment of heart failure is complex. Pathologies contributing to heart failure are diverse and are further complicated by associated comorbidities (congenital birth defects, valvular dysfunction, obesity, diabetes, hypercholesterolemia, and cardiomyopathies

stemming from idiopathic factors) [18]. However, the most prevalent causes of heart failure are myocardial infarction or hypertension [3].

1.1.1 Heart Failure Resulting from an Acute Myocardial Infarction (AMI)

In a healthy human heart, coronary arteries supply oxygen and nutrient-rich blood to the myocardium. In an acute myocardial infarction (AMI), the coronary arteries become partially or completely occluded as a result of vasospastic constriction, vulnerable atherosclerotic plaque rupture and/or platelet activated thrombus formation. Occlusion of the coronary arteries results in ischemia, which translates to reduced nutrient/oxygen delivery to cardiomyocytes and an accumulation of toxic metabolic waste, such as lactic acid, due to anaerobic metabolism [19].

An AMI is divided into three primary stages: acute injury, early remodeling and late remodeling. Initial occlusion of the coronary arteries results in a sudden drop in blood supply to the myocardium (ischemia). Simultaneously, absence or reduction in oxygen availability causes rapid accumulation of reactive oxygen species (ROS) and subsequent apoptosis/necrosis [20]. Cardiomyocyte necrosis results in cytokine release and systolic dysfunction with the resulting loss of contractile tissue [21]. Cytokine release is both necessary for modulation of myocardial repair, such as through myofibroblast differentiation and proliferation, as well as detrimental in the generation of ROS and negative matrix remodeling by inflammatory cells [22].

Treatment must be rapidly administered to prevent expansion of the infarct whether by further necrosis or apoptosis. Reperfusion of the coronary arteries may be achieved through thrombolysis, percutaneous coronary intervention (stenting or balloon angioplasty by coronary catheterization), or coronary artery bypass grafting. Reperfusion of the occluded artery will not rescue necrotic tissue and, though necessary can cause further accumulation of ROS through ischemia reperfusion (IR)-injury [23]. In many instances, however, the coronary arteries remain permanently occluded and therapeutics such as anti-platelet therapies, calcium channel antagonists and β-adrenergic antagonists (β-blockers) aim to prevent further occlusion and reduce oxygen consumption by decreasing the force of contraction and heart rate respectively.

In patients surviving the initial AMI, early remodeling results in structural and morphological changes to the myocardium [24]. After AMI, stabilization of the

weakened ventricular wall becomes critical to preventing hemorrhagic rupture as the heart undergoes eccentric hypertrophy and ventricular dilatation. Within the infarct zone, deleterious cardiomyocyte remnants are removed from the infarct by macrophage infiltration [24]. Increased hemodynamic load and cytokine stimulation signal rapid fibroblast proliferation, differentiation and scar matrix production [25]. Fibroblasts are essential mediators of extracellular matrix (ECM) remodeling through the deposition of fibrin and fibronectin in the attempt to re-establish structural integrity [26]. Within the peri-infarct region, surviving cardiomyocytes compensate for the loss of contractile tissue and increased hemodynamic stress through hypertrophic remodeling [27, 28].

Additional structural changes are observed in later remodeling. In the compensated heart, extensive fibroblast proliferation results in collagen reinforcement of the existing scar and compensatory hypertrophy of the remaining viable cardiomyocytes maintains cardiac output [29]. However, decompensation can emerge from excessive or negative remodeling and previously preserved ejection fraction can then deteriorate [30].

Myocardial stretch, caused by eccentric ventricular hypertrophy/dilatation and increased hemodynamic volume overload, coupled with simultaneous negative extracellular matrix remodeling (i.e. via matrix metalloproteases), results in myocardial slippage [31]. Myocardial slippage, misalignment of myosin and actin filaments, results in an impaired ability to contract efficiently (systolic dysfunction), further contributing to decreased oxygen delivering capabilities (i.e. ejection fraction). As the oxygen demands of the surviving cardiomyocytes rise to meet the increased mechanical load, neovascularization is essential to meet their metabolic needs [32, 33].

1.1.2 Heart Failure Resulting from Hypertension (Pressure Overload)

Hypertension is the persistent elevation of arterial blood pressure in excess of 100-140mmHg during systole and 60-90mmHg in diastole [34]. The two most prominent factors contributing to hypertension include dysfunctional arterial endothelium and excess renin-angiotensin-aldosterone system (RAAS) activity. Excess endothelial production of vasoconstrictors (e.g. endothelin-1) in contrast to vasodilators (e.g. nitric oxide, carbon monoxide (CO), and prostacyclin) can result in increased arterial resistance [35]. Arterial resistance alone does not inevitably translate into an increase in blood pressure. Coupled with impaired arterial tone, overactive RAAS contributes to

hypertension by increasing blood volume and angiotensin II production. Angiotensin II acts as a vasoconstrictor, while aldosterone overproduction contributes to hypertension by decreasing natriuresis through sodium reabsorption in the kidneys, osmotically drawing water from the renal filtrate back into the bloodstream to increase blood volume [36]. Increased arterial pressure is further propagated by subsequent stimulation of vascular smooth muscle cell (VSMC) proliferation. An increase in blood volume, concurrent with increased arterial resistance, exerts greater transmural force against the vasculature instead of exerting shear stress. Reduction in shear stress results in vascular smooth muscle proliferation [37]. Consequently, unrestricted proliferation of vascular smooth muscle cells results in decreased luminal diameter, increasing the risk of atherosclerosis and reducing renal perfusion. Decreased renal perfusion stimulates renin synthesis and exacerbates hypertension through angiotensin II production and vasoconstriction [38].

Hypertension is predominantly asymptomatic, even as pressure becomes dangerously elevated, and is therefore routinely monitored for by family physicians. Absence of symptoms results from the heart's initial ability to adapt to the gradual increase in arterial pressure [10]. To overcome the increase in peripheral resistance (afterload), the myocardium must increase the force with which it contracts. Acutely, the increase in afterload is met with compensatory concentric hypertrophy [12]. Chronically, the persistent strain on the hypertrophied heart can result in decompensation [12] and ultimately heart failure. This can result from insufficient neovascularization as well as pathological remodeling. Interstitial fibrotic remodeling occurs as increased mechanical load and transmural wall pressure stimulates fibroblast proliferation/differentiation, and induces ECM remodeling. Although hypertrophy is initially beneficial to the myocardium's adaptation to increased afterload, fibrotically fixed hypertrophy can result in decompensatory failure through decreased ventricular volume as well as both systolic and diastolic dysfunction [12].

1.1.3 Clinical Management of Heart Failure

For patients with an underlying predisposition for heart failure and those who may be unable to alter their lifestyle and cannot yet change their genetic predispositions, pharmacological intervention is required [39]. β-adrenergic receptor antagonists, such as

propranolol, inhibit the binding of epinephrine and norepinephrine to β-adrenergic receptors. Antagonism of β_1-adrenergic receptors located in the heart decreases heart rate through sympathetic inhibition. Consequently, demand for molecular oxygen declines alongside cardiac output. β_1-receptor antagonism further inhibits renin synthesis through β_1 receptors situated in the kidney. Non-selective β-antagonists, such as carvedilol, provides additional therapeutic benefit through antagonism of α_1-receptors to inhibit vasoconstriction. Pharmacological reduction of blood volume is achieved through the administration of diuretics, such as thiazides. Blood volume reduction and vasodilation is further accomplished through RAAS antagonists, such as angiotensin II receptor blockers (ARBs), angiotensin converting enzyme (ACE) inhibitors, aldosterone inhibitors, as well as the more novel chymase inhibitors [26].

In patients where cardiovascular prognosis is in decline, surgical intervention may be inevitable. Surgical intervention is significantly more complex and invasive (e.g. open heart procedures). Intervention may include procedures such as the insertion of ventricular assist devices (VADs) or cardiac transplant, which are reserved for end-stage heart failure. VADs are implanted within the failing ventricle and mechanically propel blood to the vasculature. Implantation of VADs are used as an intermediary bridge to cardiac transplantation until a suitable donor heart becomes available. Although cardiac transplants replace the injured heart altogether, the patient may have been placed on a waitlist for a prolonged period of time. The procedure is costly and includes risk of immune incompatibility, while not necessarily eliminating the factors that contributed to the initial heart failure. Despite the array of advances in interventional medicine, there exists no cure for heart failure. Current treatment options aim to alleviate symptoms and delay decompensation, however the morbidity and mortality of patients diagnosed with heart failure remain high. It is therefore critical to investigate novel therapeutic targets aimed at improving not only survival but the overall cardiac function of heart failure patients.

1.2 Preclinical Models of Heart Failure

Although patient biopsies provide valuable insight into the molecular signaling involved in the human failing heart, they are frequently obtained from cardiac tissue prior to transplant, thus providing only a brief snapshot of a complex series of molecular

mechanisms leading to the terminal stages of heart failure. Further, true molecular signaling may be masked by concomitant comorbidities and prior pharmacological intervention. Preclinical models thus provide critical insight into the detailed molecular signaling as the heart progresses into failure. Although the incipient cause of preclinical heart failure may not be identical in every aspect to those underlying patient heart failure, preclinical models are invaluable for investigating altered signaling throughout compensatory to decompensatory stages, as well as identifying novel pharmacological targets and the optimal strategies for, or limitations of, potential interventions.

The successful translation of novel pharmacological compounds from basic research to the clinic is heavily dependent upon the use of appropriate preclinical models. The vast majority of preclinical trials exclusively employ young, male, genetically inbred animals. However, clinical translation still requires assessment of therapeutic potential in preclinical models that more accurately reflect patient demographics and disease (i.e. age and sex appropriate models) [40].

1.2.1 Heart Failure by AMI

Surgical ligation of the left anterior descending coronary artery (LAD) is the principal method used to model AMI-induced heart failure [41]. Permanent occlusion of the LAD significantly reduces left ventricular perfusion and results in the rapid increase in oxidative stress markers [42] and cardiomyocyte death. Similar to the infarcted human heart, occlusion of the LAD in both murine and porcine models demonstrate characteristic increases in left ventricular volume as the infarct expands, in addition to decreased ejection fraction [42]. Although the coronary ligation model excludes clinical contributing factors (e.g. atherosclerosis) and requires surgical proficiency, it most closely reflects clinical AMI. The LAD ligation model further facilitates modeling of IR-injury, allowing for equal opportunity to model patients who are eligible for reperfusion as those that are ineligible. Other, less prominent models of volume-induced heart failure include cryoinjury, electrocautery or subcutaneous isoproterenol infusion, which generate myocardial weakening by direct cardiomyocyte necrosis [41]. Despite their simplicity, these techniques are limited in their clinical translation as the remodeling is not deemed to be as well aligned with either the LAD or IR-injury models.

1.2.2 Heart Failure by Chronic Hypertension

Preclinical modelling of hypertensive heart failure is significantly more complex. As 95% of patient hypertension is idiopathic (defined as 'primary hypertension'; [43]), many preclinical models have emerged to investigate the interplay of genetic predisposal, RAAS, sympathetic and endothelial dysfunctions. Transgenic modelling of hypertensive heart failure primarily involves the use of either Dahl salt-sensitive or spontaneously hypertensive (SHF/Mcc-facp) rat models [44]. Dahl rats develop systemic hypertension at 18-20 weeks when fed a high-salt diet. Spontaneously hypertensive rats display a gradual increase in systemic hypertension, followed by compensatory left ventricular hypertrophy with preserved ejection fraction, increased interstitial fibrosis and subsequent transition into decompensated heart failure at 18-24 months [44]. Transgenic models offer the benefit of a more clinically relevant and non-invasive model through the gradual pathogenesis of hypertension and chronic heart failure. However, Dahl salt-sensitive and spontaneously hypertensive rat models are limited by their higher financial costs; larger cohorts are required to account for discrepancies in age-matching and delayed onset (18 weeks to 2 years) extends animal care costs considerably.

In addition to genetic models, aortic banding has become the most popular model of hypertensive heart failure. Surgical placement of a restrictive band around the ascending aorta of 3 week-old rats results in the gradual constriction of the aorta as the rats mature, subsequently driving RAAS-induced heart failure through restricted renal perfusion [41]. Aortic banding in rats may be either ascending [45], transverse [46] or abdominal [47], but either demonstrates concentric left ventricular hypertrophy while maintaining ejection fraction. At approximately 18 weeks of age, systolic and diastolic dysfunction, as well as pulmonary edema, are observed [41]. That most models are performed at an age where the animals transition into full adulthood could limit the clinical parallel, yet there is clinical relevance in that a gradual development of hypertension occurs. Aortic banding requires a high degree of technical surgical proficiency in newly weaned rats, and even more so in small mice (of comparable age). Despite the technical challenge, transverse aortic constriction (TAC) remains the most broadly used model of hypertensive heart failure [41, 48]. In murine TAC, a ligature is applied around the transverse segment of the aortic arch, between the brachiocephalic and

left common carotid arteries, and is constricted over a blunted 22-27-gauge needle. As the needle is withdrawn, the aorta remains constricted to its diameter. Aortic constriction reduces perfusion to the kidneys, while simultaneously generating increased afterload to the left ventricle. TAC results in compensatory left ventricular hypertrophy, interstitial fibrotic remodeling, and decompensation accompanied by the increased secretion of inflammatory cytokines, systolic and diastolic failure. Although the TAC model does not identically reflect the gradual onset of hypertensive heart failure in older humans, it continues to provide a consistent response in the left ventricle and immediate insight into the molecular pathways responsive to hypertensive adaptation [49].

1.3 Hypoxia in Heart Failure

As the largest consumer of molecular oxygen by mass, the myocardium requires a constant supply of oxygen to maintain myocardial viability and function [50]. Without oxygen, mitochondrial energy production via the electron transport chain would cease, resulting in the accumulation of ROS, ATP deprivation, apoptosis or necrosis [51]. Persistent hypoxia, or low oxygen availability [52], such as that exhibited in the injured myocardium is detrimental to proper cardiac function and thus remains a major contributor to increased morbidity and mortality associated with heart failure [50].

1.3.1 Acute and Chronic Hypoxia in AMI- and Hypertension-Derived Heart Failure

Hypoxia occurs both acutely and chronically in AMI-derived heart failure. Acutely, occlusion of the coronary arteries prevents oxygenated blood flow to downstream tissue. In patients where percutaneous coronary intervention or a coronary artery bypass graft is appropriate, hypoxic tissue can be reperfused and a continuous supply of oxygen is reinstated. In the event of permanent coronary artery occlusion, oxygen delivery is not reinstated and downstream tissue becomes necrotic.

As heart failure emerges with progressive cardiomyocyte loss, chronic hypoxia can occur in the peri-infarct region as transfer of mechanical load from the dying to the surviving cardiomyocytes occurs. Increased hemodynamic strain results in compensatory hypertrophy of the remaining cardiomyocytes through the addition of sarcomeric units [53]. These units require additional ATP and thus increase the metabolic demand for oxygen, of which supply is already limited by poor perfusion. Adequate angiogenesis

and/or neovascularization to the peri-infarct region thus becomes essential and is indicated by an increase in capillary density.

In patients diagnosed with pressure-overload heart failure, oxygen availability is characterized by chronic hypoxia leading up to decompensation. Similar to AMI, chronic hypoxia in hypertension-derived heart failure is consequential of persistent metabolic hypoxia as well as pathological fibrotic remodeling [54]. Moreover, chronic hypoxia can occur as a result of increased interstitial fibrosis, which creates a barrier across which oxygen diffusion occurs from vessel to myocyte mitochondria (marginally increased further by myocyte hypertrophy) [16]. In the case of extensive perivascular fibrosis, this can also result in vessel constriction [54].

1.4. Molecular Response to Cellular Hypoxia

In order to adapt to decreased oxygen availability, protein expression is modulated to reduce intracellular stress, maintain cell viability and improve oxygen delivery. The molecular response to intracellular hypoxia can thus be thematically classified as: 1) attenuation of oxidative stress and inflammation and 2) the modification of oxygen delivery and/or consumption to regain oxygen homeostasis. These responses are largely mediated by the stress-inducible expression of heme-catabolizing enzyme heme oxygenase-1 (HMOX1) [55] and the pleiotropic expression of proteins regulated by transcriptional factor hypoxia inducible factor 1 alpha (HIF1α) [56].

1.4.1 Hypoxia Inducible Factors (HIF1α and HIF2α)

Hypoxia inducible factors are the primary regulators of oxygen homeostasis. Two isoforms exist: the well characterized, HIF1α and the lesser characterized, HIF2α. HIF1α is attributed to being the primary mediator of cell adaptation to hypoxia, as it is responsible for the transcriptional regulation of over 200 genes, such as vascular endothelial growth factor (VEGF), erythropoietin (EPO) and HMOX1 that increase oxygen availability through angiogenesis, erythropoiesis [57-59], and cytoprotection. HIF2α has received considerably less investigative attention. HIF1α and HIF2α are heterodimeric transcription factors belonging to a family of basic helix-loop-helix, PAS-domain proteins, which are composed of an α-subunit and a constitutively expressed β-subunit, also known as aryl hydrocarbon receptor nuclear translocator (ARNT/HIFβ) [60]. Due to the severe implications of low oxygen tension, HIF1α and HIF2α are

continually synthesized and degraded despite oxygen homeostasis; HIF1α has been reported to have a half-life of only 5 minutes [61]; though it is unclear whether differences in stability exist between HIF1α and HIF2α. In normoxia, the α-subunit undergoes oxygen-dependent prolyl hydroxylation, mediated by prolyl hydroxylases PHD1, PHD2 or PHD3, within its oxygen dependent degradation (ODD) domain. Hydroxylation of the ODD results in an increased affinity to tumor suppressor, Von Hippel-Lindau (VHL) protein, and subsequent HIFα targeting by the E3 ubiquitin ligase complex for polyubiquitination, proceeded by proteosomal degradation [60] (Figure 1.1). With intracellular hypoxia, HIFα forms a heterodimer with HIFβ, thus enabling nuclear translocation. Once in the nucleus, the heterodimer binds hypoxia response elements (HREs) within the promoter region of target genes. This results in the formation of a transcription initiation complex (TIC) with RNA polymerase and P300 coactivators, and elicits an appropriate molecular physiological response. Although intracellular oxygen availability is the primary means by which HIFs are stabilized, it is important to note the existence of other hypoxia-independent stabilizers, most notably $CoCl_2$, which, by inhibiting the hydroxylation of the ODD, results in an accumulation of HIF1α independent of oxygen availability [62-64].

HIF1α and HIF2α are highly conserved and contain many overlapping functions [61]. Both isoforms are critical to the regulation of cardiovascular development. Deletion of either isoform during development is embryonically lethal [61]. In mice lacking HIF1α, impaired cardiac development and erythropoiesis are observed [61]. In mice lacking HIF2α, vascular defects and bradycardia are observed. Similarities in dysfunction may be partially attributable to overlapping regulation of VEGF [61].

HIF1α and HIF2α also contain distinctly separate functions and are therefore are not redundant to one another, but rather appear complementary. HIF2α is a transcriptional regulator of erythropoietin (EPO) [65], while HIF1α regulates angiopoietins 1-and 2, stromal derived factor-1 and endothelin [61]. A distinct characteristic of HIF2α is the presence of an iron response element (IRE) within its transcript [66]. IREs are specific sequences located within the untranslated region (UTR) of certain mRNA transcripts that enable regulation by iron bioavailability [67]. When

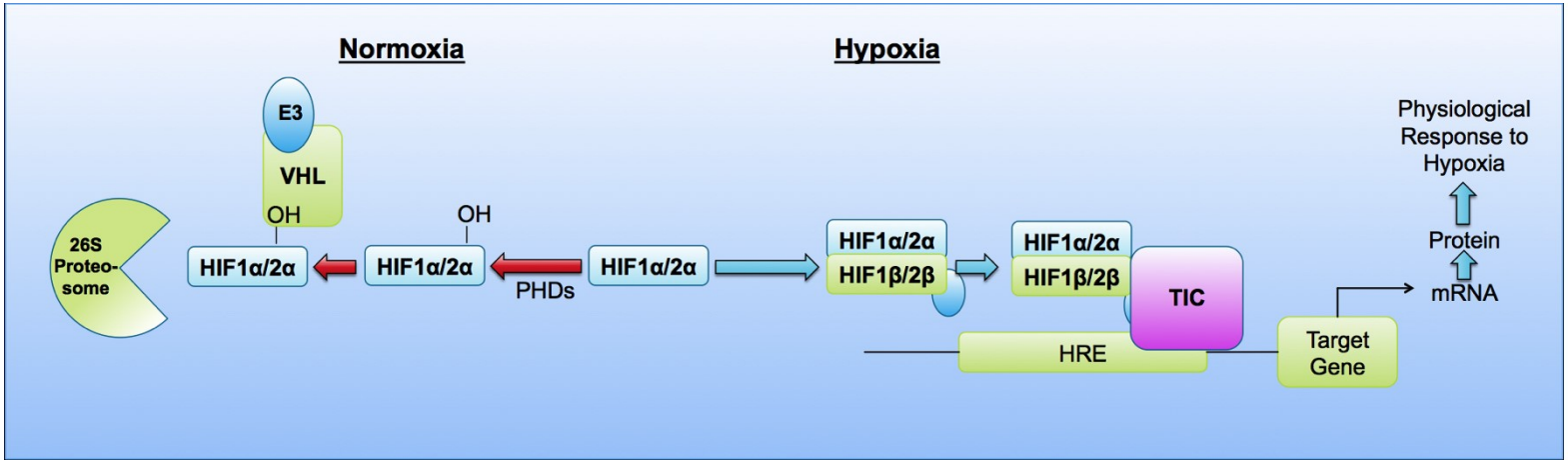

Figure 1.1. Regulation of Hypoxia Inducible Factors in Intracellular Normoxia and Hypoxia. Under normoxic conditions, hypoxia inducible factors HIF1α and HIF2α undergo hydroxylation by prolyl hydroxylases (PHDs) and are subsequently targeted by the Von Hippel-Lindau (VHL) tumor suppressor protein, enabling polyubiquitination by the E3 ubiquitin complex and proteosomal degradation. Under hypoxic conditions, HIF1α/ HIF2α forms a heterodimer with nuclear translocator HIF1β/HIF2β. Once in the nucleus, the heterodimer binds hypoxia response elements (HREs) within the promoter region of target genes resulting in the formation of a transcription initiation complex (TIC) with RNA polymerase and P300 coactivators. Adapted from Semenza, G.L. [68].

intracellular iron levels are low, IREs are bound by iron response element binding proteins (IREBPs), which inhibit mRNA translation. In the presence of iron, IREBPs are released and mRNA translation is disinhibited. IREs have been identified in a number of iron-related genes, such as ferritin [69]. As intracellular iron, such as that produced by heme catabolism, binds the IREBP on ferritin-mRNA, the IREBP dissociates to allow ferritin translation. Although most IRE-containing transcripts conform to this mode of action, others do not [70]. For example, transferrin receptor mRNA, which is responsible for intracellular re-uptake of iron, is stabilized by the presence of an IREBP. In heme metabolism, the presence of an IRE within erythroid delta-aminolevulinic acid synthase-2 (ALAS2) is a distinguishing feature from ALAS1 [71]. The presence of an IRE may explain why HIF2α has been shown to transcriptionally regulate key iron regulatory proteins including divalent metal transporter-1 (DMT-1), ferroportin, and hemoprotein duodenal cytochrome B (DcytB) [72]. Interestingly, HIF2α - not HIF1α - also contains four putative heme regulatory motifs that theoretically could enable protein interactions with heme [73].

1.4.2 Regulation of Rate-Limiting Enzymes in Heme Metabolism

Heme, iron protoporphyrin IX, is essential for oxygen-dependent life as a result of the oxygen binding capacity of its iron core [74]. Heme, the iron-containing prosthetic group of the hemoprotein hemoglobin, is essential for sustaining oxygen-dependent function through its roles in cellular respiration, formation of cytochromes, and globins. The oxygen binding capacity of heme's iron core enables it to serve in electron transport and catalyze redox reactions. Proteins including the heme prosthetic/cofactor are termed 'hemoproteins' and include a wide array of function, such as the generation of immune reactions in peroxidases, generating ATP or metabolizing drugs in Cytochrome C and Cytochrome P450, and oxygen transport and storage in hemoglobin and myoglobin. Thus heme is synthesized ubiquitously and is critical to cellular homeostasis and metabolic processes involving oxygen. Although essential to cellular function, free heme can be cytotoxic as its highly lypophilic regions enables destabilization of lipid membranes and DNA by peroxidation and intercalation [75].

Heme is synthesized by a sequence of 8 enzymatic reactions, of which the first and last 3 steps take place within the mitochondria [76] (Figure 1.2). Heme biosynthesis

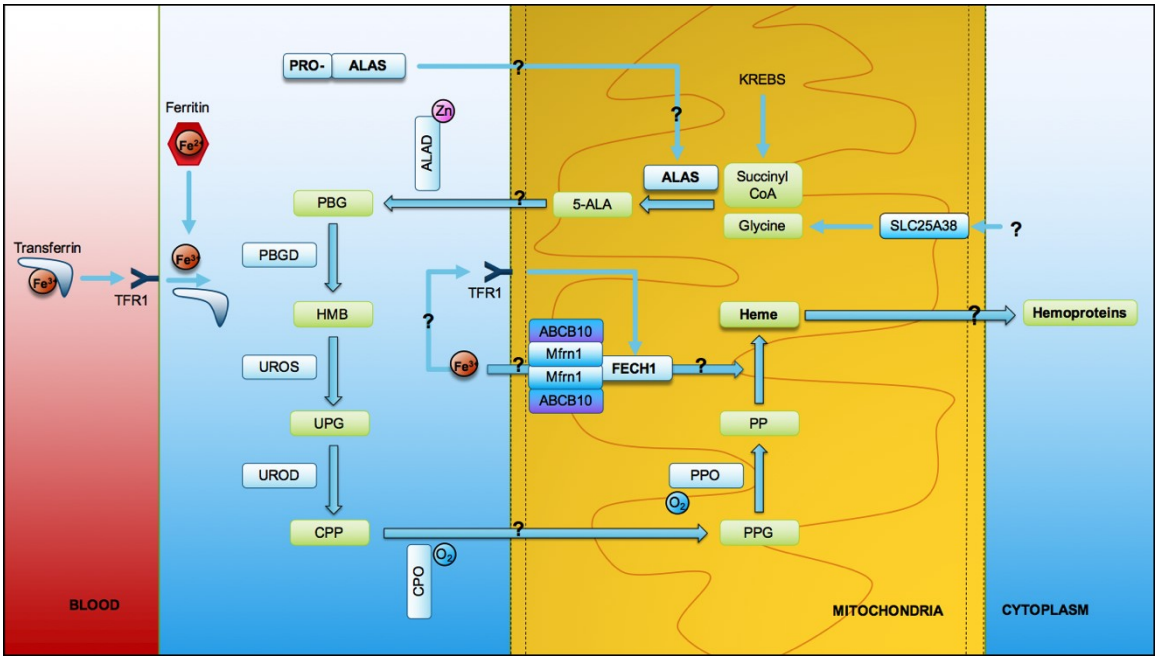

Figure 1.2. Regulation of Heme Synthesis by Rate-Limiting Delta-Aminolevulinic Acid Synthase (ALAS1 and ALAS2). Delta-aminolevulinic acid synthase (ALAS1 or ALAS2) mediates the conversion of glycine and succinyl Co-A to 5-aminolevulinic acid (5-ALA) in the mitochondria. Zinc-coupled 5-aminolevulinic acid dehydratase (ALAD) converts 5-ALA into porphobilonogen (PBG) in the cytosol. PBG is then converted to hydroxymethylbilane (HMB) by porphobilonogen deaminase (PBGD). HMB is converted to uroporphyrinogen III (UPB) by uroporphyrinogen III synthase (UROS). UPB is subsequently converted into coproporphyrinogen III (CPP) by uroporphyrinogen decarboxylase (UROD). Within the mitochondria, the conversion of CPP to protoporphyrinogen IX (PPG) is catalyzed by coproporphyrinogen III oxidase (CPO) and oxygen. PPG is then converted to protoporphyrin IX (PP) by protoporphyrinogen oxidase (PPO) and oxygen before chelating iron (Fe^{2+}) via ferrochelatase (Fech1) to form heme. (ABCB10, ATP-binding cassette subfamily-B member-10; Mfrn1, mitoferrin-1; SLC25A38, Solute carrier family 25 member 38; TFR1, transferrin receptor-1).

is catalyzed from glycine and succinyl Co-A by the rate-limiting enzyme ALAS [77]. Two highly conserved isoforms have been identified: ALAS1 and ALAS2. ALAS1, also named ALAS-H for its purported housekeeping properties, is believed to be constitutively expressed while ALAS2 (ALAS-E) is the primary isoform responsible for heme incorporation into red blood cells and is predominantly expressed in erythroid cells [78].

Heme is catabolized by heme oxygenases, of which, two active isoforms have been characterized, an inducible HMOX1 and a constitutive HMOX2 [79]. HMOX1 and HMOX2 are responsible for the catabolism of heme into biliverdin, carbon monoxide (CO), and essential Fe^{2+} (Figure 1.3). HMOX1 is tightly regulated by its transcriptional repressor Bach1 [80]. In the presence of heme, Bach1 is released from the HMOX1 promoter and subsequently targeted for proteasomal degradation outside of the nucleus. Historically, little attention was paid to HMOX1 or its metabolites, which were largely considered to be waste products when discovered in 1968 by Tenhunen *et al.*[79] until 1992 when Nath *et al.* [81] characterized HMOX1 as cytoprotective against renal injury. Since then, exploration of HMOX1 as a potential cytoprotective strategy has dramatically increased, especially in the context of ischemic injury [82].

HMOX1 collectively exerts its cytoprotective benefits by catabolism of pro-oxidant free heme into potent antioxidant biliverdin; vasodilator and anti-inflammatory agent, CO; and Fe^{2+} which is rapidly sequestered by ferritin [82]. The binding of heme to HMOX1 results in targeted cleavage of heme's α-methine bridge and opening of its heterocyclic pyrrole ring to form the bile pigment biliverdin. Biliverdin is then converted to bilirubin by biliverdin reductase, where it can then be bound to albumin and cleared by the liver. However, bilirubin serves as an antioxidant by accepting electrons from free radicals, thus attenuating ROS levels. The potency of bilirubin as an antioxidant stems from its subsequent conversion back to biliverdin upon electron acceptance [83]. Heme catabolism further results in endogenous CO production. Similar to nitric oxide, CO acts as a vasodilator through activation of soluble guanalyl cyclase [4]. This is an important property in the context of tissue hypoxia as vasodilation enables increased passage of oxygenated blood to the hypoxic tissue. CO additionally serves as an anti-inflammatory agent [84] through CO-mediated thrombosis inhibition, preventing aggregation and

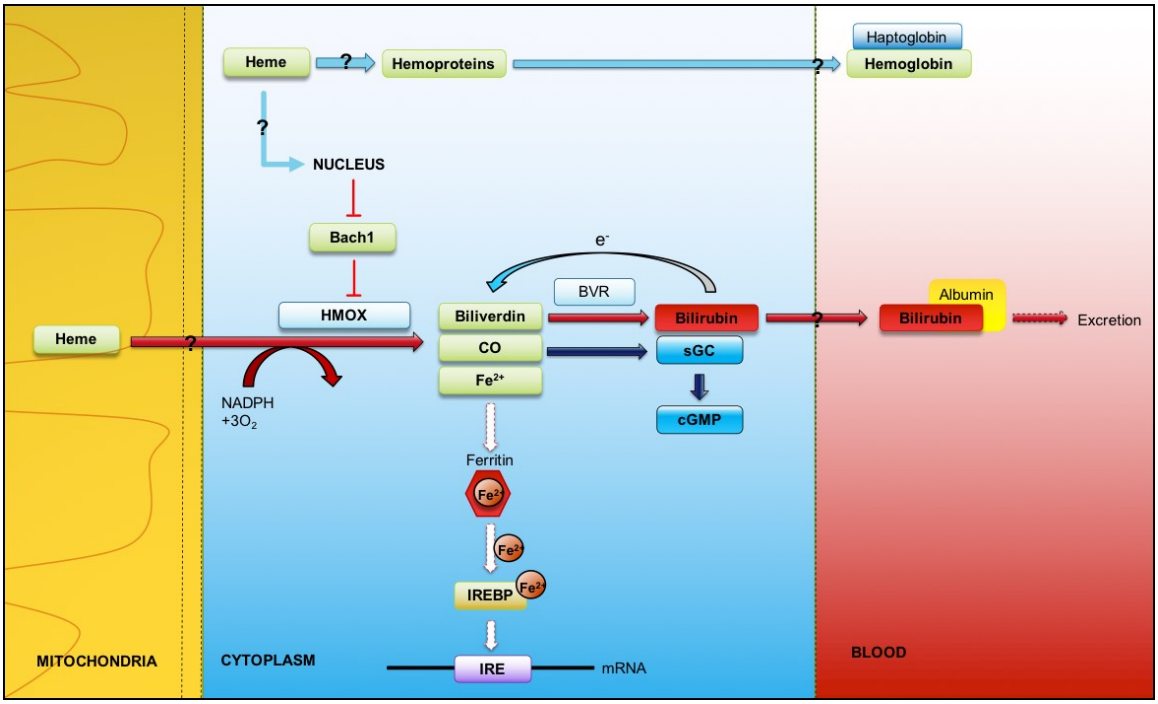

Figure 1.3. Regulation of Heme Catabolism by Heme Oxygenases (HMOX1 and HMOX2). Heme oxygenase 1 (HMOX1) is transcriptionally repressed by Bach1 in the absence of heme. HMOX1 and HMOX2 catabolize heme into biliverdin, carbon monoxide (CO) and Fe^{2+}. Biliverdin is reduced to bilirubin by biliverdin reductase (BVR) and is excreted by the liver. CO activates hemoprotein soluble guanalyl cyclase (sGC) to produce cyclic guanosine monophosphate (cGMP). Fe^{2+} is chelated by ferritin. Upon release from ferritin, Fe^{2+} dissociates iron response element binding proteins (IREBPs) from target iron response elements (IREs), enabling translation of the target mRNA. (NADPH, nicotinamide adenine dinucleotide phosphate-oxidase).

activation of platelet cytokine cascades.

Finally, catabolism of heme results in the release of Fe^{2+}. Although an essential source of iron, iron derived from heme catalysis can contribute to the production of hydroxyl radicals and the perpetuation of excess ROS formation through the Fenton reaction [85]. Coordinating with HMOX1 transcriptional activation is the simultaneous upregulation of ferritin [5]. Ferritin, a 450 kDa globular protein cage, is the primary intracellular site of iron storage in the cytosol. Release of iron from ferritin occurs by lysosomal autophagy [86].

1.5 HMOX1 in Heart Failure

Current interventional strategies in heart failure management focus heavily on attenuating RAAS signaling and sympathetic drive. Yet, morbidity and mortality in heart failure persists. Targeting of the heme metabolism pathway provides a novel approach to manage heart failure.

1.5.1 Therapeutic Potential of HMOX1 Induction

Modulation of the heme catabolism pathway has extensively been shown to mitigate myocardial damage following AMI-induced heart failure. In Lewis rats, pre-emptive delivery of adeno-associated HMOX1 gene reduced infarct size by 62% and improved mortality by 25% 1 year after IR-injury [6]. In a similar study, pre-emptive HMOX1 delivery attenuated decreased ejection fraction by 27% 1.5 months after IR-injury, while recovering ejection fraction fully after 3 months [87]. This was supported by earlier findings that cardiac-specific (α-myosin heavy chain) HMOX1 transgenic mice demonstrated a 40% reduction in AMI injury [7]. Due to the present translational obstacles involved with HMOX1 gene delivery, hemin has also been investigated as a novel strategy to ameliorate heart failure outcomes. Hemin, trade name Panhematin®, is an FDA-approved heme surrogate used in the treatment of porphyrias. Hemin is derived from red blood cells and differs from heme only by the presence of a chloride group bound to heme's iron core. Similar to endogenous heme, hemin acts as both inducer and substrate of HMOX1. Hemin administration has been shown to reduce infarct expansion and improve survival by approximately 40% when compared to vehicle-treated controls in a preclinical models of permanent-ligation AMI [8]. Although less is known about the therapeutic potential of targeting the heme metabolism pathway in pressure-overload

heart failure, gene delivery studies have demonstrated delayed hypertension onset and lowered blood pressure in spontaneously hypertensive rats [88].

1.5.2 Paradoxical Expression of HMOX1 in Human Failing Hearts

Although largely reported as an exclusively cytoprotective enzyme, recent reports have shown that HMOX1 can also exacerbate cardiovascular disease. HMOX1 levels in obese patients act as positive predictors of chronic metabolic inflammation and insulin resistance [89]. Within the same study, deletion of hepatic and adipose HMOX1 in preclinical models of obesity independently prevented the reported negative effects. Furthermore, transgenic mice overexpressing HMOX1 under the control of an α-myosin heavy chain promoter demonstrated accelerated cardiac dysfunction, despite attenuated interstitial fibrosis, following TAC, while simultaneously eliciting protection in isoproterenol-induced cardiomyopathy [90]. These studies highlight an underlying limitation to our basic understanding of HMOX1 that could limit its translation as a therapeutic. Moreover, Khechaduri *et al.* [91] challenged our understanding of HMOX1 as a stress/heme-inducible enzyme, showing an increase in heme content and heme synthesizing enzyme ALAS2 in human heart failure *without* evidence of HMOX1 induction. Collectively, these studies highlight a biased understanding of HMOX1 towards its therapeutic benefits or context (temporally/spatially) and raises important questions: If HMOX1 is known to be cytoprotective *and* proportionally increased in the presence of stress (oxidative, hypoxic or both) and heme - why is it insufficient to prevent heart failure? Are there injuries/disease conditions or times at which HMOX1's benefits are limited by heme bioavailability? Is HMOX1 induction desensitized during decompensatory heart failure? How is heme metabolism regulated in the progression of heart failure and how might heme bioavailability be affected during heart failure or influenced by hypoxia?

1.6 Summative Rationale

The morbidity and mortality of heart failure is high, despite progress in pharmacological interventions (e.g. ACE inhibitors and β-blockers). Heart failure is the inability of the heart to meet the metabolic demands of the body as a consequence of reduced blood ejection capacity (i.e. left ventricular ejection fractions <40%). Heart failure is caused by various cardiovascular disease etiologies; AMI and hypertension are

the two most prevalent [3]. AMI causes ischemic necrosis and the surviving myocardium's oxygen demands increase during compensation to the added mechanical load (volume-overload). Scarring and insufficient neovascularization can cause cardiomyocytes to become isolated and chronically hypoxic. The myocardium in hypertension also experiences increased oxygen demands as it compensates for the increased afterload due to peripheral resistance. This results in hypertrophy, perivascular and interstitial fibrosis, and without adequate neovascularization, the partial pressure of oxygen diffusion is reduced (pressure-overload). With increased oxygen demand (during compensation), metabolic inefficiency (during decompensation) and with hypoxia, there is an increased state of oxidative stress. The HMOX1 pathway has long been recognized as integral to cytoprotection of cardiomyocytes during hypoxia (via HIF1α transactivation) and oxidative stress (via Nrf2 transactivation) [92], which can be augmented further by the presence of inflammation (via concomitant NF-kB transactivation) [92]. HMOX1 exerts cytoprotection by catabolizing pro-oxidant free-heme into antioxidant biliverdin. Additionally, HMOX1 catabolism of heme releases Fe^{2+} and CO, which indirectly (by ferritin and cGMP mechanisms) reduce oxidative stress and apoptosis, respectively. In pre-clinical models of AMI-driven heart failure, induction of HMOX1 reduces mortality and preserves ventricular function [6], however, overexpression of HMOX1 simultaneously exacerbates heart failure in pressure overload [90]. We hypothesize that the paradoxical effects of HMOX1 in heart failure result from differences in transcriptional regulation of heme metabolism by hypoxia severity or duration.

Targeting of the heme metabolism pathway remains a novel approach to manage heart failure. Understanding the molecular mechanisms regulating heme metabolism is essential to expedite translation to the clinic and prevent adverse side effects using existing medication strategies (eg. Pan-Hematin^{TM}). In particular, the elucidation of the role of HIFs in maintaining heme homeostasis, using clinically parallel degrees and duration of hypoxia, would be a critical step. The HIFs are potential key transcriptional regulators of heme bioavailability in the failing heart. HIF1α transcriptionally regulates over 200 genes in response to acute hypoxia, including HMOX1. Yet, HMOX1 levels remain unchanged in recent findings from human failing hearts despite increased heme

synthesis and hypoxia [91, 93]. The understanding of clinical-hypoxia is based on experiments performed principally in acute, intense hypoxia models that do not reflect the degree or duration of hypoxia experienced by cardiac patients. This is further propagated in our understanding of HMOX1 regulation by HIF1α, which is purported to be the primary mediator of hypoxia-induced expression. Contrary to HIF1α, the role of HIF2α in hypoxia has been given short shrift and is often presumed to be a redundancy to the roles of HIF1α. Although less is known about HIF2α and its role in maintaining oxygen homeostasis in heart failure, it is a potentially key regulator of heme bioavailability. Similar to HIF1α, HIF2α has the capacity to bind hypoxia response elements (HREs), binding sites putatively identified in HMOX1, ALAS1 and ALAS2 promoters. Unlike HIF1α, HIF2α contains four putative heme-regulatory motifs [73] and an iron response element (IRE; the IRE-binding protein inhibits mRNA translation in the presence of excess iron) within its transcript [66]. HIF2α has been shown to regulate divalent metal transporter-1 (DMT-1), erythropoietin (EPO) and ferroportin-1 (FPN1), independent of HIF1α [61], thus implicating it as the predominant regulator of ferro-heme homeostasis.

1.7 Hypothesis and Objectives

We hypothesize that HIF2α regulates heme metabolism in heart failure. Specifically, we propose that HIF2α, not HIF1α, maintains heme homeostasis through regulation of ALAS and HMOX in chronic hypoxia, typified in heart failure progression. To elucidate the role of the HIFs in regulating heme metabolism in hypoxia, and thus heart failure, the following objectives will be addressed:

1) Characterize HIF1α, HIF2α, ALAS1, ALAS2, HMOX1, HMOX2 (heme regulatory enzymes) levels in clinical heart failure using *in silico* microarray analyses of human failing hearts obtained from the Gene Expression Omnibus (GEO);

2) Quantify heme content (by enzymatic assay) and heme regulatory enzymes (by qPCR and immunoblotting) throughout the progression of both volume- and pressure overload pre-clinical models of heart failure;

3) Quantify heme content and regulatory enzymes using *in vitro* models of acute and chronic, moderate or severe hypoxia, by manipulating atmospheric O_2 concentrations;

4) Quantify heme regulatory enzyme expression in heme-replete hypoxia by administration of hemin (heme surrogate) to recapitulate heme-replete conditions reported by Khechaduri *et al.* in human heart failure [91];

5) Investigate the roles of HIF1α/2α in mediating heme regulatory enzymes in hypoxia and heme-replete hypoxia by using adenoviral overexpression/shRNA vectors;

CHAPTER 2
Materials and Methods

2.1 *In Silico* Microarray Analyses of Human Failing Hearts

The National Center for Biotechnology Information's (NCBI's) Gene Expression Omnibus Gene Expression and Hybridization Array Repository (GEO; [94, 95]) is comprised of user submitted high-throughput datasets from original research, in compliance with the NCBI's stringent Minimum Information About a Microarray Experiment (MIAME) submission standards [96]. Microarray datasets pertaining to human heart failure were obtained through the open-access data deposited in GEO (Figure 2.1). Heme regulatory enzyme mRNA expression was investigated in biopsies of male and female patients diagnosed with either dilated heart failure (Series Accession GSE3586; [97]) or idiopathic heart failure (Series Accession GSE1145). Cardiac biopsies derived from either the left ventricle or the septal-wall were obtained from explanted hearts prior to cardiac transplantation. Control biopsies were obtained from organ donors whose hearts were unable to be transplanted. Data are expressed as relative mRNA (log_2-transformed).

2.2 Animal Care and Preclinical Models

Animal care and experimental procedures were approved by the Animal Care Committee at the University of Guelph, and were carried out in accordance with the guidelines established by the Canadian Council on Animal Care. Animals were maintained on a 12:12 hour light:dark cycle with food and water provided *ad libitum*.

2.2.1 Volume Overload Heart Failure (AMI)

Adult male C57B1/6 mice (8 weeks of age) were subjected to AMI by permanent ligation of the left anterior descending coronary artery (LAD) [98]. Animals were anesthetized with 2%:100% isofluorane:O_2, intubated, and ventilated (Harvard Apparatus) at a rate of 200 breaths/min. Under sterile surgical conditions, a para-sternal thoracotomy was performed and the LAD was ligated immediately below the atrioventricular border using 7-0 Surgipro™ II polypropylene suture (Covidien; Figure 2.2). The thoracic incision was closed using 7-0 Prolene™ (Covidien). Sham-operated animals underwent an identical operation, but without arterial ligation. Animals were monitored twice daily for post-surgical complications. Age-matched sham and volume

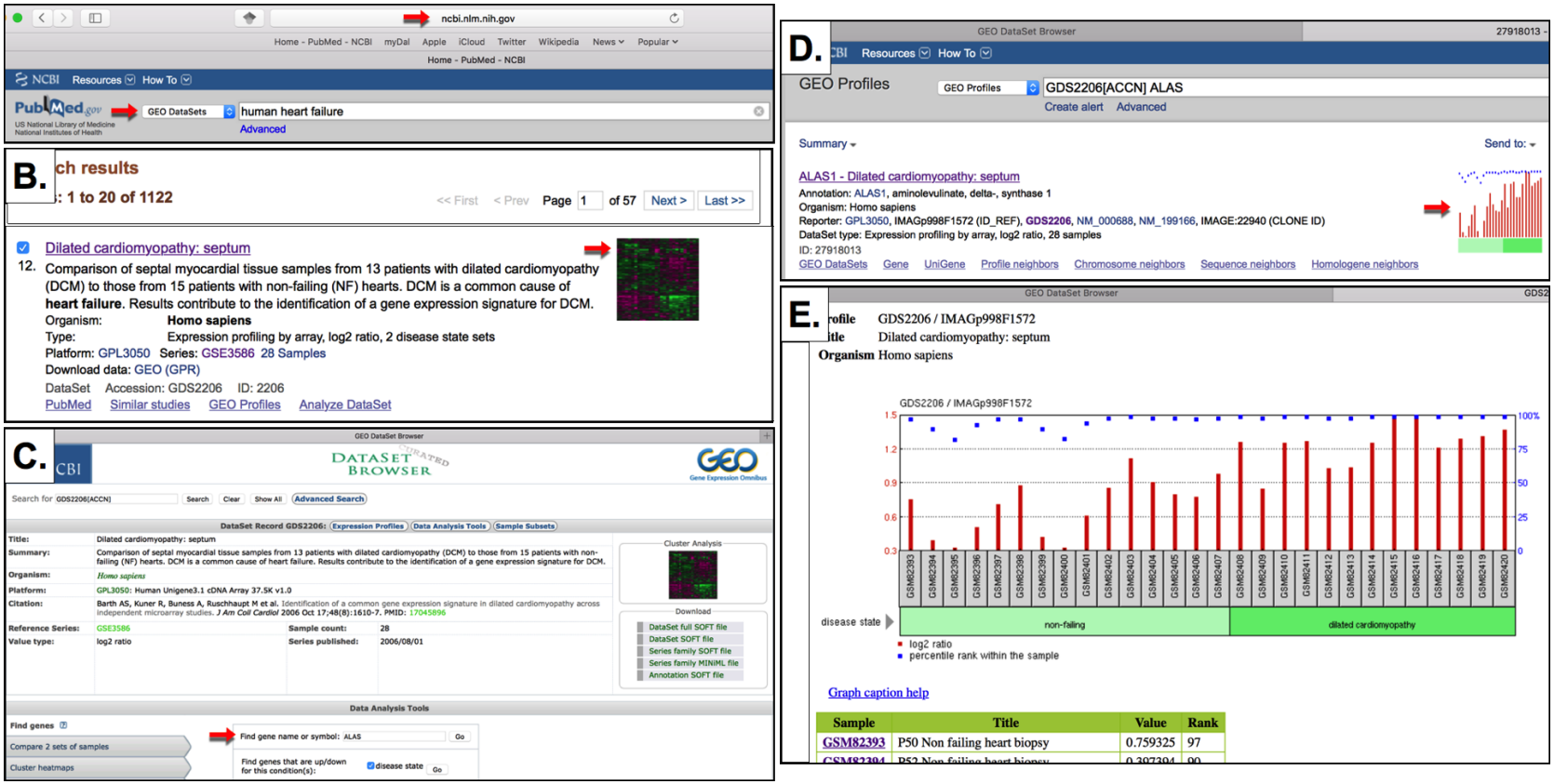

Figure 2.1. Retrieval of Human Heart Failure GEO Profiles via the NCBI Database. (A) GEO DataSets were accessed from http://www.ncbi.nlm.nih.gov/geoprofiles/ using the keywords "human heart failure." **(B)** Search results containing microarray datasets displayed both a Series Accession number (GSE#) and thumbnail image of a microarray cluster heat map. **(C)** GEO DataSet Browser identified experimental protocols, sample type, microarray platform, and raw data. Genes of interest were queried in the Data Analysis search box. **(D)** Curated gene-of-interest GEO Profiles displayed thumbnail images of normalized data. **(E)** An expanded view of the normalized dataset included disease state, sample identification and normalized data values.

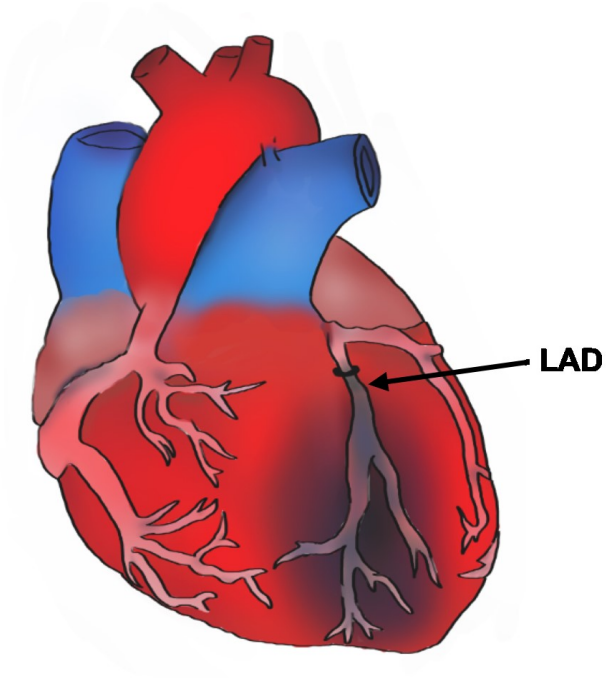

Figure 2.2. Surgical Model of Volume-Overload Heart Failure by Acute Myocardial Infarction (AMI). Permanent ligation of the left anterior descending coronary artery (LAD) occludes blood flow and results in necrosis and scarring of the downstream myocardium.

overload animals were sacrificed under anesthesia at 3 days, 1 week, 2 weeks, and 4 weeks after AMI.

2.2.2 Pressure Overload Heart failure by Transverse Aortic Constriction (TAC)

Adult male C57B1/6 mice (8 weeks of age) were subjected to cardiac pressure overload by transverse aortic constriction [99]. Animals were anesthetized with 2%:100% isofluorane:O_2, intubated, and ventilated at a rate of 200 breaths/min. A parasternal thoracotomy was performed and a ligature was applied around the transverse segment of the aorta, between the brachiocephalic trunk and the left common carotid artery, and constricted over a blunted 22-gauge needle using a silk 7-0 suture (Figure 2.3). Age-matched sham and pressure overload animals were sacrificed under anesthesia at 2, 4 and 18 weeks post TAC surgery.

2.2.3 Tissue Collection and Preparation

Hearts were rapidly excised, frozen in liquid nitrogen and stored at -80˚C until further analysis. In AMI, the infarct was isolated by its characteristic pallor. Samples were ground to powder in liquid nitrogen using a porcelain mortar and pestle. Samples (10-15mg) were homogenized on ice for 30 seconds in 120ul NP-40-based lysis buffer (1% NP-40) using a stainless steel tissue homogenizer (Omni-International). Lysis buffer was prepared immediately before use with 10ul protease inhibitor cocktail (Sigma-Aldrich), 10ul phosphatase inhibitor cocktail (Calbiochem), and 10ul activated sodium orthovanadate (Calbiochem) per 100ul lysis buffer stock. Samples were placed on ice for 30 minutes and centrifuged at 2000 x rcf for 2min at 4ºC to remove insoluble lipids and matrix from the lysate. The supernatant was transferred to a fresh 1.5ml tube and centrifuged at 1200 x rcf for 30 minutes at 4ºC to pellet any residual insoluble material. The supernatant was then transferred to a fresh 1.5ml tube using a 28 ½-gauge insulin syringe (Becton Dickinson) to shear DNA remaining in the sample. Total protein concentration was determined using the bicinchonic acid (BCA) method (Pierce®) according to the manufacturer's instructions.

2.2.4 Neonatal Rat Cardiomyocyte (NRCM) Isolation

Neonatal Sprague-Dawley rat pups, between 1 and 2 days of age, were sacrificed by decapitation. A total of 18 rat hearts were excised and placed in 50ml ice-cold 1X phospho-buffered saline (PBS; Corning). The atria and non-cardiac tissue were removed

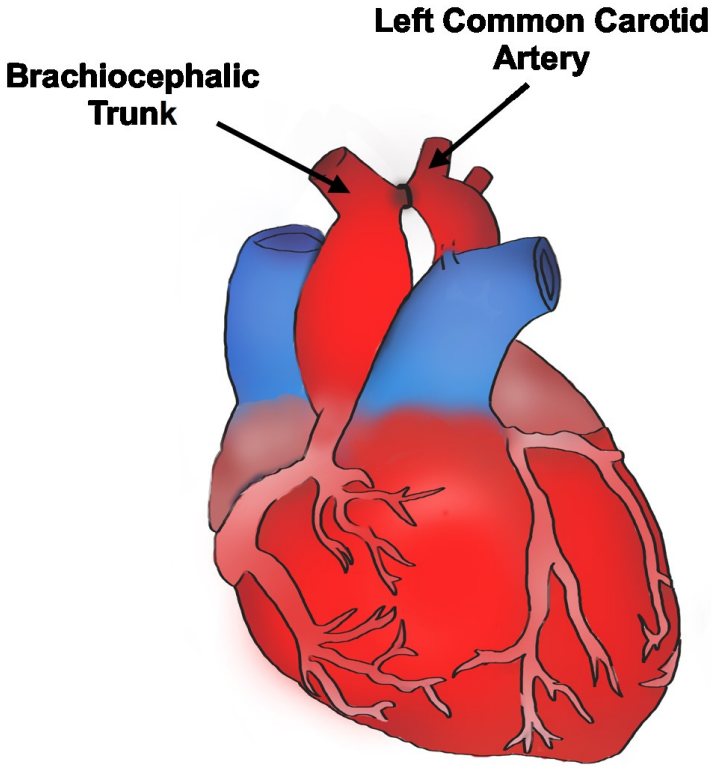

Figure 2.3. Surgical Model of Pressure-Overload Heart Failure by Transverse Aortic Contriction (TAC). Ligation of the aortic arch between the trunk of the brachiocephalic and left common carotid arteries increases afterload in the left ventricle while decreasing renal perfusion.

from each heart in a petri dish containing 1X PBS. An incision was made in the hearts to remove any blood remaining in the ventricles. Once complete, all hearts were transferred to 50ml fresh ice-cold 1X PBS for a final rinse. Hearts were finely minced over a fresh petri dish containing 1X PBS. Subsequent steps were performed in a Labconco® Biological Safety Cabinet under sterile conditions.

Minced hearts were transferred to a T-25 cell culture flask (Corning) with a sterile Pasteur pipette. Sterile 1X PBS (17ml), containing 1ml freshly prepared, sterile-filtered (0.22um) Collagenase Type 2 (Worthington), 1ml DNase I (Worthington), and 0.5ml Trypsin (Worthington), was added for tissue dissociation. The flask was incubated at 37ºC on a rotary shaker for 20min. The dissociated hearts were transferred to a 50ml tube containing 20ml DF20 media: 500ml Dulbecco's Modified Eagle Medium (DMEM)/F12 Medium; (Sigma-Aldrich) supplemented with 125ml fetal bovine serum (FBS; Sigma-Aldrich), 1% penicillin/streptomycin (Invitrogen), and 50µg/ml gentamycin (Invitrogen). Hearts were centrifuged at 800rpm for 1 minute at room temperature. Supernatant was discarded and 17ml ice cold 1X PBS was added to the remaining pellet. The resuspended cells were transferred to a new T-25 flask, supplemented with 1ml Collagenase, 1ml DNase, and 0.5ml Trypsin, and incubated at 37ºC on a rotary shaker for 20min. Cells were once again transferred to a 50ml tube containing 20ml DF20 media and were centrifuged at 300 x rcf for 7min at 4ºC. Supernatant was discarded and 12 ml plating media, containing 500ml DMEM/F12 media, 60ml horse serum (Invitrogen), 30ml FBS, 1% pen/strep, and 50µg/ml gentamycin, was added to the remaining pellet.

The cell suspension was transferred to a fresh 50ml tube over a 100um cell strainer (BD Falcon) and triturated. The cell filtrate was transferred to a T-25 flask and incubated at 37ºC for 1h. NRCMs suspended in the media were transferred to a new T-25 flask, without disrupting the bottom surface of the flask, and were incubated for an additional hour at 37ºC. The supernatant was transferred to a sterile 15ml tube and centrifuged at 1000 rpm for 2 minutes at room temperature. The supernatant was aspirated and the remaining NRCM pellet was diluted in 18ml plating media. Viable cells were counted by hemocytometer and Trypan Blue Solution 0.4% (Amresco); viable cells were defined by Trypan Blue impermeability. NRCMs were seeded at $2x10^6$ cells/35mm Primaria™ (Corning) plate and were incubated at 37ºC for 24h prior to treatment.

2.3 Cell Culture

H9C2 embryonic rat left ventricular cardiomyoblasts were expanded from frozen stocks purchased from the American Type Culture Collection (ATCC) using plating media containing Dulbeco's Modified Eagle Medium-High Glucose (DMEM-HG; Gibco®) supplemented with 10% FBS (Seradigm). For experiments, cells were seeded at $2x10^4$ cells/35mm plate and cultured to 80% confluency at 37ºC in a 95% air, 5%CO_2 humidified atmosphere. All experiments were conducted on cells that were passaged at least once following recovery from cryogenic storage and did not exceed 19 passages. Cells were cultured for a minimum of 24h after passaging prior to experimental treatment.

2.3.1 Serum Deprivation, Hypoxia and Drug Treatment

Proliferative H9C2 cells were converted to quiescent myotubules by complete deprivation of FBS for 6 days [100], renewing the media with DMEM-HG without FBS (differentiation media) every 72h. Experimental conditions were initiated on the 6^{th} day of differentiation. Experiments conducted in hypoxia were incubated in a HERAcell 150.i CO_2 incubator (Thermo Scientific) with adjustable atmospheric O_2/N_2 content. For experiments conducted in hypoxia in excess of 24h, media was renewed with hypoxia-conditioned media every 24h. A 10mM Hemin stock (Sigma-Aldrich) was prepared in dimethyl sulfoxide (DMSO; Amresco) and was sonicated in a water bath for 40min. Stock hemin in DMSO was stored at 4ºC for a maximum of 3 months. Hemin stock was sonicated for 10min prior to use and was diluted in media immediately preceding treatment. N-Acetyl-L-Cysteine (NAC; Amresco) was prepared as a 3mM stock in sterile 1X PBS. NAC was sonicated in PBS for 10min prior to use and was diluted in media immediately before treatment. Stock NAC was stored at 4ºC and was used within 2 months.

2.3.2 Cell Viability Assay

Cell viability was determined using the resazurin method. H9C2 cells were seeded at $12x10^3$ cells/well in a 96-well plate with 100ul media/well. Following cell treatment, media was carefully aspirated from the wells. All wells were rinsed twice with 100ul sterile 1X PBS. Fresh media supplemented with 10% PrestoBlue™ Cell Viability Reagent (Invitrogen) was added to each well and cells were incubated at 37ºC for 3

hours. Spectral absorbance was measured using a Synergy H4 Hybrid Reader (Biotek) with excitation and emission wavelengths of 560 and 590nm respectively. Cell viability was calculated through subtraction of the 560/590nm media-only control from its respective cell treatment group.

2.4 Adenoviral Vector Transduction

2.4.1 HIF1α and HIF2α Constructs

Overexpression and knockdown of HIF1/2α was accomplished by transduction of bicistronic adenoviral vectors developed in collaboration with Vector Biolabs (Figure 2.4). Human HIF overexpression vectors (Ad-RFP-h-HIF1α-HA and Ad-GFP-h-HIF2α-Myc) were regulated by the cytomegalovirus (CMV) promoter in addition to a downstream intermediate ribosomal entry site (IRES). Histidine tags (HA or Myc) were integrated into the C-terminus of the human HIF proteins in the overexpression vectors. Adenoviral knockdown was accomplished using mouse or rat-gene specific targeted short-hairpin-loop RNA (shRNA; Ad-RFP-m-HIF1α-shRNA and Ad-GFP-r-HIF2α-shRNA) under the control of the U6 promoter (Table 1.). Both overexpression and shRNA adenovectors encoded fluorescent tags, red fluorescent protein (RFP) or green fluorescent protein (GFP), permitting visualization of transduction. Adenoviruses were aliquoted and stored at -80º in buffer containing DMEM supplemented with 2% bovine serum albumin (BSA) and 2.5% glycerol. Titers ranged from $2.2x10^{10}$ to $6.0x10^{10}$ plaque forming units (PFU)/ml, as determined by Vector Biolabs.

2.4.2 Transduction of Adenoviral Vectors into Host Cells

H9C2 were plated as previously described. After 72h culture in differentiation media, cells were transduced in fresh differentiation media containing 100 multiplicities of infection (100 MOI) of adenovirus expressing either human HIF1α or HIF2α, or mouse/rat-targeted HIF1α shRNA. After 72h transduction (day 6 of differentiation), media was renewed and treatment was initiated. Transduction efficiency was assessed after 72h viral exposure at 85-95% by GFP/RFP visualization by fluorescence microscopy and further confirmed by flow cytometry. Gene overexpression and knockdown were confirmed by Western blot and qPCR analyses.

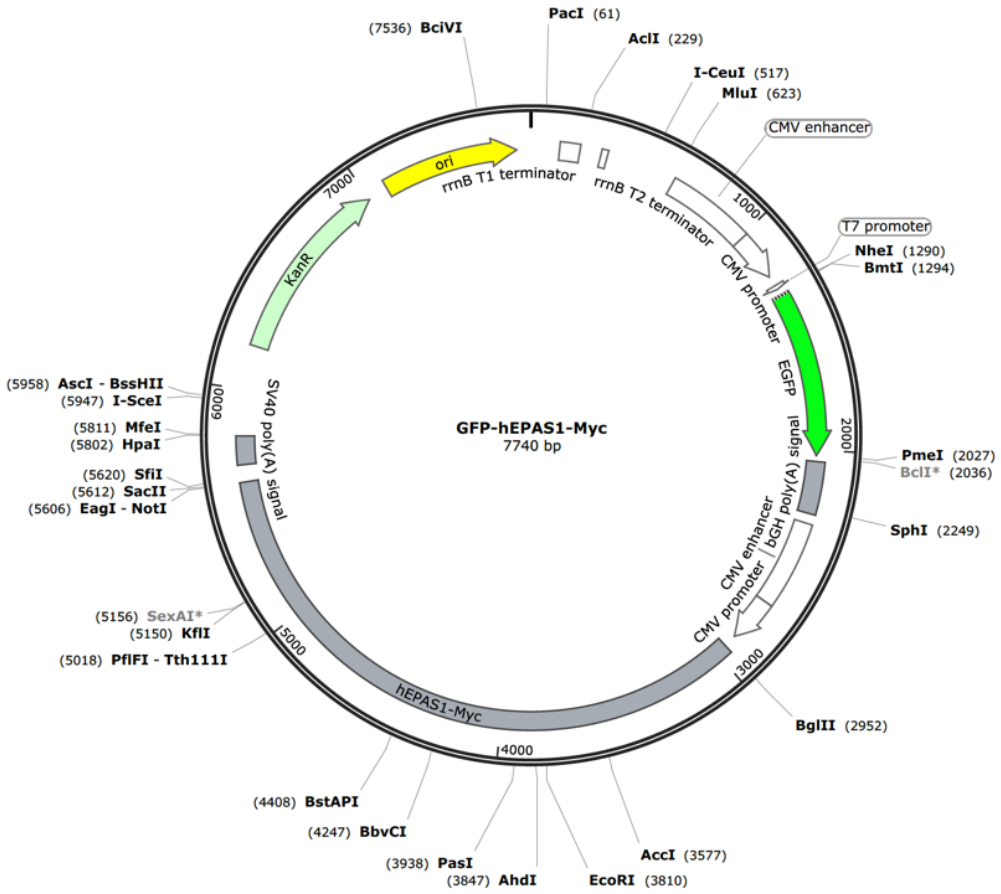

Figure 2.4. Adenoviral Vector Construct Map. Representative bicistronic adenoviral vector construct containing a CMV/U6 promoter region, reporter gene (ex. EGFP), downstream intermediate ribosomal entry site (IRES), and a specific gene sequence (ex. HIF2α, a.k.a. EPAS1) with tag (ex. Myc). Map image courtesy of Vector Biolabs.

Table 1. Adenoviral shRNA Sequences

Vector	shRNA sequence (hairpin underlined)
Ad-RFP-m/r-HIF1α-shRNA	CCGG-AGTCGACACAGCCTCGATATGCTCGAGCATATC-GAGGCTGTGTCGAC-TTTTTG
Ad-GFP-r-HIF2α-shRNA	CCGG-AGCTTCCTGCGAACACATAAACTCGAGTTTATG-TGTTCGCAGGAAGC-TTTTTG

GFP, green fluorescent protein; HIF, hypoxia inducible factor; m, mouse; r, rat; RFP, red fluorescent protein.

2.5 Microscopy

Images were acquired using an EVOS™ XL Cell Imaging System transmitted-light microscope (Invitrogen) using appropriate Em:488±10nm/Ex:520±20nm detection filters.

2.6 Flow Cytometry

2.6.1 Hypoxia Detection

For all flow cytometry, a minimum of 10, 000 cells/events were included for analysis. Pimonidazole [101], gold (III) chloride trihydrate [102] ($HAuCl_4$) and Alexa Fluor®-conjugated maleimide were used to detect intracellular hypoxia. All reagents, cell plates and tubes containing hypoxia-sensitive dyes were covered in aluminum foil and experiments were conducted under reduced light conditions. A 10mM pimonidazole (Sigma-Aldrich) stock, commercially recognized as Hypoxyprobe™, was prepared in ddH_2O and sonicated in a water bath for 10min. Stock pimonidazole was stored at 4ºC for up to 3 months. Pimonidazole stock was sonicated for 5min and diluted to working solutions of either 100 or 200 uM in media immediately prior to use. Cells ($4x10^5$ H9C2/60mm dish) were incubated with pimonidazole in hypoxia for 24h. Media was subsequently aspirated and cells were rinsed with 1X PBS. Cells were incubated with Trypsin EDTA, 1X (Corning) for 5min at 37ºC. Once non-adherent, cells were transferred to a sterile 15ml tube containing an equal volume of media and then centrifuged at 500 x rcf for 5min at 4ºC. The supernatant was carefully aspirated and cell pellets were gently resuspended in 1 to 2ml media. Approximately $4x10^5$ viable cells were counted by hemocytometer with Trypan Blue solution and transferred to fresh 5ml polystyrene tubes (BD Falcon). Cells were pelleted by centrifugation at 500 x rcf for 5min at 4ºC, the supernatant was carefully aspirated and cells were rinsed in 1X PBS; centrifugation and wash with 1X PBS was repeated. Cells were resuspended in 1ml 1X PBS and fluorescence-activated cell sorting (FACS) analysis was performed using a Gallios 10-color flow cytometer (Beckman Coulter) to determine the presence or absence of pimonidazole within the cells.

A 20mM $HAuCl_4$ (Sigma-Aldrich) stock was prepared in sterile 1X PBS and sonicated for 30min before passing the solution through a 0.2um syringe filter. Stock $HAuCl_4$ was stored at 4ºC for up to 4 months. $HAuCl_4$ stock was sonicated for 5min and

diluted to a working solution of 10uM in media immediately prior to use. Incubation and preparation of $HAuCl_4$-exposed cells for FACS analysis was performed identically to that previously outlined with pimonidazole. $HAuCl_4$ was measured at an emission wavelength of 532nm.

A 1mM stock solution of Alexa Fluor® 633-conjugated C5-maleimide (Thermo Scientific) was prepared in DMSO. Stock maleimide was stored at 4ºC for up to 4 months. Maleimide stock was diluted to a working solution of 10uM in media immediately prior to use. Following exposure to hypoxia, media was rapidly replaced with media containing 10uM maleimide, covered in aluminum foil and returned to either normoxia or hypoxia for 2h. Cells were counted and washed in 1X PBS as previously described. Maleimide was measured at an emission wavelength of 622 to 640nm.

Cobalt (II) chloride ($CoCl_2$) acts as a hypoxia mimetic by inhibiting the hydroxylation and subsequent proteosomal degradation of the HIFα subunit [62], thus artificially increasing HIF1α levels through stabilization. To ensure that the hypoxia-sensitive dyes were responsive to hypoxia, independent of HIFα stabilization, $CoCl_2$ was used as a negative control. A 10mM stock solution of $CoCl_2$ (Santa Cruz) was prepared in ddH_2O and sonicated for 15min. Stock $CoCl_2$ was stored at 4ºC for up to 5 months. $CoCl_2$ stock was sonicated for 5min, diluted to a working solution of 100uM in media immediately prior to use and incubated with the cells during hypoxia for up to 24h.

2.6.2 CM-H2DCFDA Measurement of ROS

Intracellular measurement of oxidative stress was performed using chloromethyl 2',7'-dichlorodihydrofluorescein diacetate (CM-H_2DCFDA; Life Technologies). A 1mM CM-H_2DCFDA stock was prepared in DMSO. Stock CM-H_2DCFDA was stored at -80ºC for no longer than 1 month. CM-H_2DCFDA stock was diluted to a working solution of 5uM in media immediately prior to use. Following treatment, cells were incubated with CM-H_2DCFDA for an additional 30 minutes at experimental oxygen condition(s). Media was rapidly aspirated and cells were quickly rinsed with 1X PBS. Cells were incubated for 5min with Accutase™ Cell Detachment Solution (Innovative Cell Technologies) at 37ºC. Viable cells were immediately counted (approximately $4x10^5$ H9C2/60mm plate) and transferred to fresh flow cytometer tubes. Cells were pelleted by centrifugation at 500 x rcf for 5min at 4ºC; the supernatant was carefully aspirated and cells were rinsed in 1X

PBS. Centrifugation and wash with 1X PBS was repeated. Cells were resuspended in 1ml 1X PBS. Fluorescence was measured at an emission wavelength of 520nm.

2.7 Quantitative Polymerase Chain Reaction (qPCR)

2.7.1 TRIzol Extraction of RNA from Tissue

RNA was isolated by TRIzol® extraction (Invitrogen) in accordance with the manufacturer's instructions. Tissue was briefly homogenized in 1ml TRIzol® prior to extraction. RNA samples were purified by DNase treatment (Qiagen) and RNA integrity was verified by Agilent 2100 BioAnalyzer analysis (Agilent Technologies). RNA concentration was determined spectrophotometrically using a NanoDrop ND1000 (Thermo Scientific). cDNA was synthesized using SuperScript II Reverse Transcriptase (Invitrogen). qPCR was performed by Real-Time PCR 7500 detection system (Applied Biosystems) using Platinum SYBR Green qPCR Supermix (Invitrogen).

2.7.2 TRIzol® Extraction of RNA from Cell Culture

RNA was isolated by TRIzol® extraction in accordance with the manufacturer's instructions. Media was aspirated and cells were rinsed with 1X PBS. Cells were scraped and harvested in 1ml of 1X PBS. Samples were collected in 1.5ml RNase/DNase-free tubes and centrifuged at 10,000 x rcf for 5min at 4ºC. PBS was aspirated and the cell pellet was sonicated for at 20kHz, 30% amplitude (QSonica Sonicators) in 500ul TRIzol® reagent for 10s. An additional 500ul of TRIzol® and 200ul chloroform (Sigma-Aldrich) were added. Samples were repeatedly inverted by hand for 15s before incubation at room temperature for 3min. Samples were centrifuged at 12,000 x rcf for 15min at 4ºC to separate the phases: the upper, colorless aqueous phase was transferred to a fresh RNase/DNase-free tube, while the lower phenol-red organic and interphases were discarded. Ice-cold 100% isopropanol (500ul; Sigma-Aldrich) was added to the aqueous phase and the tubes were repeatedly inverted by hand for 15s before incubation at room temperature for 10 minutes. Samples were centrifuged at 12,000 x rcf for 10 minutes at 4ºC to pellet the RNA (faint white to semi-translucent). Once the supernatant was carefully discarded, the RNA pellet was rinsed and vortexed in 1ml ice-cold 75% ethanol (Commercial Alcohols) prepared in UltraPure™ RNase/DNase-free ddH_2O (Invitrogen). Samples were centrifuged at 7500 x rcf for 5 minutes at 4ºC. The ethanol wash was discarded and the RNA pellet was briefly air-dried for 5min by inverting the tubes onto a

clean surface. The pellet was suspended in 25ul RNase/DNase-free H_2O, vortexed and briefly spun down.

RNA was examined for degradation using the automated QIAxcel Advanced microcapillary electrophoresis system (Qiagen) in accordance with the manufacturer's guidelines. Briefly, 1ul of QRNA Ladder (Qiagen) and 1ul of Denaturing Buffer (Qiagen) were added to the first strip tube in a series of 12. In subsequent tubes, 4ul Denaturing Buffer was added to 4ul sample RNA. To avoid equipment damage, all tubes were topped to a total volume of 10ul with Dilution Buffer (Qiagen) before running. RNA migration was internally normalized to a Qiagen Intensity Marker. Total RNA, as well as the 260:280nm ratio, were quantified using the Take3 microplate spectrophotometer (Biotek) and Synergy H4 Hybrid Reader. Reverse transcriptase reactions were conducted prior to RNA storage at -80ºC.

2.7.3 Complementary DNA (cDNA) Synthesis

A 20ul cDNA reaction mix was prepared by loading the volume equivalency of 1µg RNA template and 4ul 5X qScript™ cDNA SuperMix (Quanta Biosciences) into RNase/DNase-free strip-tubes and topping the remaining volume to 20ul with UltraPure™ ddH_2O. The reaction mix was briefly vortexed and centrifuged prior to incubation at 25ºC for 5 minutes, 42ºC for 30 minutes, 85ºC for 5 minutes and then held at 4ºC using a Mastercycler Nexus Gradient Thermocycler (Eppendorf). cDNA was stored at -20ºC.

2.7.4 Applied Biosystems® SYBRGreen qPCR

Primer-pairs (Invitrogen, Table 2) were designed using OLIGO Primer Analysis Software V6.31 (Molecular Biology Insights, Inc.) and incorporated all transcript variants identified in NCBI's GenBank RefSeq database. To design primers specific to a single species (ex. human or rat-specific HIF2α), human and rat mRNA sequences were first aligned using Clustal Omega (V1.2.2). Aligning segments were deleted and primers were designed using the remaining base pair fragments. Predicted primer products were cross-referenced with NCBI's Basic Local Alignment Search Tool (BLAST) to ensure target gene sequence specificity. Primer-pairs were investigated for dimerization using the automated QIAxcel Advanced microcapillary electrophoresis system. For each primer pair under investigation, a reaction mix was prepared by addition of 5ul pooled cDNA,

Table 2. Primer Sequences and Annealing Temperatures of Oligonucleotides used in qPCR

Target		Primer sequence (5'-3')	Annealing temperature (ºC)
MsActB	F1	TGTGATGGTGGGAATGGGTCAGA	51
	R1	TGTGGTGCCAGATCTTCTCCATGT	
MsAlas1	F1	CATACCCACATAGTAGCCAGAAT	57
	R1	GTCAACAGCAGAAACACCTAAC	
MsAlas2	F1	ACATCATCTCTGGAACTCTTGG	57
	R1	GGTCAGGTTCTGCTTTGTCT	
MsBach1	F1	CCAGAACCTTGAGTCGGAAAT	57
	R1	GGTCAGGTTCTGCTTTGTCT	
MsHMOX1	F1	CTCTCTTCTCTTGGGCCTCTAA	58
	R1	TGTCAGGTATCTCCCTCCATTC	
MsHMOX2	F1	GGGACCCAATTCTACCTGTTT	58
	R1	CTCCTCCACAATCCTCTCTTTG	
MsHPRT1	F1	GGCCTCCCATCTCCTTCATG	60
	R1	CAGTCCCAGCGTCGTGATTA	
MsHIF1α	F1	CCCATTCCTCATCCGTCAAATA	57
	R1	GGCTCATAACCCATCAACTCA	
HuHIF2α	F1	ATG CGC TAG ACT CCG AGA A	60
	R1	TGC AGG TTG CGA GGG TTG TAG A	
RtHIF2α	F1	AGT TGG AAA GCC GGA AGA	60
	R1	CGT AGG GCC TAA ATG TAA TGG T	
MsRpl32	F1	CACCAGTCAGACCGATATGTGAAAA	61
	R1	TGTTGTCAATGCCTCTGGGTTT	

ActB, β-actin; ALAS, aminolevulinic acid synthase; F1, forward primer; HIF, hypoxia inducible factor; HMOX, heme oxygenase; Hu, human; Ms, mouse; R1, reverse primer; Rpl32, ribosomal protein L32; Rt, rat.

37.5ul AccuStart II GelTrack PCR SuperMix (2X; Quanta Biosciences™), 0.375ul 100uM forward primer, 0.375ul 100uM reverse primer, and 31.75ul nuclease-free water to a 0.5ml tube. The reaction mix was briefly vortexed and centrifuged prior to incubation at 94ºC for 1min, 10 cycles of incubation at 94ºC for 30s, 65ºC for 30s and 72ºC for 40s, 25 cycles of incubation at 94ºC for 30s, 55ºC for 30s and 72ºC for 40s, incubation at 72ºC for 4min and then held at 4ºC. PCR product was column purified by MinElute PCR Purification Kit (Qiagen) to remove nucleotide fragments and primers prior to quantification by QIAxcel (DNA High Resolution) microcapillary electrophoresis in accordance with the manufacturer's guidelines. Only one band was observed. Total copy number (molecules) was calculated using the quantified amplicon amount (ng) and dsDNA amplicon length (base pairs):

$$\frac{\mathrm{X\,ng} * 6.0221 \times 10^{23}\mathrm{molecules/mole}}{\left(\mathrm{N} * \frac{660\mathrm{g}}{\mathrm{mole}}\right) * 1 \times 10^{9}\mathrm{ng/g}}$$

where X was equal to the total amount of amplicon (ng) and N was equal to the length of dsDNA (base pairs). The average mass of 1 base pair of dsDNA was expressed as 660g/mole. To form an 8-point standard curve, PCR product was serially diluted in RNase, DNase-free ddH_2O from $1x10^8$ to $1x10^2$ copies/ul. A no-template control (NTC) consisting of nuclease-free water served as the 8th point. Sample cDNA (10ul) was diluted to 1 in 3 in RNase/DNase-free water.

Diluted cDNA and standard curves (2ul) were added to a 96-well qPCR plate in duplicate. qPCR mastermix was prepared by combining 5ul PerfeCTa SYBR Green FastMix Low ROX (2X), 1ul forward primer (100uM), 1ul reverse primer, and 1ul nuclease-free water. The mastermix was gently vortexed and 8ul was added to each well containing either standard curve, NTC or sample cDNA. The qPCR plate was sealed and briefly centrifuged. The reaction mix was incubated at 95ºC for 20s, 35 cycles of incubation at 95ºC for 1s and 60ºC for 20s, and 20ºC for 5min (ViiA7 96-well fast block; Applied Biosystems). Relative mRNA levels were normalized to MsHPRT1 expression and expressed as ΔΔCT.

2.8 Immunoblotting

2.8.1 Cell Collection and Lysate Preparation

Cells were harvested on ice by aspirating the media, gently rinsing cells with 1X PBS and scraping the cells in freshly prepared lysis buffer (60-120ul/35mm plate) containing sodium orthovanadate and protease and phosphatase inhibitor cocktails as previously described. Harvest of hypoxic cells was performed with plates on ice in less than 60 seconds to minimize re-oxygenation effects. Cell lysates were transferred to fresh 1.5ml tubes and were left on ice for 30 minutes before sonicating the samples on ice for 10 seconds at 20kHz, 30% amplitude using the QSonicator. Total protein concentrations were quantified by BCA. Protein samples (8-25µg) were boiled at 99ºC for 5min in 4X Laemmli Buffer with dithiothreitol (DTT).

2.8.2 Western Blotting

Boiled samples (8-25µg) were separated (3.5% stacking gel) and resolved via 10% Mini-Protean sodium dodecyl sulfate-polyacrylamide gel electrophoresis (SDS-PAGE) or by 4-20% Criterion™ TGX™ PreCast Gels (BioRad). Samples were loaded alongside 10ul Precision Plus Protein™ Standards Kaleidoscope™ ladder (BioRad) and were run at constant voltage until the dye front migrated to the bottom edge of the gel (approximately 2 hours). Mini-Protean self-cast gels were run at 90V at room temperature in 1X Tris/Glycine/SDS Electrophoresis Buffer (BioRad); Criterion™ gels were run at 90V for 30 minutes and 120V on ice. Samples were wet-transferred to nitrocellulose (0.2um; BioRad) at 100V for 1 hour 30 minutes at 4ºC. Membranes were briefly rinsed in ddH2O and equal protein transfer was confirmed by incubating the membranes in Pierce® Reversible Memcode Stain for 5 min. The stained blot was labeled and imaged using a ChemiDoc™ MP Imaging System before removing the stain using Pierce® Stain Eraser. Membranes were then blocked in 5% skim-milk in 1X Tris-Buffered-Saline-Tween 20 (TBS-T) for 45 minutes. Membranes were subsequently incubated at 4ºC overnight in primary antibody (1% skim-milk in TBS-T with sodium azide) targeting ALAS1 (1:1000, #VMA00203KT, BioRad), ALAS2 (1:1000, #sc-166-139, Santa Cruz), HIF1α (1:400, #AF1935, R&D Systems), HIF2α (1:1000, #VMA00083Kt, BioRad), HMOX1 (1:2000, #ab82585, Abcam), or Myogenin (1:1000, #14688, ProteinTech). Blots were then incubated with secondary horseradish peroxidase

(HRP)-conjugated anti-goat (1:1000, #sc-2056, Santa Cruz), HRP-conjugated anti-mouse (1:2000, #sc-2055, Santa Cruz), or HRP-conjugated anti-rabbit (1:2000-5000, #sc-2054, Santa Cruz) IgG for 2h in 5% milk at room temperature. Immunoreactivity was detected using Clarity™ Western Enhanced Chemiluminescence Substrate (BioRad) or SuperSignal® West Dura Extended Duration Substrate with a ChemiDoc™ MP Imaging System. Membranes were then stripped by incubation in 25ml 0.5M Tris-HCl/SDS buffer supplemented with 125ul β-mercaptoethanol (OmniPur®) for 1 hour and reprobed.

2.8.3 Densitometry

Densitometric measurements were completed using ImageLab™ Software v5.0 (BioRad). Relative integrated density was calculated as the density of the target protein normalized to the total protein density of the respective memcode-stained lane. As such, quantitative results were only statistically analyzed from a single membrane blot with multiple N-values or biological replicates. Otherwise, blot-to-blot analysis was performed qualitatively as a fold change relative to a common control (as stated). [Note: variation in Western blot conditions and development, as well as statistical validity in twice-normalized samples precludes statistical analysis across blots. Membrane blots that best represented the degree of change from multiple independent trials were used as representative blots (i.e. 2-trials, the blot with the least degree of change was shown; 3-trials, the blot most approximating the mean degree of change was shown. Rearrangement of bands within an individual blot was denoted by a vertical dashed line.

2.9 Heme Content Assay

Heme content in tissue and cell lysates was quantified by Heme Colorimetric Assay (BioVision). Lysates were diluted, so as to fall within the linear portion of the hemin standard curve (> 40fmol and < 200fmol). Tissue lysates were diluted between 1 in 100 (TAC) and 1 in 3500 in ddH_2O (AMI, peri-infarct). Cell lysate was diluted 1 in 800 in ddH_2O. Samples (10ul) were directly added to the wells of a clear-bottomed 96-well plate (in triplicate) and were topped with 40ul assay buffer. The hemin standard was dissolved in 100ul DMSO (10uM) immediately before use. The 10uM standard was subsequently diluted to 100nM by transfer of 10ul hemin standard to 990ul Assay Buffer, and further diluted by addition of 100ul of 100nM standard into 900ul assay buffer (10nM). In triplicate, 20, 16, 12, 8, 4, and 0ul of the 10nM hemin standard was added to

their corresponding wells and were topped with 30, 34, 38, 42, 46, and 50ul assay buffer respectively. At that time, the hemin probe was warmed to 37ºC for 2 minutes and the enzyme mix was dissolved in 500ul assay buffer. Due to the light-sensitivity of the assay probe, subsequent steps were completed in a semi-dark room, protected from light. Immediately before use, a reaction mix (50ul/sample) was prepared by addition of reagents in the following order: enzyme mix (3ul), hemin substrate (2ul), assay buffer (43ul), and hemin probe (2ul). The reaction mix was quickly added to both standard and sample wells while taking care to avoid bubble formation within the well. The 96-well assay was immediately placed in a Synergy H4 Hybrid Reader at room temperature and the optical density (OD)/Absorbance at 570nm was read in Kinetic Mode at 2 minute intervals for 2 hours. Heme content per ug protein was extrapolated from the standard curve OD and sample data were plotted as fmol heme/µg protein or fmol heme/ng protein.

2.10 Statistical Analyses

Results are expressed as mean ± standard deviation (SD) unless otherwise stated. Statistical significance between treatments was determined in GraphPad Prism 6 (GraphPad Software Inc.) using Student's two-tailed t-Test (comparisons involving two groups) or One-way analysis of variance (ANOVA) followed by Tukey's multiple comparison test (P-value <0.05 was considered significant). In the event of high variability, as determined by Brown-Forsythe test, a Kruskal-Wallis test was performed. Sample populations were considered significantly different if both Kruskal-Wallis and Tukey's multiple comparison tests demonstrated P-values <0.05.

In silico and *in vivo* analyses, N-values were representative of individual patients or animals. *In vitro*, an independent trial was defined as the replication of an experiment on a separate occasion/date. A biological replicate was defined as cell culture wells or plates placed under identical experimental conditions for an independent trial (i.e. different day replicates). A technical replicate was defined as a cell culture wells or plates under identical experimental conditions within an independent trial (i.e. same-day replicate).

CHAPTER 3
Results

3.1 Heme Metabolism and Hypoxia Gene Expression in Human Failing Hearts

To independently confirm whether patients in heart failure differentially express rate-limiting enzymes for heme metabolism (ALAS/HMOX) and/or the two major isoform proteins regulating gene expression in hypoxia (HIF1α/HIF2α), we analyzed open-access microarray data-sets from the Entrez Gene Expression Omnibus (GEO) (http://www.ncbi.nlm.nih.gov/geoprofiles/). First, we searched for studies in GEO related to human heart failure using mesh terms [10]. Five potential data-profiles were discovered. Two data-profiles were sufficiently diverse and complete for a comparison of the genes of interest; yet, data for either ALAS2 or HMOX2 were not reported in the microarray analysis data sets analyzed. The first data-set pertained to idiopathic heart failure (GSE1145) and the second to dilated heart failure (GSE3586, [97]). ALAS1 gene expression was elevated in both idiopathic and dilated heart failure (Figure 3.1-A, E, respectively) in the subjects under study. Relative HMOX1 expression in heart failure subjects did not vary significantly from control subjects in either data set (Figure 3.1-B, F). HIF1α expression compared to control samples was significantly lower in idiopathic heart failure (Figure 3.1-C), but did not vary significantly from controls in dilated heart failure (Figure 3.1-G). HIF2α expression did not vary significantly from controls in either idiopathic or dilated heart failure (Figure 3.1-D, H). These data indicate that at end-stage heart failure (where hearts are explanted for transplantation) gene expression of heme synthesizing enzyme, ALAS1, is significantly increased, but that hypoxia sensitive transcription factor HIF1α is decreased in heart failure in subjects from a study of idiopathic heart failure, but not dilated heart failure.

3.2 Heme Metabolism and Hypoxia Gene Expression in Preclinical Models of Heart Failure

AMI and TAC are two widely used preclinical models used to investigate heart failure. Here we sought to determine whether the rate-limiting heme regulatory enzymes or hypoxia sensitive transcription factors would be altered throughout the progression of

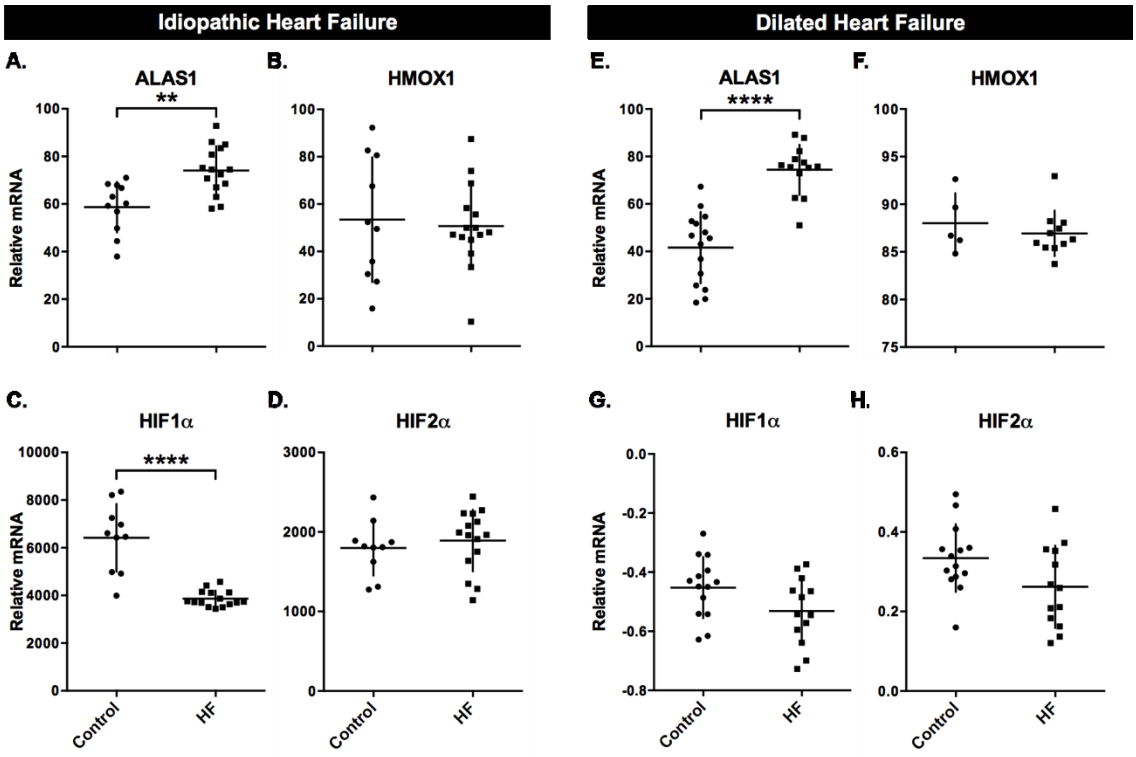

Figure 3.1. Microarray Analysis of Rate-Limiting Heme Metabolism Enzymes and Hypoxia Inducible Factors in Human Idiopathic and Dilated Heart Failure. mRNA (log_2-transformed) was analyzed in heart failure (HF) patients using public microarray datasets. **(A-D)** Left ventricular biopsies were obtained from patients with idiopathic heart failure at the time of explant (N=15); control biopsies were obtained from non-failing donor hearts (N=10). **(E-H)** Cardiac septal wall and left ventricle apex (HMOX1) biopsies were obtained from dilated cardiomyopathy heart failure patients (N=11-15) and control biopsies (N=5-13). ALAS1 was higher in **(A)** idiopathic and **(E)** dilated cardiomyopathy heart failure. **(B, F)** HMOX1 did not vary significantly with heart failure. **(C)** HIF1α was lower in idiopathic heart failure. **(D)** HIF2α did not vary significantly in idiopathic heart failure. Neither **(G)** HIF1α nor **(H)** HIF2α varied significantly in dilated heart failure. (**, $P \leq 0.01$; ****, $P \leq 0.0001$).

heart failure. Traditionally, the actin gene has been used to internally normalize gene expression in the heart, however, actin gene levels varied wildly throughout AMI and TAC progression (data not shown). The degree of cytoskeletal remodeling involved in both models necessitated the use of an alternate housekeeping gene to normalize gene expression samples; thus, gene expression was normalized to ribosomal subunit protein L32 (Rpl32). Real-time quantitative PCR analyses was conducted during the compensatory phase after onset of AMI or TAC at 2-weeks and the decompensatory phase at 18-weeks (as determined by cardiac functional analysis). Quantitative PCR showed no significant difference in cardiac expression of ALAS1 or ALAS2 2 weeks after AMI in mice, relative to sham (Figure 3.2-A, B). In 18week post-AMI mice, both ALAS1 and ALAS2 cardiac gene expression was significantly lower compared to sham animals (Figure 3.2-A, B). However, ALAS1 was lower, whereas ALAS2 was significantly higher in 2 week TAC (Figure 3.2-G, H). Cardiac HMOX1 expression was higher in both 2 and 18 week AMI and TAC mice (Figure 3.2-C, I). HMOX2 expression did not vary significantly in either AMI or TAC hearts (Figure 3.2-D, J). HIF1α expression was not different at 2weeks but was significantly higher in 18 week AMI hearts compared to sham (Figure 3.2-E,). HIF1α was significantly higher in 18 week TAC, relative to both sham and 2 week TAC (Figure 3.2-K). HIF2α expression did not vary significantly with AMI at either 2 or 18 weeks (Figure 3.2-F) but was significantly lower in 2 week TAC (Figure 3.2-L).

We do not find exact alignment between clinical subjects and pre-clinical models of heart failure of gene expression profiles of heme regulating enzymes or hypoxia sensing transcription factors. However, both human and murine data clearly demonstrated altered gene expression in heme synthesizing ALAS enzymes. In AMI, both ALAS1 and ALAS2 expression is reduced by up to 50%, which is similar to 2 week TAC for ALAS1, but not ALAS2 (increased by up to 50%) and, in human subjects, ALAS1 was as much as 2-fold elevated. HIF1α was lower in human subjects and elevated in late stage murine models of heart failure. Consistent with HMOX2 being a low level constitutive enzyme, no changes were discovered. Likewise, consistent with HMOX1 being induced during stress, we found significantly increased expression in both AMI and TAC during both the compensatory and decompensatory phase of the murine models of heart failure – yet no

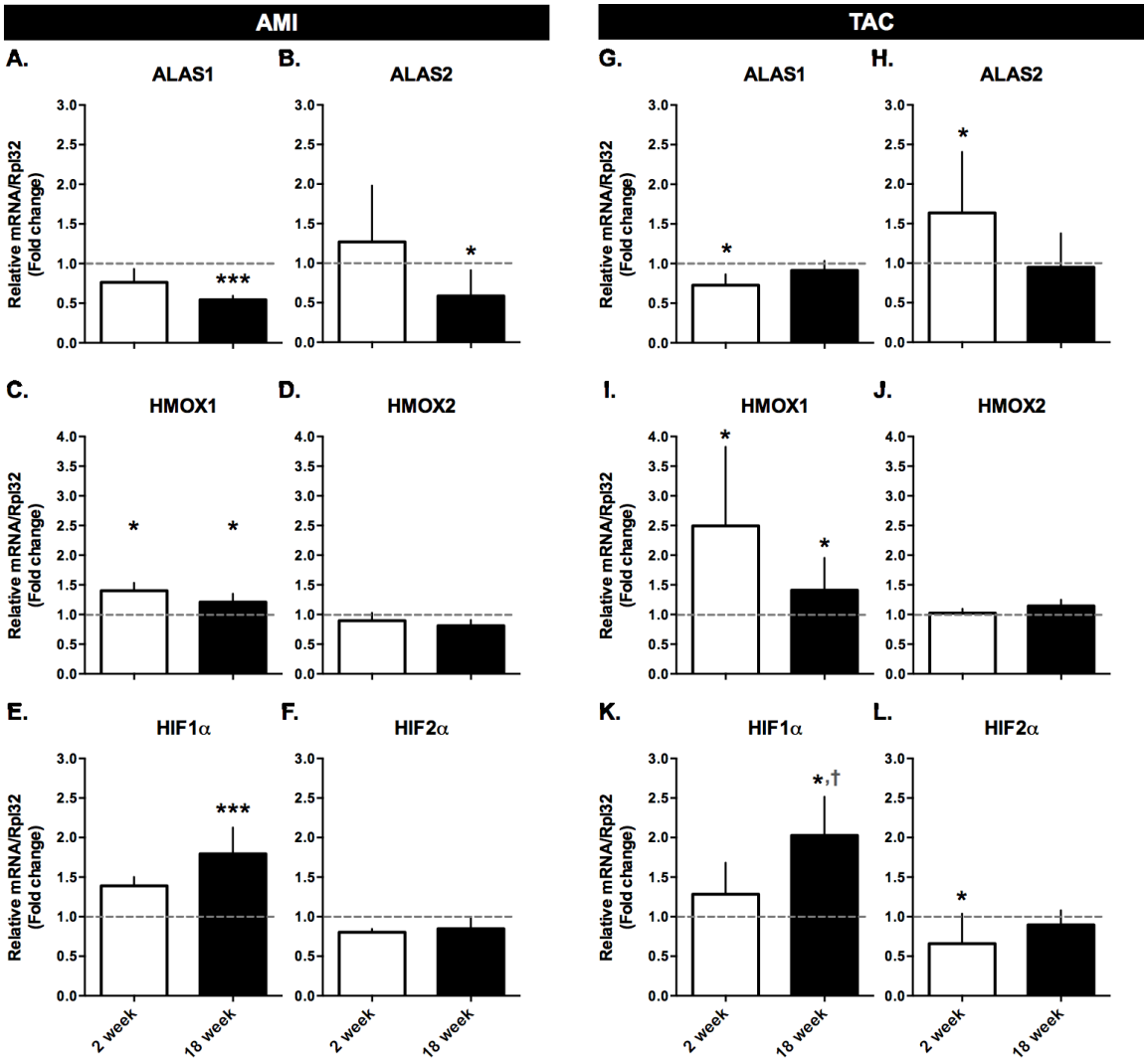

Figure 3.2. Gene Expression of Rate-Limiting Heme Metabolism Enzymes and Hypoxia Inducible Factors in Pre-Clinical Models of Heart Failure. Hearts were harvested from C57B1 mice following 2 and 18 week AMI (**A-F**; N=3-4) and TAC (**E-L**; N=4-5). Gene expression was internally normalized to Rpl32 and relative to sham (N=4-5). **(A-B)** ALAS1 and ALAS2 were lower in 18 week AMI. **(G)** ALAS1 was lower in 2 week TAC. **(H)** ALAS2 was significantly higher in 2 week TAC**. (C)** HMOX1 was significantly higher with AMI. **(B)** HMOX2 did not vary significantly in AMI. **(I)** HMOX1 was significantly higher with TAC. **(E)** HIF1α was higher in 18 week AMI. **(F)** HIF2α did not vary significantly with AMI. **(K)** HIF1α was higher in 18 week TAC relative to both sham and 2 week TAC. **(L)** HIF2α was lower in 2 week TAC. (*, P≤0.05; ***, P≤0.001; * Indicates significance vs. sham, † indicates significance between 2 and 18 week groups).

difference was observed in HMOX1 in human heart failure subjects. Interestingly, human subjects showed either a decline or no change in HIF1α, whereas in the murine models HIF1α was significantly higher in the decompensatory phase of both AMI and TAC. These results could be due to fundamental differences in heart failure stages, regional cardiac anatomical sampling differences or speciation. However, gene expression *per se* does not determine the degree of protein expression, nor the degree of heme bioavailability (i.e. nominal, deplete, replete or toxic) and these remained to be explored.

3.3 Heme Metabolism and Hypoxia Protein Expression in Preclinical Models of Heart Failure

3.3.1 Heme Metabolism and Hypoxia Protein Expression in the Infarcted Left Ventricle

In order to distinguish between changes in heme metabolism regulating enzymes in the surviving myocardium compared to the more fibrotic scar, heme regulatory enzyme expression was investigated in the infarcted left ventricle and the peri-infarct region of AMI mice by western blotting. In the isolated infarct, ALAS1 was significantly decreased at 1-week post-AMI (Figure 3.3-A, and blot quantified, D), while ALAS2 did not vary significantly from sham (Figure 3.3-B, and blot quantified, E). HMOX1 levels were gradually increased from sham to 1-week post-MI; HMOX1 returned to baseline by 2 weeks post MI (Figure 3.3-C, and blot quantified, E). It is noteworthy to appreciate the changes in protein profiles by whole membrane staining, likely indicative of the reduced myofiber and increased fibrotic proteins (Figure 3.3-G), however whole lane quantification of membranes did not show any significant bias to lane normalization.

3.3.2 Heme Metabolism and Hypoxia Protein Expression in the Peri-Infarct Tissue

In the peri-infarct tissue, ALAS1 was significantly decreased in 2 and 4 week AMI (Figure 3.4-A, and blot quantified, D). ALAS2 was gradually and significantly increased by 2 and 4 week AMI in the peri-infarct tissue (Figure 3.4-B, and blot quantified, E). In contrast to the isolated infarct, HMOX1 levels were significantly increased by 3 days post-MI, but returned to baseline by 1-week post-MI (Figure 3.4-C, and blot quantified, F). These data show that region selection (infarct zone and peri-infarct zone), for AMI tissues, influence the altered state of heme regulatory enzyme expression. HMOX1 was significantly elevated by 3-days post-AMI and sustained

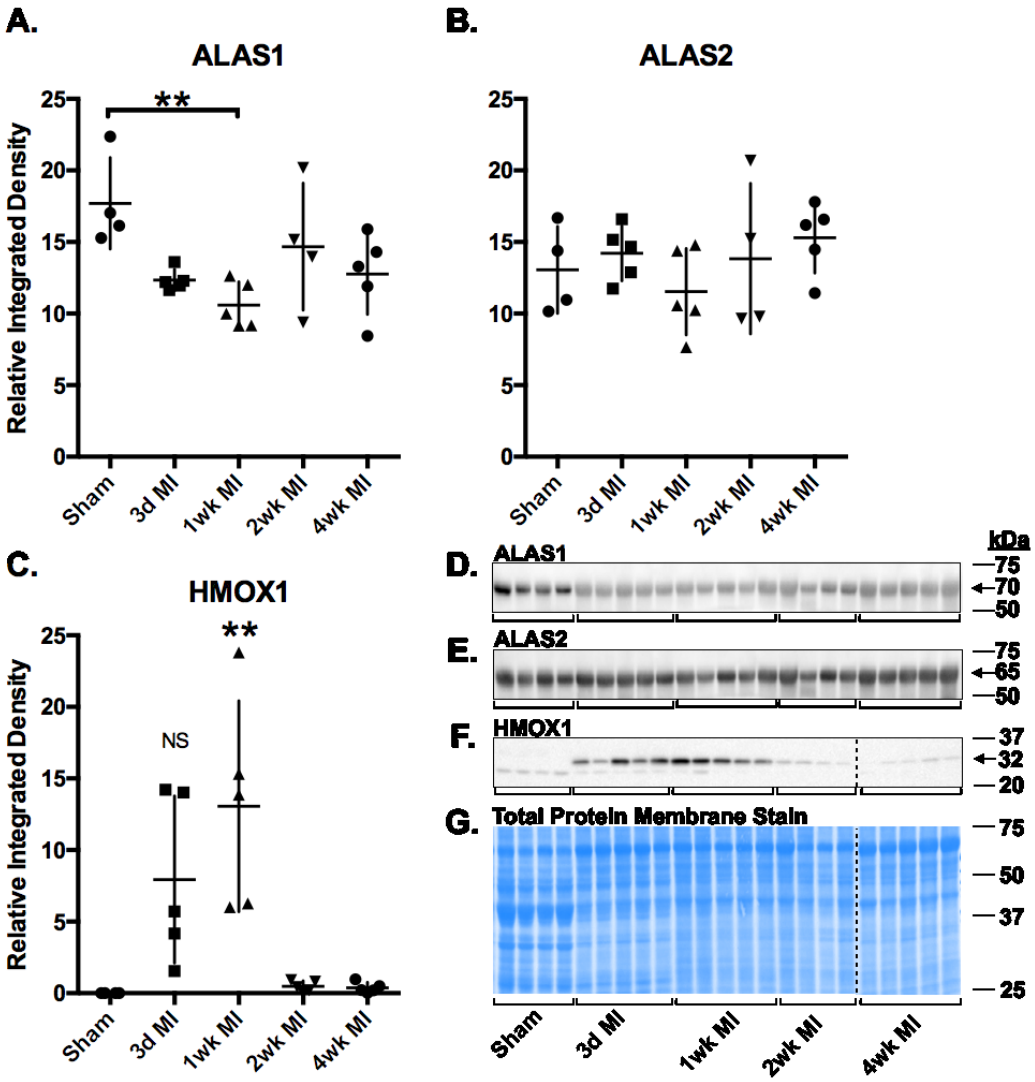

Figure 3.3. Infarcted Left Ventricle Expression of Rate-Limiting Heme Metabolism Proteins Over Time. Infarcts were obtained from C57B1 mouse hearts 3 days (N=4), 1 week (N=5), 2 weeks (N=4), and 4 weeks (N=5) post AMI surgery; control hearts were obtained from mice post sham surgery (N=4). **(A)** ALAS1 was significantly decreased at 1 week post-myocardial infarct (MI). **(B)** ALAS2 did not vary significantly with MI. **C)** HMOX1 was significantly increased at 1 week post MI. **(D)** Representative ALAS1-probed membrane displayed specific prominent ALAS1-bands at 70 kDa. **(E)** Representative ALAS2-probed membrane displayed specific prominent ALAS2-bands at 65 kDa. **(F)** Representative HMOX1-probed membrane displayed specific prominent HMOX1-bands at 32 kDa. **(G)** Pierce® Memcode staining demonstrated uniform protein loading on the membrane prior to antibody probe. (ns, $P>0.05$; *, $P\leq0.05$; **, $P\leq0.01$).

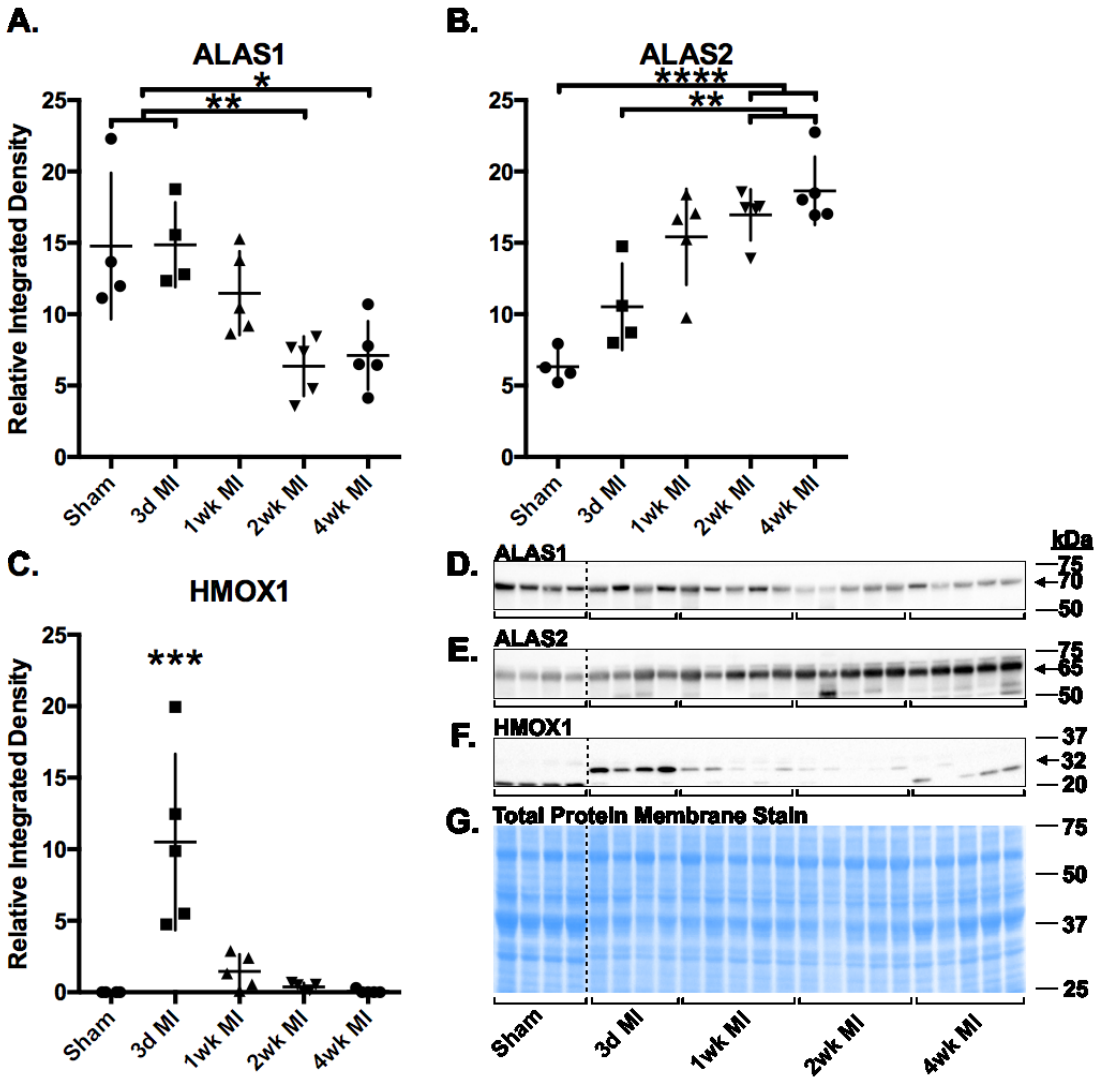

Figure 3.4. Peri-Infarct Left Ventricle Expression of Rate-Limiting Heme Metabolism Proteins Over Time. The peri-infarct regions of the myocardium were obtained from C57B1 mouse hearts 3 days (N=4), 1 week (N=5), 2 weeks (N=5), and 4 weeks (N=5) post AMI surgery; control hearts were obtained from mice post sham surgery (N=4). **(A)** ALAS1 was significantly decreased at 2 and 4 weeks post MI relative to sham and 3 days post MI. **(B)** ALAS2 was significantly increased at 2 and 4 weeks post MI relative to sham and 3 days post MI. **(C)** HMOX1 was significantly increased at 3 days post MI, however expression was returned to sham-like levels from 1 to 2 weeks post MI. **(D)** Representative ALAS1-probed membrane displayed specific prominent ALAS1-bands at 70 kDa. **(E)** Representative ALAS2-probed membrane displayed specific prominent ALAS2-bands at 65 kDa. **(F)** Representative HMOX1-probed membrane displayed specific prominent HMOX1-bands at 32 kDa. **(G)** Pierce® Memcode staining demonstrated uniform protein loading on the membrane prior to antibody probe. (ns, $P>0.05$; *, $P\leq0.05$; **, $P\leq0.01$; ***, $P\leq0.001$; ****, $P\leq0.0001$).

expression for up to 1-week in the infarct but not peri-infarct tissues. Interestingly, the protein expression of HMOX1 in AMI is more transient, resolving by 2-weeks in contrast to our gene expression data. Likewise, the protein expression of ALAS1 and ALAS2 were in agreement with gene expression data, but demonstrably greater differences in the peri-infarct region show that ALAS1 protein expression is significantly reduced in exchange for significantly elevated ALAS2 expression. In order to determine whether this contributes to a change in heme bioavailability we next quantified heme content in the peri-infarct regions of post-AMI cardiac tissues (Figure 3.5). There was substantial variability in heme content across samples in 3-day, 1-week and 2-week AMI and no significant difference was determined. However, in comparison to sham and 4-week AMI the early peri-infarct heme content appears to be in a state of flux and in some animals was increased 3-6 fold comparatively to the tightly clustered sham levels of heme, suggesting some animals are in a heme-replete state during the early post-AMI peri-infarct myocardium (a more powered analysis may be appropriate).

3.3.3 Heme Metabolism and Hypoxia Protein Expression in TAC Hearts

In TAC hearts, ALAS1 was significantly decreased in 2, 4 and 18-week TAC (Figure 3.6-A, and blot quantified, D). ALAS2 did not vary significantly with TAC (Figure 3.6-B, and blot quantified, E). HMOX1 protein was significantly decreased in 18-week TAC (Figure 3.6-C, and blot quantified, F). In agreement with the gene expression data there was a significant reduction in ALAS1 protein by 2-weeks. However, though gene expression returned to sham levels, ALAS1 protein expression remained significantly lower than sham. A reduction in ALAS1 was observed in both AMI and TAC animals (unlike human subjects where ALAS1 gene expression was elevated). TAC hearts did not show a commensurate increase in ALAS2, as was observed in TAC gene expression and peri-infarct AMI. Likewise, TAC myocardium showed a significant reduction in HMOX1 protein expression contrary to the increased gene expression in TAC and unlike the AMI (see Table 3. for a summary report). To determine whether TAC myocardium heme bioavailability was altered, heme content analysis was performed. Interestingly, heme content was progressively and significantly higher by 18-week TAC (Figure 3.7-C). This onset of a heme-replete state is curious given that there was a reduction in the rate-limiting ALAS1 heme-synthesis enzyme. Further, this heme-

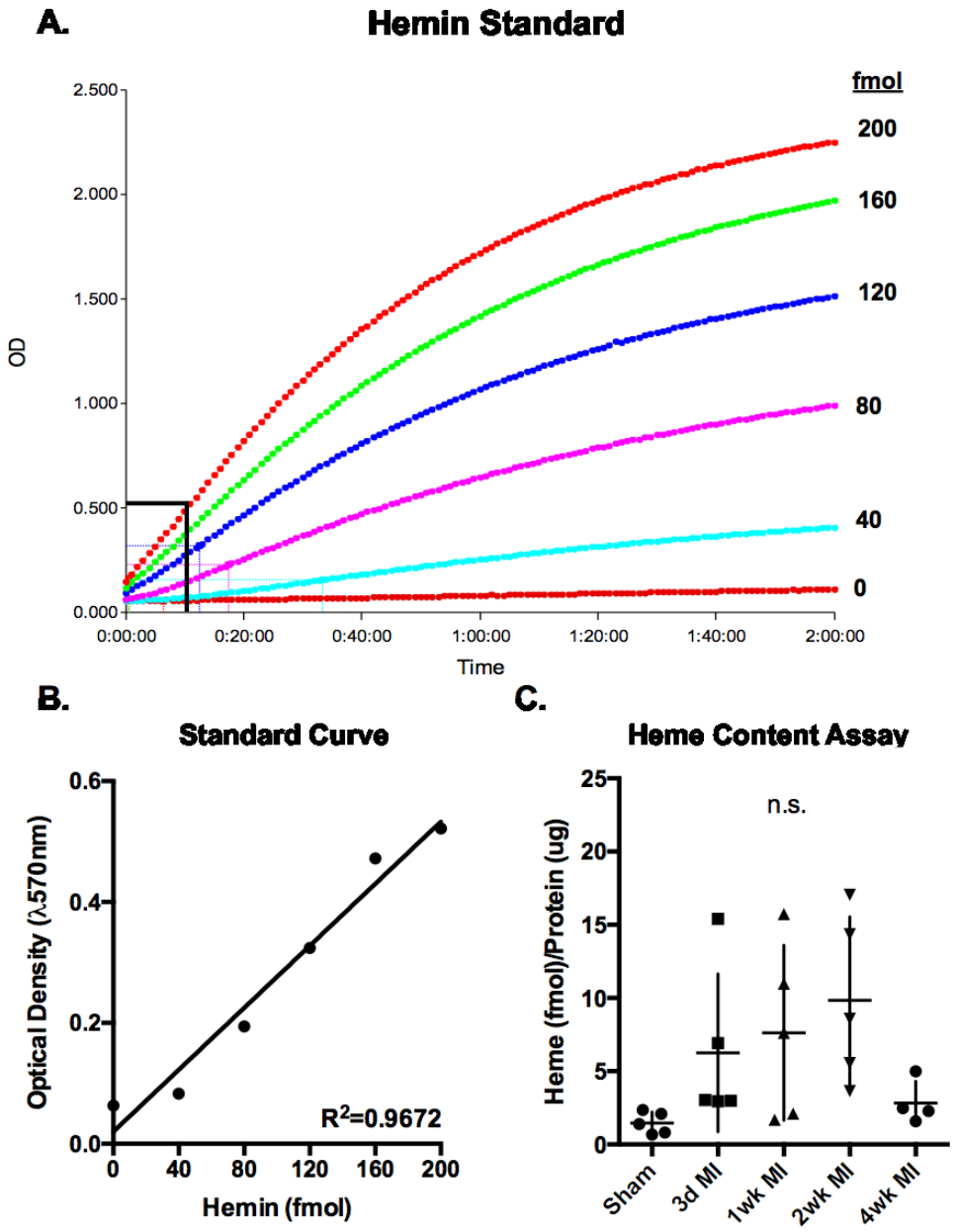

Figure 3.5 Time-Dependent Changes in Cardiac Heme Content of Peri-Infarct Left Ventricle Tissue. (A) Raw kinetic plotting of hemin-standard reaction progression. Standard curve optical densities (OD) were derived from the phase of linear growth at time = 10 minutes. **(B)** Heme content was interpolated through linear regression from a hemin standard curve (R^2=0.9672). **(C)** Cardiac heme content in the peri-infarct region at 3 days (N=5), 1 week (N=5), 2 weeks (N=5), and 4 weeks (N=4) post AMI surgery; control hearts were obtained from mice post sham surgery (N=5). Heme content did not vary significantly in AMI (ns, P>0.05).

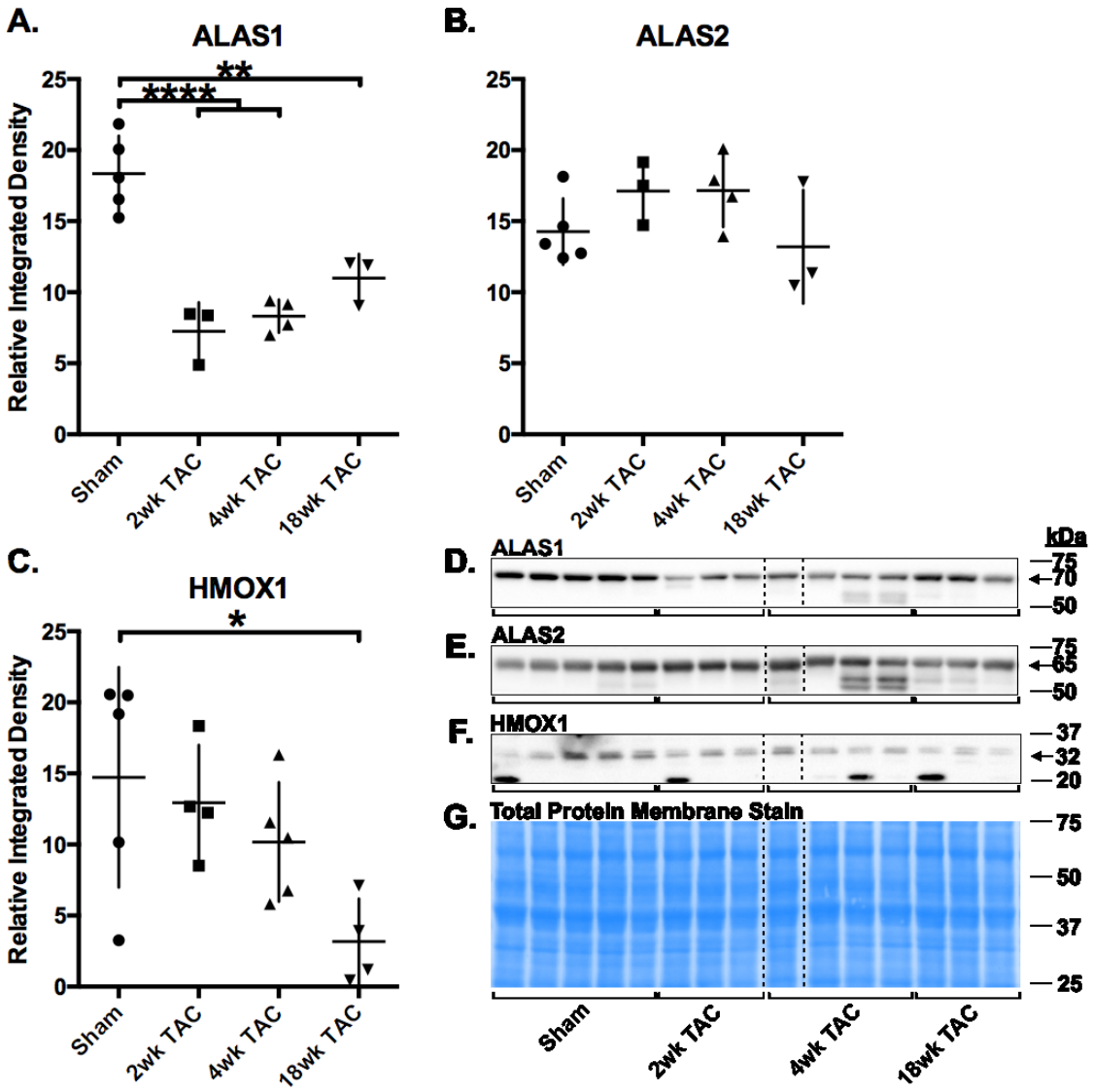

Figure 3.6. Time-Dependent Changes in Cardiac Heme Regulatory Enzyme Protein Expression after TAC. Hearts were obtained from C57B1 mice 2 weeks (N=3-4), 4 weeks (N=4-5), and 18 weeks (N=3-4) post TAC; control hearts were obtained from mice post sham surgery (N=5). **(A)** ALAS1 was significantly decreased with TAC. **(B)** ALAS2 did not differ significantly with TAC. **(C)** HMOX1 was significantly decreased at 18 week TAC. **(D)** Representative ALAS1-probed membrane displayed specific prominent ALAS1-bands at 70 kDa. **(E)** Representative ALAS2-probed membrane displayed specific prominent ALAS2-bands at 65 kDa. **(F)** Representative HMOX1-probed membrane displayed specific prominent HMOX1-bands at 32 kDa. **(G)** Pierce® Memcode staining demonstrated uniform protein loading on the membrane prior to antibody probe. (*, P≤0.05; **, P≤0.01; ****, P≤0.0001).

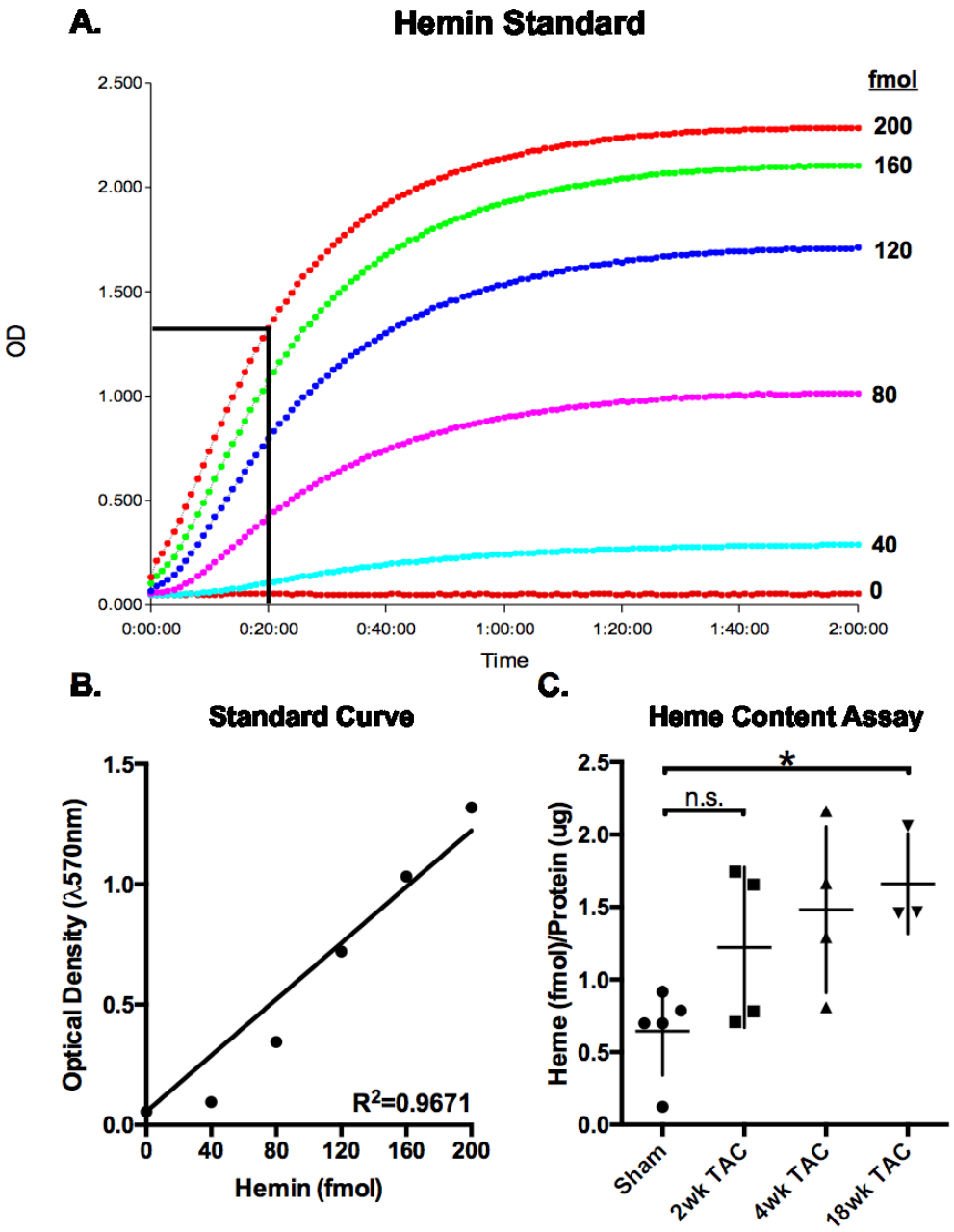

Figure 3.7. Time-Dependent Changes in Cardiac Heme Content after TAC. (A) Raw kinetic plotting of hemin standard reaction progression. Standard curve optical densities (OD) were derived from the phase of linear growth at time = 20 minutes. **(B)** Heme content was interpolated through linear regression from a hemin standard curve (R^2=0.9671). **(C)** Heme content in the mouse myocardium at 2 weeks (N=5), 4 weeks (N=4), and 18 weeks (N=3) post TAC surgery; control hearts were obtained from mice post sham surgery (N=5). Heme content was significantly higher in the mouse myocardium following 4 and 18 week TAC. (ns, P>0.05; *, P≤0.05).

replete state was evident without enacting an increase in the heme-inducible HMOX1 catalytic enzyme. The mechanisms that would regulate these changes remain to be defined, but could be related to the degree of tissue hypoxia and/or oxidative stress caused by the model of heart failure.

We next sought to identify protein changes in HIF1α and HIF2α, but these were not readily detectable in mouse myocardium (Figure 3.8-B,D) by Western Blot. To ensure that the antibodies used were valid as commercially indicated, we conducted an immuno-validation study. Only two primary Anti-HIF1α and Anti-HIF2α antibodies were capable of detecting the respective antigen by western blot *in vivo* and *in vitro*. The R&D Systems #AF1935 (Figure 3.8-A) Anti-HIF1α detected faint bands in mouse and rat myocardium in the range of molecular weight for HIF1α and exactly at the predicted molecular weight for human HIF1α during hypoxia in rat H9C2 cells expressing a human HIF1α transgene (Figure 3.8-B). However, a HIF2α primary antibody from BioRad #VMA00083KT (Figure-3.8C) was only capable of detecting the respective human antigen by western blot *in vitro* (HEPG2 hepatocarcinoma cells) as confirmed by exposure to 1% O_2 for 24h alone and with overexpression of a human HIF2α transgene (Figure 3.8-D). We defined a valid western blot antibody as being: commercially designed to react (or predicted to react) with human, mouse and rat antigen; at or near the predicted molecular weight of the full-length protein; confirmed to demonstrate both a physiological response to hypoxia and gain or loss of antigenicity by genetic manipulation (such as, by over-expressing a transgene or knocking down the protein of interest using shRNA). Numerous commercial HIF1α antibodies failed to meet these minimal validity standards (Figure 3.9-A), many of which produced extensive non-specificity or detection of what might be degraded antigen. There are few commercial HIF2α antibodies available and we were limited only to human antigenicity (Figure 3.9-B). Molecular validation of HIF1α and HIF2α was thus limited by western blotting and may require *de novo* antibody generation or other methodological approaches, such as nuclear isolation, non-denaturing conditions, immunocytochemistry or immunohistochemistry approaches. Given the challenge of evaluating the molecular mechanisms of heme regulating enzymes by hypoxia inducible factors in vivo, a more

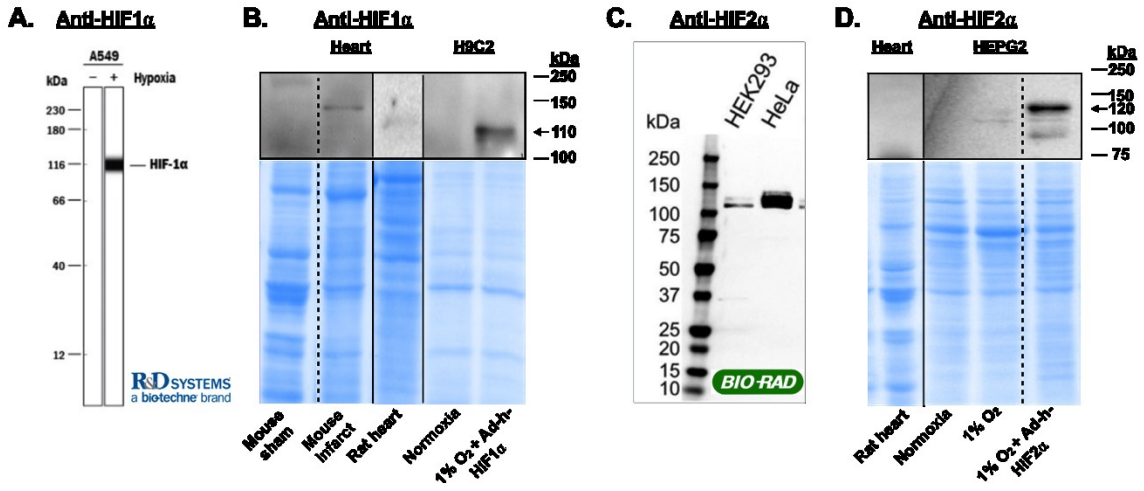

Figure 3.8 Detection of HIF1α and HIF2α by Western Blot. (A) Commercial product datasheet of polyclonal Goat Anti-Human/Mouse/Rat HIF1α primary antibody (Cat#AF1935; R&D Systems) demonstrated physiological induction of HIF1α in A549 human lung carcinoma cells exposed to 1% O_2 for an unspecified amount of time. **(B)** HIF1α was detected in H9C2 myotubules overexpressing HIF1α in 1% O_2 for 24h, but was undetectable in mouse or rat heart by Western blot of whole tissue lysates. **(C)** Commercial product datasheet of monoclonal Mouse Anti-Human/Mouse/Rat HIF2α primary antibody (Cat#VMA00083KT). **(D)** HIF2α induction was faintly detected in HEPG2 hepatocarcinoma cells following 24h at 1% O_2, and detected readily in HEPG2 overexpressing HIF2α at 1% O_2 for 24h. HIF2α was undetectable in rat whole heart by Western blot of whole tissue lysates.

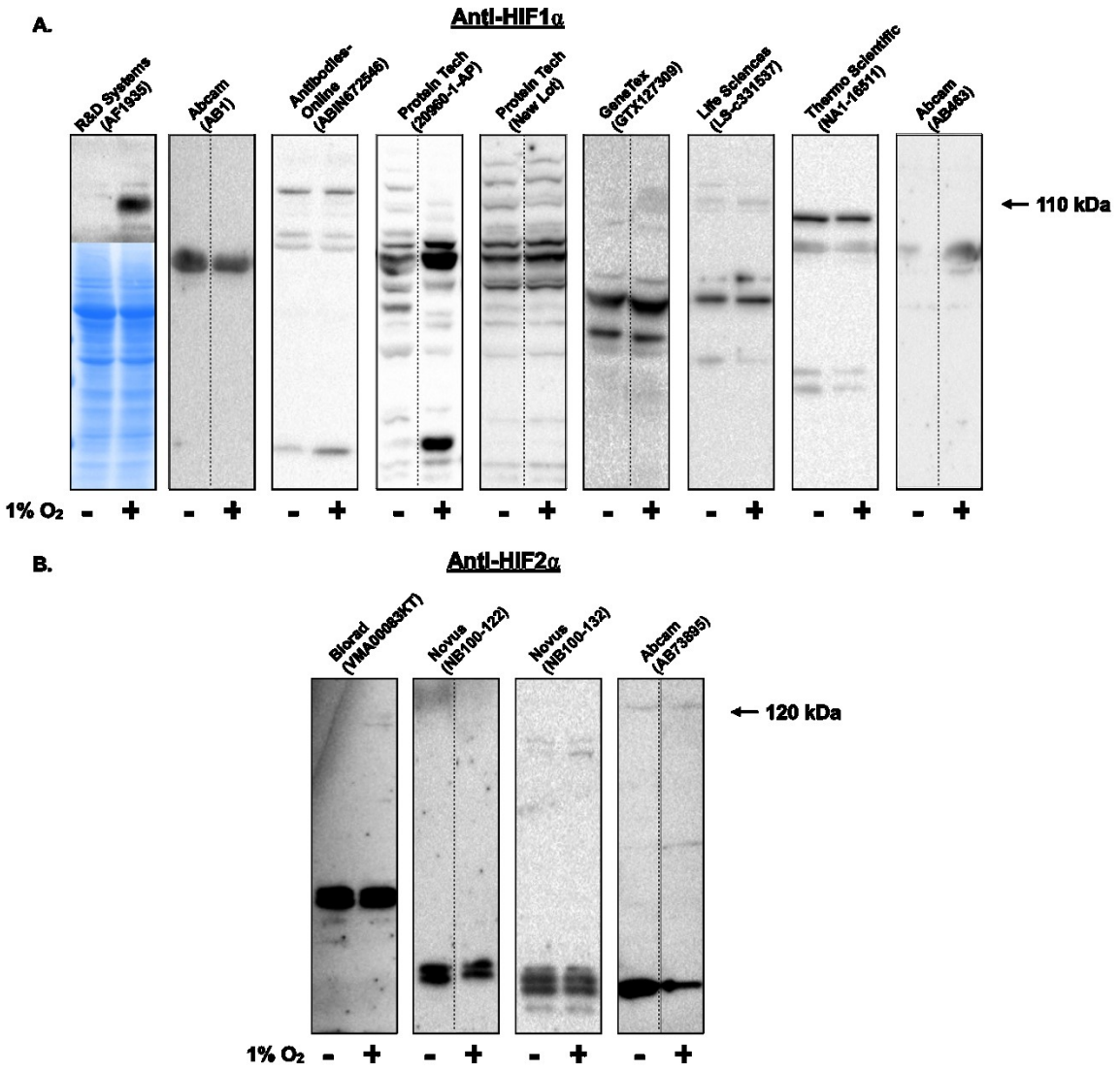

Figure 3.9 In Vitro Validation of Primary Anti-HIF1α and Anti-HIF2α Antibodies. **(A)** Anti-HIF1α (110 kDa) primary antibodies were tested in H9C2 cells exposed to either normoxia (21% O_2) or 1% O_2 for 24h. Primary antibody AF1935 of R&D Systems was validated in H9C2 myotubules. A total of (N=13) antibodies were trialed; 12 failed to detect physiological induction of HIF1α in hypoxia. **(B)** Anti-HIF2α (120 kDa) primary antibodies were tested in HEPG2 cells exposed to either normoxia (21% O_2) or 1% O_2 for 24h. Primary antibody VMA00083KT (BioRad) was validated in HEPG2 only.

defined *in vitro* conditional experimental approach was appropriate.

3.4 A HIF-Independent *In Vitro*-Indicator of Hypoxia at Low Oxygen Tension

The most common means of confirming intracellular hypoxia is to measure increased HIF1α protein expression/stability. However, other means of stabilizing HIF1α, independent of intracellular hypoxia, are known [62-64]. Further, not all cells demonstrate physiologically/metabolically similar states of hypoxic stress (i.e. lung vs bone parenchyma) at the same low-oxygen tensions or durations [103-107]. Thus, it was necessary to confirm intracellular hypoxia in our *in vitro* model independent of HIF1α expression to ensure that hypoxia was present under experimental conditions (1% atmospheric oxygen (1% O_2) in H9C2 cells).

Detection of low oxygen tension by FACS was used to quantitatively assess metabolic hypoxia in H9C2 cells (Figure 3.10). The commercial hypoxia indicator, HypoxyProbe™ (Pimonidazole; Figure 3.10-A), or $HAuCl_4$ (Figure 3.10-B), failed to demonstrate an increase in fluorescent intensity in response to 24h 1% O_2 in H9C2 cells. These initial assays may require additional amplification, for example by secondary anti-body labeling (as suggested by the commercial supplier in the case of HypoxyProbe), and thus were not sufficiently sensitive to our purpose. However, AlexaFluor 633 Cy5-conjugated Maleimide (Figure 3.10-C) demonstrated a marked increase in fluorescent intensity in response to 1% O_2 for 24hr. Importantly, the maleimide intensity did not increase in response to the hypoxia-mimetic, $CoCl_2$. The mechanism by which Maleimide is indicative of low oxygen tension is shown in Figure 3.11. Thus, in addition to proving cellular hypoxia in an *in vitro* model of low oxygen through stabilization of HIF1α, we were able to confirm the presence of intracellular hypoxia using one of three reported biochemical means of detection.

3.5 Heme Metabolism and Hypoxia Inducible Factor Protein Expression in Acute Moderate or Severe Hypoxia

The effect of acute moderate (8% O_2) and severe hypoxia (1% O_2) in H9C2 myotubules is shown in Figure 3.12. HIF1α was increased in myotubules exposed to 1% O_2 for 24h (+15-fold; +23-fold vs. normoxia 24h), but there was no observable difference in 8% O_2 (Figure 3.12-A). ALAS1 did not vary markedly in hypoxia (Figure 3.12-B; -1.3-fold, -1-fold, 8% O_2 vs normoxia; +1.2-fold, +2-fold , 1% O_2 vs normoxia). HMOX1

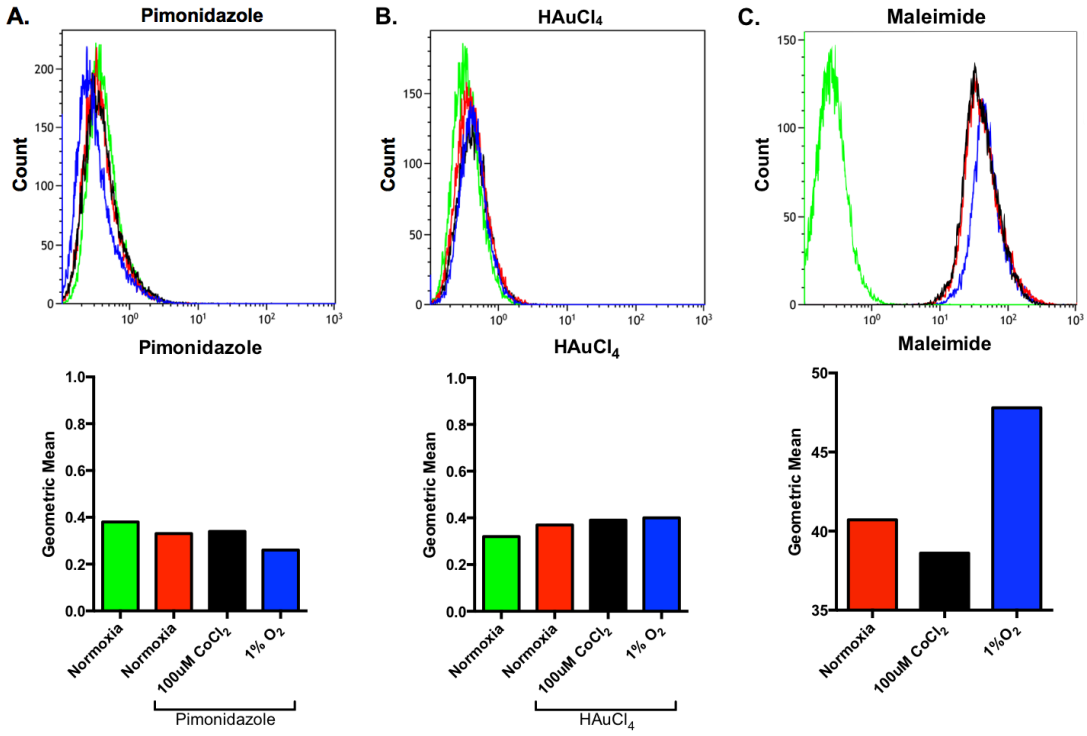

Figure 3.10. Maleimide is Indicative of Low Oxygen Tension by Fluorescence-Activated Cell Sorting (FACS). Fluorescence-activated cell sorting of proliferative H9C2 cells exposed to normoxia alone (21% O_2; green), normoxia with 100uM CoCl2 (black), or 1% O_2 for 24h (blue) with either **(A)** 100uM Pimonidazole, **(B)** 10uM $HAuCl_4$, or **(C)** 10uM AlexaFluor 633 C5 Maleimide. **(A-B)** Fluorescence did not increase markedly in cells exposed to 1% O_2. **(C)** Maleimide fluorescence increased empirically in hypoxic cells in comparison to normoxic and $CoCl_2$-treated cells.

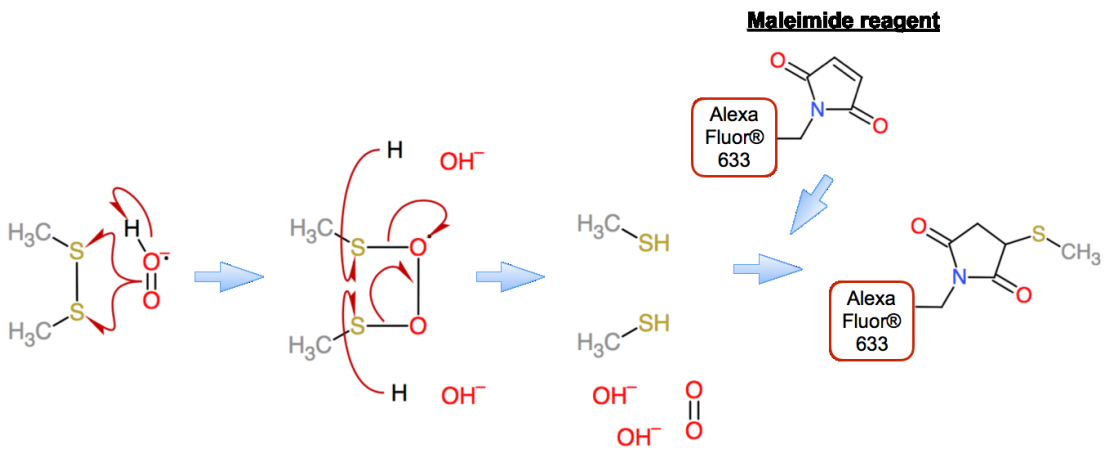

Figure 3.11. Thiol Formation and Maleimide Binding in Hypoxia. Cellular disulfide bonds are more readily broken in low oxygen tension as a result of increased intracellular reactive oxygen species formation that, in conjunction with decreased pH from hypoxia, form thiol (sulfhydryl) groups that react with Maleimide and retain it within the cell along with its fluorophore-conjugate for detection.

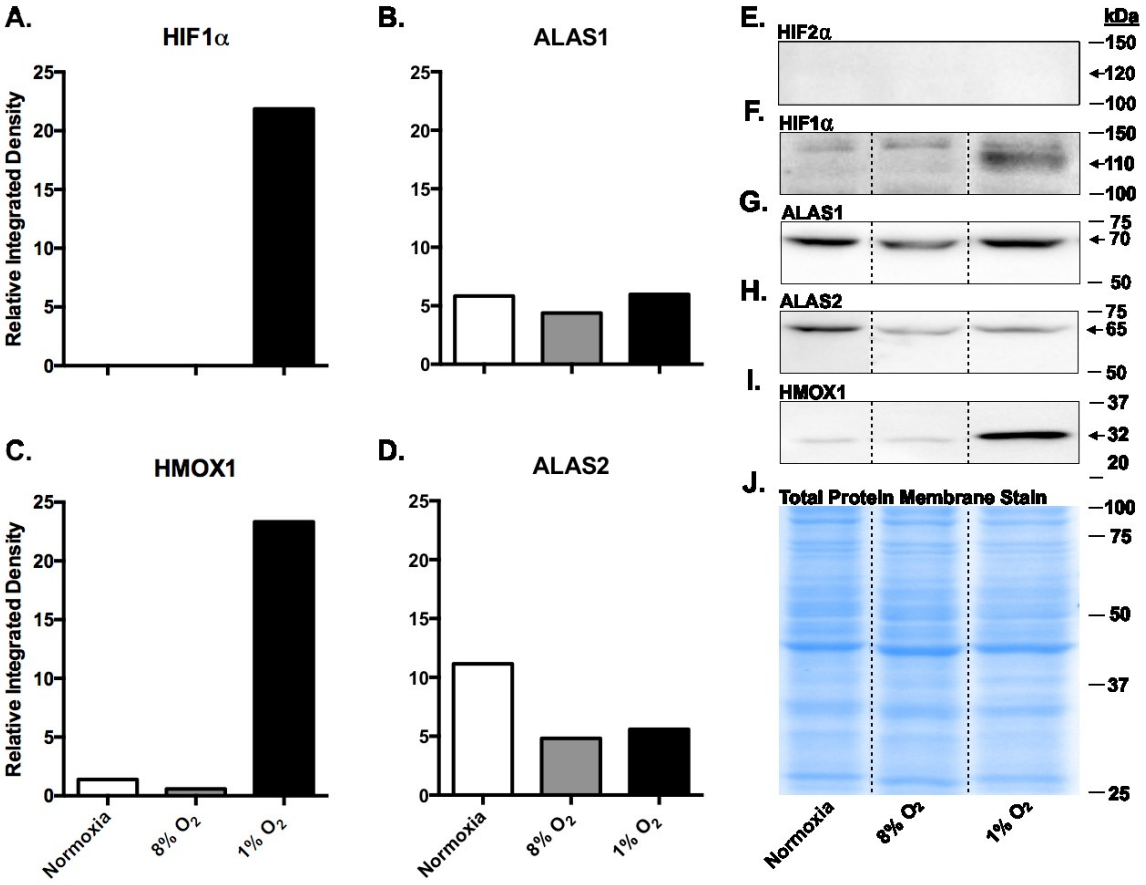

Figure 3.12. Dose-Dependent Effects of Acute Moderate or Severe Hypoxia on Heme Regulatory Enzyme Expression. Proliferative H9C2 cells were differentiated without FBS for 6 days and exposed to either normoxia (21% O_2), 8% O_2 or 1% O_2 for 24h. **(A)** HIF1α was increased after 24h in 1% O_2, but not in 8% O_2. **(B)** ALAS1 did not vary markedly in hypoxia$_2$. **(C)** HMOX1 was increased in 1% O_2 after 24h, but not in 8% O_2. **(D)** ALAS2 decreased with hypoxia. **(E)** Representative HIF2α-probed membrane; HIF2α was probed on a fresh membrane but was not detectable in H9C2 cells. **(F)** Representative HIF1α-probed membrane displayed prominent HIF1α-bands at 110 kDa. **(G)** Representative ALAS1-probed membrane displayed prominent ALAS1-bands at 70 kDa. **(H)** Representative ALAS2-probed membrane displayed prominent ALAS2-bands at 65 kDa. **(I)** Representative HMOX1-probed membrane displayed prominent HMOX1-bands at 32 kDa. **(J)** Pierce® Memcode staining demonstrated uniform protein loading on the membrane prior to antibody probe. Results are representative of 2 independent trials.

induction was observed in 1% O_2 (+22-fold, +116-fold vs normoxia) but there was no observable difference in 8% O_2 (Figure 3.12-C). ALAS2 was decreased in 8% O_2 (-2.4-fold, -1.4-fold vs normoxia) and 1% O_2 (Figure 3.12-D; -2.6-fold, -1.4-fold vs normoxia). Heme content was increased in 8% O_2 and 1% O_2 after 24h (Figure 3.13 C).

3.6 Heme Metabolism and Hypoxia Inducible Factor Protein Expression in Chronic Moderate or Severe Hypoxia

The effect of chronic (72h) moderate and severe hypoxia in H9C2 myotubules is shown in Figure 3.14. There was no observable difference in HIF1α protein expression in 8% O2; HIF1α was only increased in 1% O_2 after 24h (+15-fold, +23-fold vs normoxia 24h) and 72h at 1% O_2 (+1-fold, +1.1-fold vs 1% O_2 24h). (Figure 3.14-A). There was no observable difference in ALAS1 with chronic hypoxia in comparison to acute hypoxia (Figure 3.14-B). HMOX1 expression was increased after 24h at 1% O_2 (+5.2-fold, +22-fold vs normoxia 24h) and was elevated in normoxia over time under culture conditions (+3.2-fold, +3.3-fold vs normoxia 24h), 8% O_2 (+2.8-fold, +5-fold vs normoxia 24h) and 1% O_2 (+3.9-fold, +8.1-fold vs normoxia 24h) after 72h. (Figure 3.14-C). ALAS2 could be modestly decreased in normoxia (-1.4-fold, -3.5-fold vs normoxia 24h), or 8% O_2 (-4.5-fold, +2-fold vs 8% O_2 24h) after 72h (Figure 3.14-D). There was no observable difference in ALAS2 protein expression in 1% O_2 after 72h vs normoxia 72h (Figure 3.14-D).

3.7 Effect of HIF1α/2α Overexpression and HIF1α Knockdown on Heme Synthesizing Enzymes under Hypoxic Conditions

To elucidate the role of HIF1α and HIF2α in heme regulation, H9C2 myotubules were transduced with adenoviral vectors carrying the transgene, or shRNA for either of the HIF isoforms. Confirmation of adenoviral transduction was visually achieved by fluorescence microscopy (Figure 3.15). Adenoviral vectors targeting HIF1α were visualized by RFP (Figure 3.15-B). Vectors targeting HIF2α were visualized by GFP (Figure 3.15-C). Transduction efficiency and MOI were determined by FACS (Figure 3.16). H9C2 cells transduced with an MOI of 300 demonstrated a 2.7-fold increase in GFP intensity compared to cells transduced with an MOI of 100. However, cells transduced with an MOI of 100 demonstrated a transduction efficiency of >95%., whereas cells transduced with an MOI of 300 demonstrated a transduction efficiency

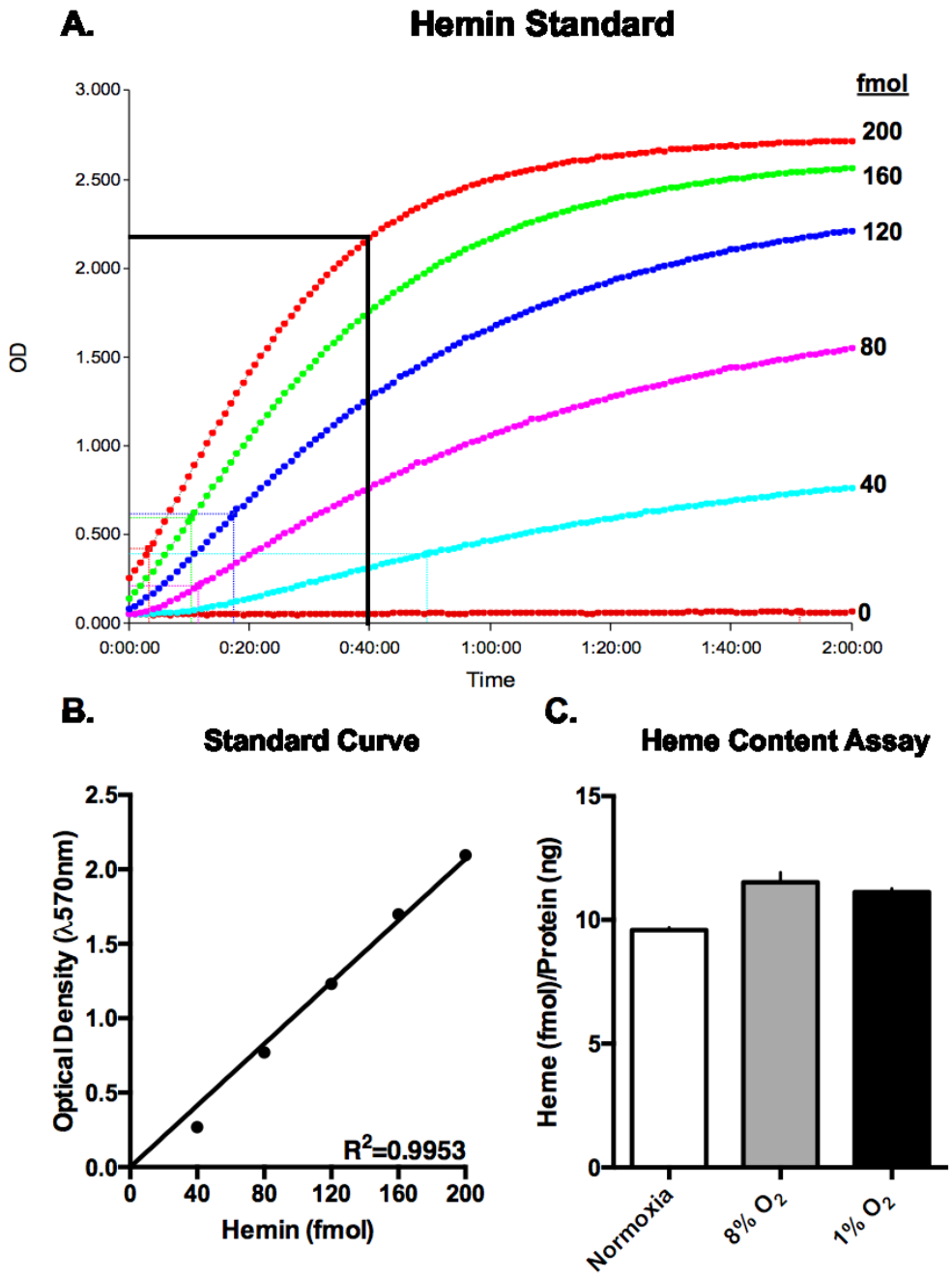

Figure 3.13. Increased Heme Content in H9C2s Exposed to Acute Moderate or Severe Hypoxia. (A) Raw kinetic plotting of hemin standard reaction progression. Standard curve optical densities (OD) were derived from the phase of linear growth at time = 40 minutes. **(B)** Heme content was interpolated through linear regression from a hemin standard curve (R^2=0.9953). **(C)** Heme content in H9C2 myotubules exposed to normoxia (21% O_2), 8% O_2 or 1% O_2 for 24h. Heme content was increased when exposed to either 8% O_2 or 1% O_2. Error bars are representative of mean ± standard error of the mean (SEM) of 3 technical replicates.

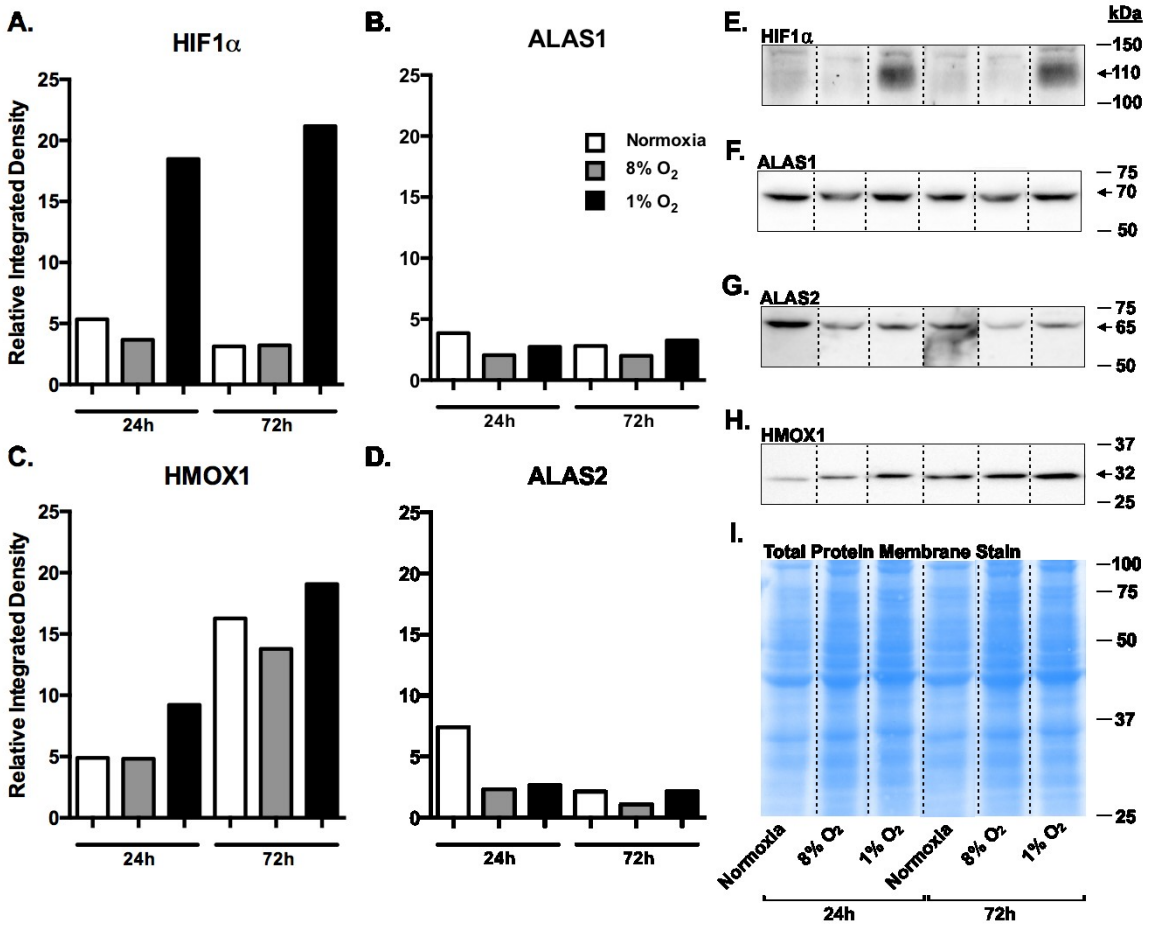

Figure 3.14. Protein Expression of Rate-Limiting Heme Metabolism Enzymes and Hypoxia Inducible Factor in Moderate or Severe Hypoxia. H9C2 cells were differentiated without FBS for 6 days and exposed to either normoxia (21% O_2), 8% O_2 or 1% O_2 for 24h or 72h. **(A)** HIF1α was increased after 24h and 72h in 1% O_2, but was not increased in 8% O_2. **(B)** ALAS1 did not vary markedly between acute (24h) and chronic (72h) hypoxia. **(C)** HMOX1 was increased after 24h in 1% O_2. After 72h, HMOX1 was increased in all treatments with highest expression observed in cells exposed to 1% O_2. **(D)** ALAS2 remained decreased in 72h hypoxia in 8% O_2 and 1% O_2. ALAS2 was decreased in normoxia after 72h. There was no observable difference in ALAS2 between 72h time points.**(E)** Representative HIF1α-probed membrane displayed prominent HIF1α-bands at 110 kDa. **(F)** Representative ALAS1-probed membrane displayed prominent ALAS1-bands at 70 kDa. **(G)** Representative ALAS2-probed membrane displayed prominent ALAS2-bands at 65 kDa. **(H)** Representative HMOX1-probed membrane displayed prominent HMOX1-bands at 32 kDa. **(I)** Pierce® Memcode staining demonstrated uniform protein loading on the membrane prior to antibody probe. Results are representative of 2 independent trials.

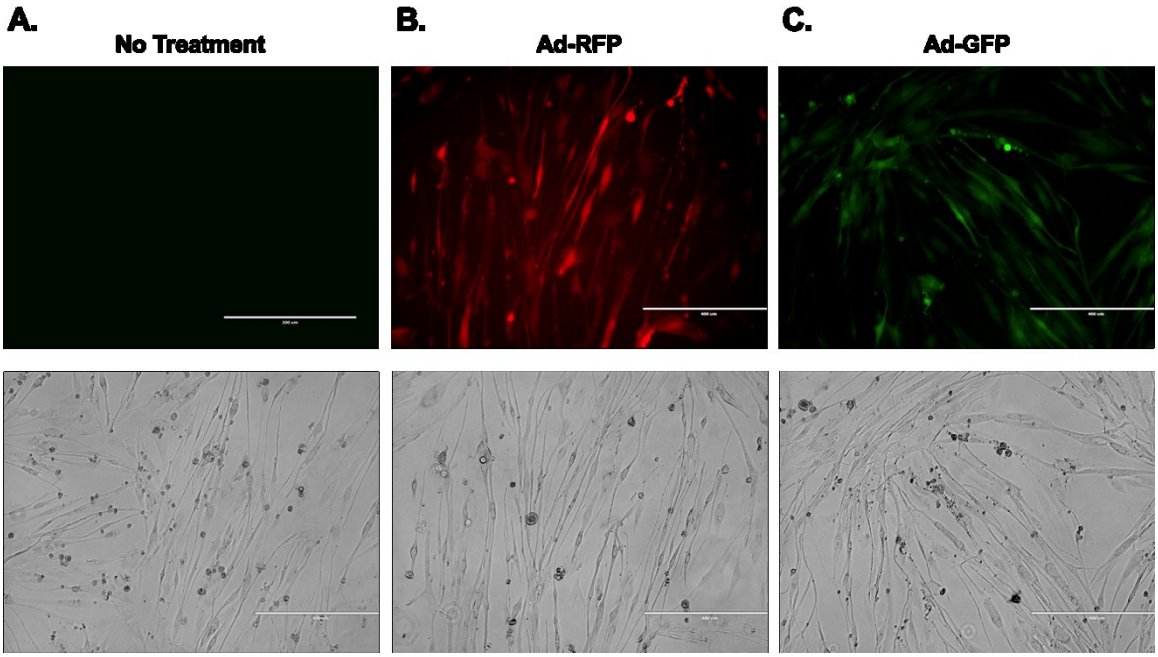

Figure-3.15. Confirmation of Adenoviral Transduction by Fluorescence Microscopy. Bright-field and fluorescence-filtered images of H9C2 myotubules after 3-day transduction with adenoviral vectors. **(A)** Non-transduced cells did not display fluorescence by microscopy, however **(B)** Ad-RFP- and **(C)** Ad-GFP- transduced cells displayed red and green fluorescence respectively.

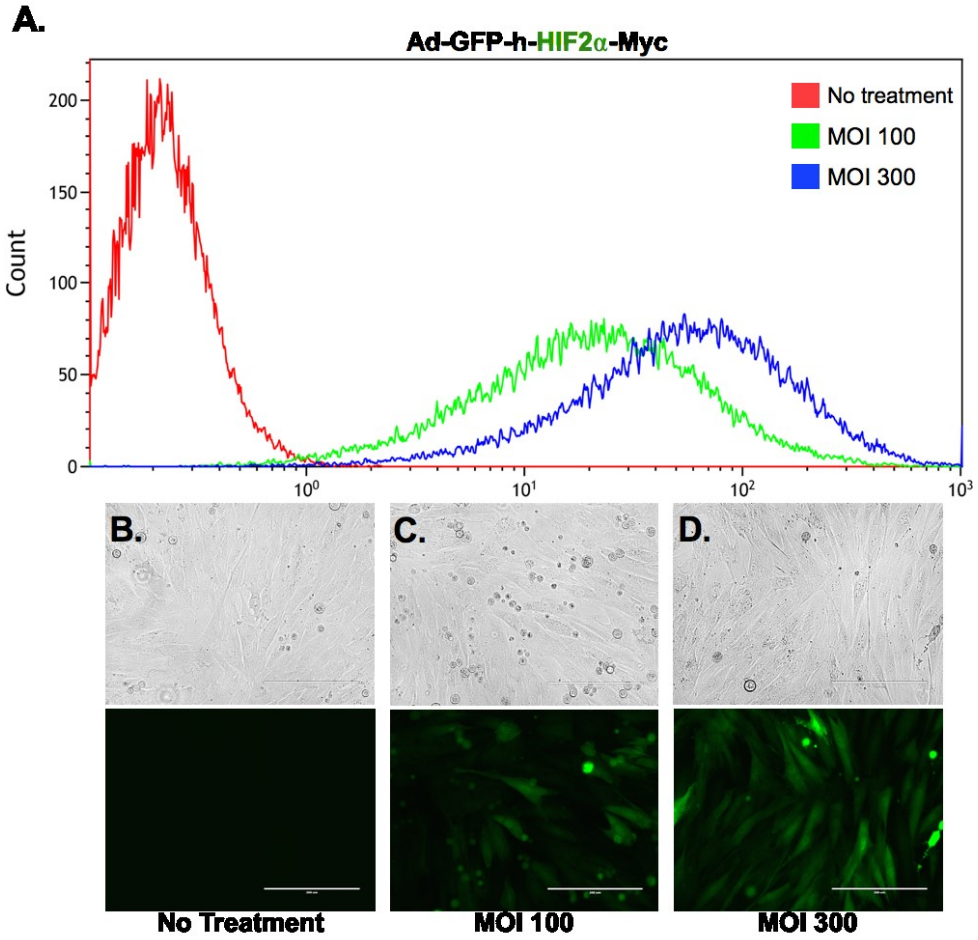

Figure 3.16. Optimizing Adenoviral Transduction Efficiency by Fluorescence-Activated Cell Sorting (FACS). Proliferative H9C2 cells were transduced with Ad-h-HIF2α-Myc for 72h at either 100 or 300 multiplicity of infection (MOI). **(A)** H9C2 cells transduced with an MOI of 300 (green) demonstrated a 2.7-fold increase in GFP intensity compared to cells transduced with an MOI of 100 (blue). **(B)** Bright-field and GFP-filtered views of H9C2 cells without adenoviral transduction. **(C)** Bright-field and GFP-filtered views of H9C2 cells transduced with a MOI of 100. **(D)** Bright-field and GFP-filtered views of H9C2 cells transduced with an MOI of 300.

>99% - only a 4% increase despite the usage of 3-fold more vector. An MOI of 100 was thus used thereafter for experimentation.

To confirm precise shRNA design, HIF1α/2α shRNA targets were aligned with their respective mRNA sequences by Clustal Omega (V1.2.2) to confirm sequence specific targeting (Figure 3.17). Western blot analysis was performed to confirm adenoviral overexpression and knockdown of HIF1α (Figure 3.18). HIF1α protein expression was increased in H9C2 myotubules exposed to 1% O_2 for 24h (+5-fold, +6.1-fold, +18-fold vs normoxia) and was subsequently knocked down with Ad-m/r-HIF1α-shRNA (-5-fold, -5.2-fold, -30-fold vs 1% O_2 24h). HIF1α was induced in normoxia by Ad-h-HIF1α-HA (+2.1-fold, +2.8-fold, +4.9-fold vs normoxia 24h) transduction and was markedly increased in conjunction with 1% O_2 for 24h (+1.4-fold, +2.2-fold, +4.5-fold vs 1% O_2 24h). To confirm targeting of HIF2α by adenoviral vectors, qPCR was performed in H9C2 myotubules incubated with either HIF1α/2α overexpression or knockdown vectors and exposed to 1% O_2 for 24h (Figure 3.19). qPCR was performed using human (Hu) and rat (Rt)-specific primers. Gene expression was internally normalized to HPRT1 and compared to a normoxic control for fold change expression. H9C2 myotubules transduced with Ad-h-HIF2α-Myc overexpression vector demonstrated >2000-fold increase in human-specific mRNA (Figure 3.19-A). HIF2α overexpression did not demonstrate cross-over effects on HIF1α. Rat-specific HIF2α primers were unable to confirm knockdown of endogenous HIF2α (Figure 3.19-B).

To verify whether adenoviral HIF1α expression was affected by HIF2α overexpression, HIF1α was measured in H9C2 myotubules overexpressing human HIF2α in normoxia or 1% O_2 for 24h (Figure 3.20). HIF1α levels were generally not affected by HIF2α overexpression in either normoxia (-2.5-fold, -1.4-fold, +1-fold, HIF2α overexpression vs non-transduced cells) or 1% O_2 (-1.1-fold, +1.1-fold, +1.1-fold vs non-transduced cells at 1% O_2).

To investigate the effect of HIF1α overexpression and knockdown on heme regulatory enzymes, H9C2 myotubules were incubated with adenoviral vectors and exposed to either normoxia or 1% O_2 for 24h. ALAS1 (+1.4-fold, +1.9-fold vs normoxia

A.

```
Human HIF1α mRNA (RefSeq:BC012527.2)   CTTTAGATAGCAAGACTTTCCTCAGTCGACACAGCCTGGATATGAAAATTTTCTTATTGTG  1020
Mouse HIF1α mRNA (RefSeq:NM_010431.2)  CTTTAGATAGCAAGACATTTCTCAGTCGACACAGCCTCGATATGAAAATTTTCTTACTGTG  1189
Rat HIF1α mRNA (RefSeq:AF057308.1)     CTTTAGACAGCAAGACATTTCTCAGTCGACACAGCCTCGATATGAAAATTTTCTTACTGTG  792
Ad-m/r-HIF1α-shRNA Target              ----------------------AGTCGACACAGCCTCGATATG----------------  21
                                                              ************** ******
```

B.

```
Human HIF2α mRNA (RefSeq:NM_001430.4)  CATGCGACTGGCAATCAGCTTCCTGCGAACACACAAGCTCCTCTCCTCAGTTTGCTCTGAAAACGAGTCCGAAGCCGAAGCT  759
Mouse HIF2α mRNA (RefSeq:NM_010137.3)  CATGCGCCTGGCCATCAGCTTCCTTCGGACACATAAGCTCCTGTCCTCAGTCTGCTCTGAAAATGAATCTGAAGCTGAGGCC  668
Rat HIF2α mRNA (RefSeq:NM_023090.1)    CATGCGCCTGGCCATCAGCTTCCTGCGAACACATAAACTCCTGTCTTCAGTGTGCTCTGAAAATGAATCTGAAGCCGAGGCT  329
Ad-r-HIF2α-shRNA Target                ----------------AGCTTCCTGCGAACACATAAA-------------------------------------------  21
                                                        ******** ** ***** **
```

Figure 3.17 Confirmation of Vector shRNA Sequence Alignment by Clustal Omega. Human, mouse, and rat **(A)** HIF1α and **(B)** HIF2α nucleotide mRNA sequences were aligned by Clustal Omega (V1.2.2.) and labeled (boxed sequences) according to the adenoviral shRNA target sequences respectively. Identical nucleotide alignment across all species and shRNA target was denoted by *. Gaps in * and boxing identified single nucleotide changes between aligned sequences. **(A)** Ad-m/r-HIF1α-shRNA aligned 100% with both mouse and rat reference sequences thus a single vector was predicted to block either species expression. **(B)** A rat-specific shRNA targeted sequence was required due to alignment of the gene across species.

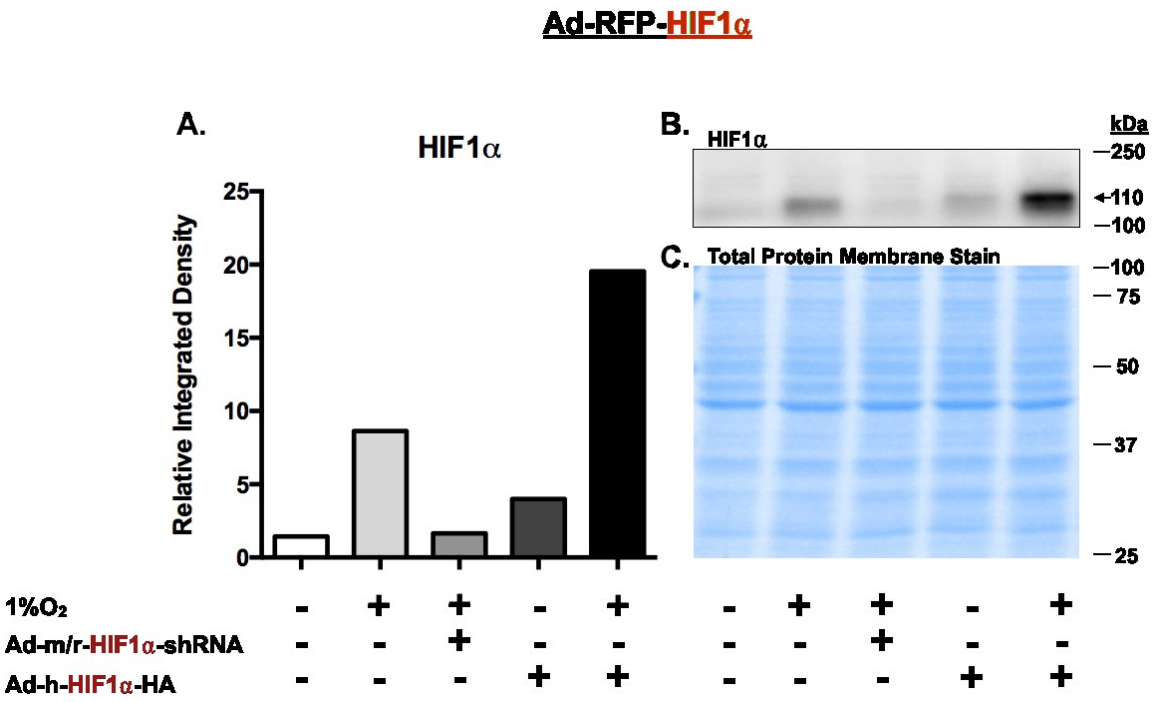

Figure 3.18. HIF1α Overexpression and Knockdown by Adenoviral Vectors under Hypoxic Conditions. H9C2 cells were differentiated without FBS for 6 days (of which the final 3 days were incubated with adenoviral vectors) and exposed to either normoxia (21% O_2) or 1% O_2 for 24h. **(A)** HIF1α was decreased in cells transduced with Ad-m-HIF1α-shRNA and exposed to 1% O_2. HIF1α was increased in cells transduced with Ad-h-HIF1α-HA in normoxia, and further elevated in 1% O_2. **(B)** Representative HIF1α-probed membrane displayed prominent HIF1α-bands at 110 kDa. **(C)** Pierce® Memcode staining demonstrated uniform protein loading on the membrane prior to antibody probe. Results are representative of 3 independent trials.

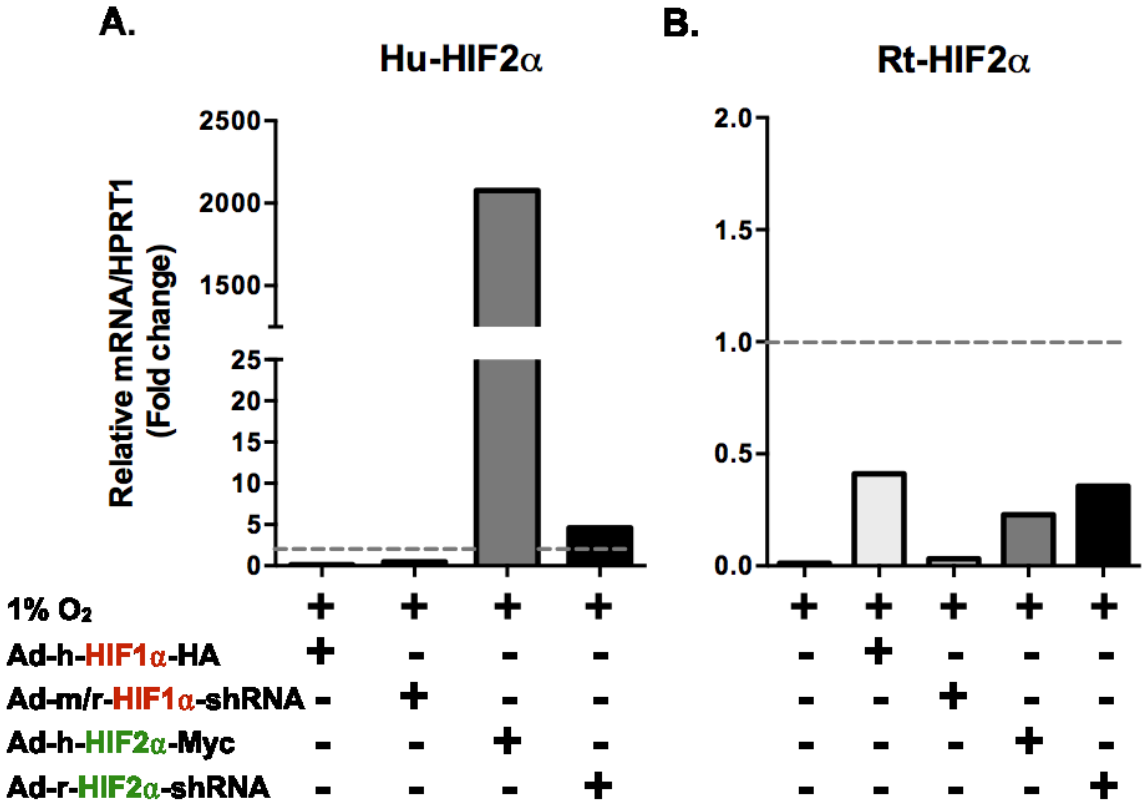

Figure 3.19 HIF2α Overexpression and Knockdown by Adenoviral Vectors under Hypoxic Conditions-without Cross-Over Effects during HIF1α Overexpression or Knockdown under Hypoxic Conditions. H9C2 cells were differentiated without FBS for 6 days (of which the final 3 days were incubated with adenoviral vectors) and exposed to either normoxia, (21% O_2) or 1% O_2 for 24h. Gene expression was internally normalized to HPRT1 and compared to a normoxic control for fold change expression. **(A)** H9C2 myotubules transduced with Ad-h-HIF2α-Myc overexpression vector displayed >2000-fold increase in human-specific mRNA. Ad-h-HIF1α-HA overexpression vectors did not affect the expression of HIF2α. **(B)** H9C2 cells transduced with Ad-r-HIF2α-shRNA did not confirm knockdown of endogenous HIF2α. Primers designed to target rat (Rt) HIF2α did not cross-react with the human overexpression mRNA.

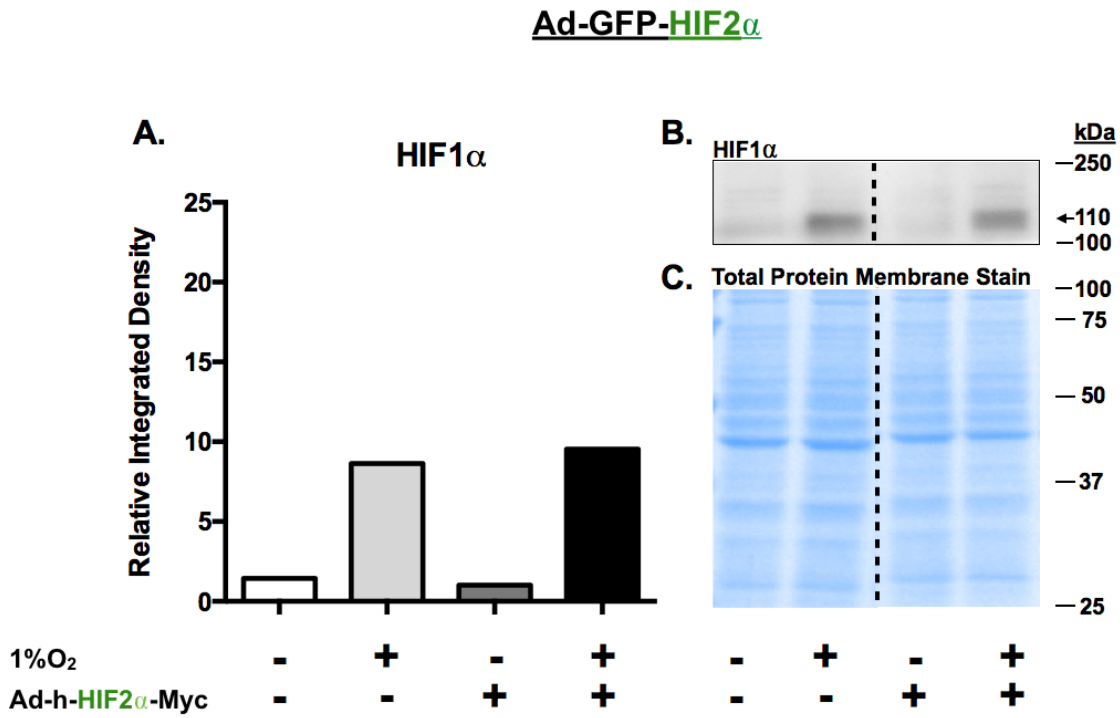

Figure 3.20. HIF1α Expression has no Cross-Over-Effects during HIF2α Overexpression under Hypoxic Conditions. H9C2 cells were differentiated without FBS for 6 days (of which the final 3 days were incubated with adenoviral vectors) and exposed to either normoxia (21% O_2) or 1% O_2 for 24h. **(A)** HIF1α expression in normoxia and 1% O_2 was not increased or decreased with Ad-h-HIF2α-Myc transduction. **(B)** Representative HIF1α-probed membrane displayed prominent HIF1α-bands at 110 kDa. **(C)** Pierce® Memcode staining demonstrated uniform protein loading on the membrane prior to antibody probe. Results are representative of 3 independent trials.

24h) and ALAS2 (+1.2-fold, -1.1-fold vs normoxia 24h) were slightly increased or generally unaffected by HIF1α overexpression in normoxia after 24h (Figure 3.21-A, B). In cells exposed to 1% O_2 for 24h, HIF1α knockdown increased ALAS1 (+4.2-fold, +4.6-fold vs 1% O_2 24h); there was no observable difference in ALAS2 from hypoxic controls (Figure3.21-A, B respectively). HIF1α overexpression in 1% O_2 also increased ALAS1 levels (+3.5-fold, +3.5-fold vs 1% O_2 24h). There was no observable difference in HMOX1 in response to HIF1α overexpression in normoxia (Figure 3.22). HMOX1was increased with HIF1α overexpression in conjunction with 1% O_2 (-2-fold, +1.4-fold, +1.7-fold vs 1% O_2 24h). Increased HMOX1 in 1% O_2 was attenuated with HIF1α knockdown (-1.57-fold, -2.2-fold, -24-fold vs 1% O_2 24h).

To investigate the effect of HIF2α overexpression on heme regulatory enzymes, H9C2 myotubules were incubated with adenoviral vectors and exposed to either normoxia or 1% O_2 for 24h. ALAS1 was increased in response to HIF2α overexpression in both normoxia (+1.3-fold, +2.5-fold vs normoxia 24h) and 1% O_2 (+1.3-fold, +2-fold vs normoxia 24h) after 24h (Figure 3.23-A). There was no observable difference in ALAS2 with HIF2a overexpression (Figure 3.23-B). Interestingly, HMOX1 was increased with HIF2α overexpression in normoxia (+26.7-fold, +62-fold, +126.7-fold vs normoxia 24h) and synergistically increased in conjunction with 1% O_2 (+5.5-fold, +6.9-fold, +10-fold vs 1% O_2 24h) after 24h (Figure 3.24). Heme content was increased with HIF2α and HIF1α overexpression in normoxia and in 1% O_2 after 24h compared to sham (Figure 3.25-C). HIF1α knockdown resulted in increased heme content levels in normoxia, elevated beyond the increase observed in hypoxia.

3.8 Dose- and Time-Dependent Changes in Heme Regulatory Enzyme Protein Expression with Hemin

To investigate the interplay of increased heme on heme regulatory enzyme and HIF expression *in vitro*, we first established a non-toxic, heme-replete state in H9C2 cells. First, cell viability was measured by PrestoBlue assay in both proliferative and quiescent H9C2 in response to increased hemin concentration (Figure 3.26). Proliferative H9C2 viability was sustained above 85% from 5-200uM hemin after 24h; survival of proliferative H9C2 was distinctly reduced with 400uM hemin after 24h (Figure 3.26-A).

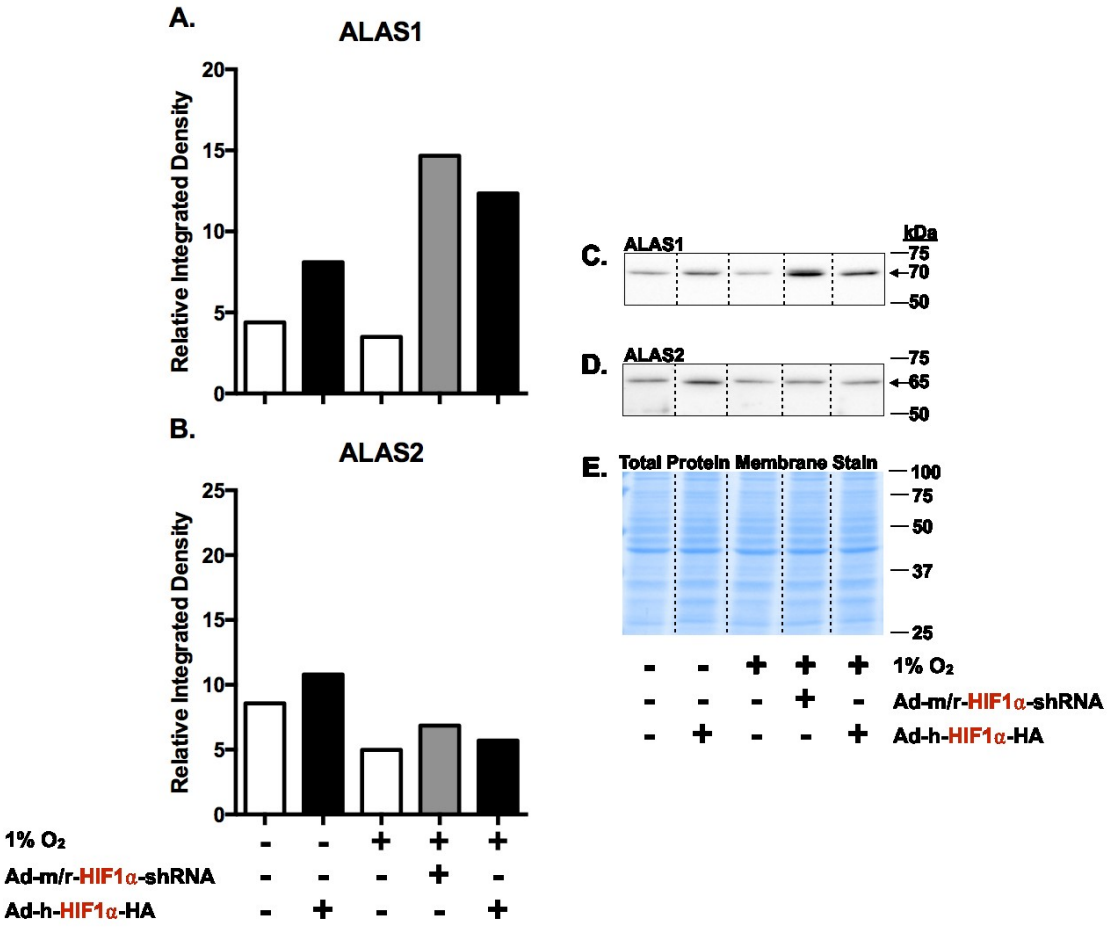

Figure 3.21. Effect of HIF1α Overexpression and Knockdown on Heme Synthesizing Enzymes under Hypoxic Conditions. H9C2 cells were differentiated without FBS for 6 days (of which the final 3 days were incubated with adenoviral vectors) and exposed to either normoxia (21% O_2) or 1% O_2 for 24h. **(A)** ALAS1 was moderately increased with HIF1α overexpression and was decreased in 1% O_2, HIF1α knockdown increased ALAS1 in normoxia and hypoxia. **(B)** ALAS2 was moderately increased with HIF1α overexpression in normoxia and decreased in 1% O_2. ALAS2 was relatively unchanged with HIF1α transduction in 1% O_2 for 24h. **(C)** Representative ALAS1-probed membrane displayed prominent ALAS1-bands at 70 kDa. **(D)** Representative ALAS2-probed membrane displayed prominent ALAS2-bands at 65 kDa. **(E)** Pierce® Memcode staining demonstrated uniform protein loading on the membrane prior to antibody probe. Results are representative of 2 independent trials.

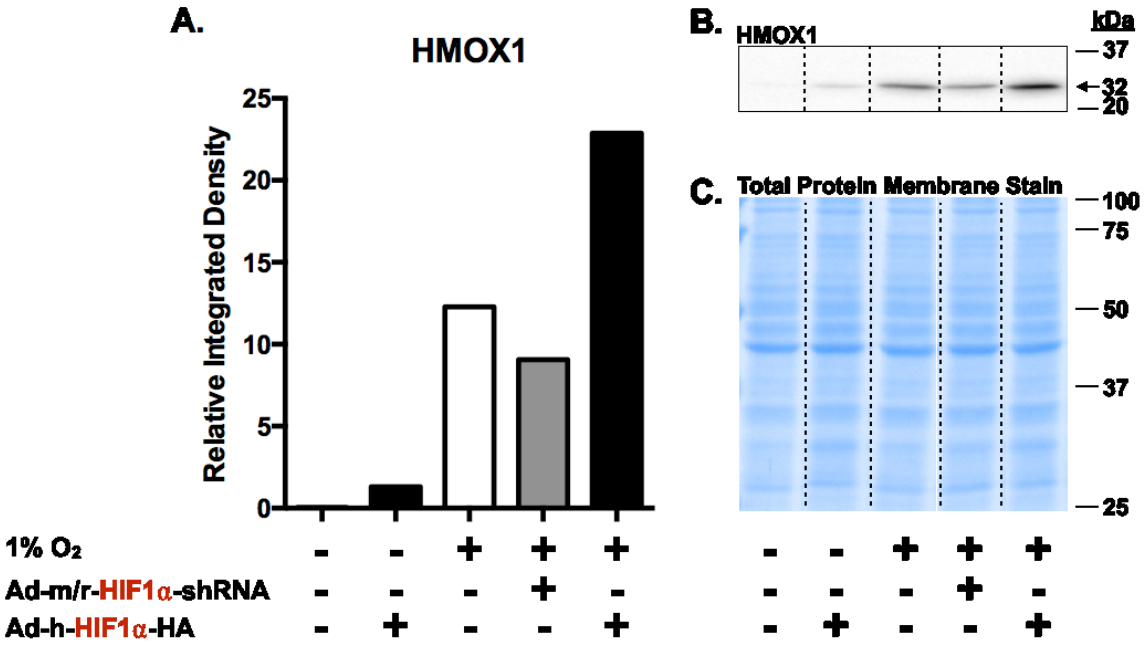

Figure 3.22. Effect of HIF1α Overexpression and Knockdown on HMOX1 Expression under Hypoxic Conditions. H9C2 cells were differentiated without FBS for 6 days (of which the final 3 days were incubated with adenoviral vectors) and exposed to either normoxia (21% O_2) or 1% O_2 for 24h. **(A)** HMOX1 was slightly increased in cells transduced with HIF1α overexpression in normoxia. HMOX1 was increased in hypoxia and was further increased with HIF1α overexpression. HMOX1 levels in hypoxia were attenuated in cells transduced with HIF1α-shRNA. **(B)** Representative HMOX1-probed membrane displayed prominent HMOX1-bands at 32 kDa. **(C)** Pierce® Memcode staining demonstrated uniform protein loading on the membrane prior to antibody probe. Results are representative of 3 independent trials.

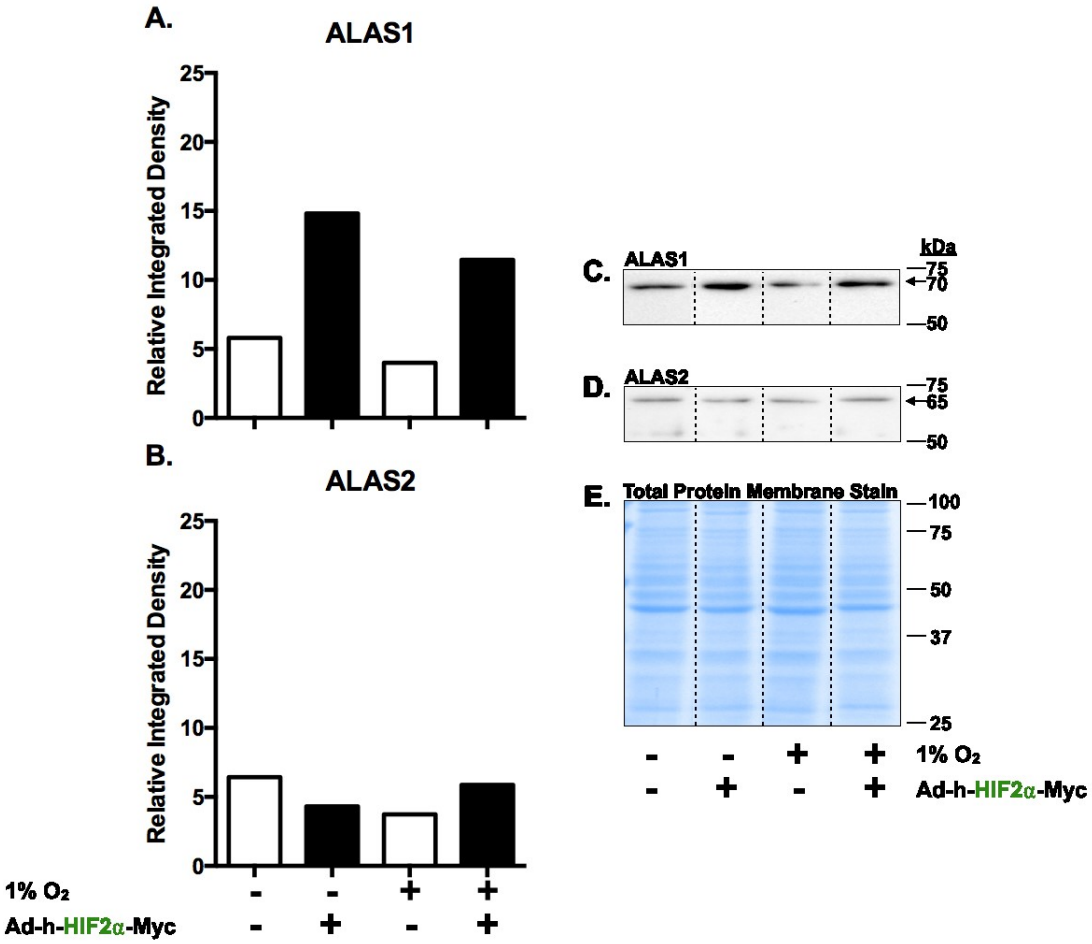

Figure 3.23. Effect of HIF2α Overexpression on Heme Synthesizing Enzymes under Hypoxic Conditions. H9C2 cells were differentiated without FBS for 6 days (of which the final 3 days were incubated with adenoviral vectors) and exposed to either normoxia or 1% O_2 for 24h. **(A)** ALAS1 was modestly increased with HIF2α overexpression.. **(B)** ALAS2 did not vary markedly with HIF2α overexpression. **(C)** Representative ALAS1-probed membrane displayed prominent ALAS1bands at 70 kDa. **(D)** Representative ALAS2-probed membrane displayed prominent ALAS2-bands at 65 kDa. **(E)** Pierce® Memcode staining demonstrated uniform protein loading on the membrane prior to antibody probe. Results are representative of 2 independent trials.

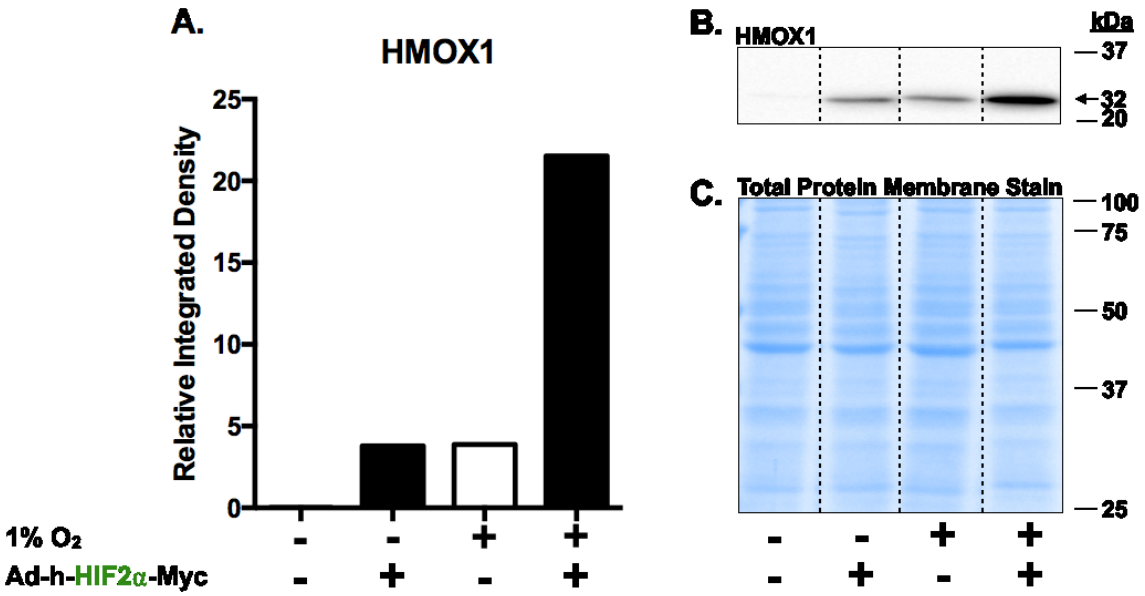

Figure 3.24. Effect of HIF2α Overexpression on HMOX1 Expression under Hypoxic Conditions. H9C2 cells were differentiated without FBS for 6 days (of which the final 3 days were incubated with adenoviral vectors) and exposed to either normoxia or 1% O_2 for 24h. **(A)** HMOX1 was increased with HIF2α overexpression in normoxia. HMOX1 expression was further increased in hypoxia with HIF2α overexpression. **(B)** Representative HMOX1-probed membrane displayed prominent HMOX1-bands at 32 kDa. **(C)** Pierce® Memcode staining demonstrated uniform protein loading on the membrane prior to antibody probe. Results are representative of 3 independent trials.

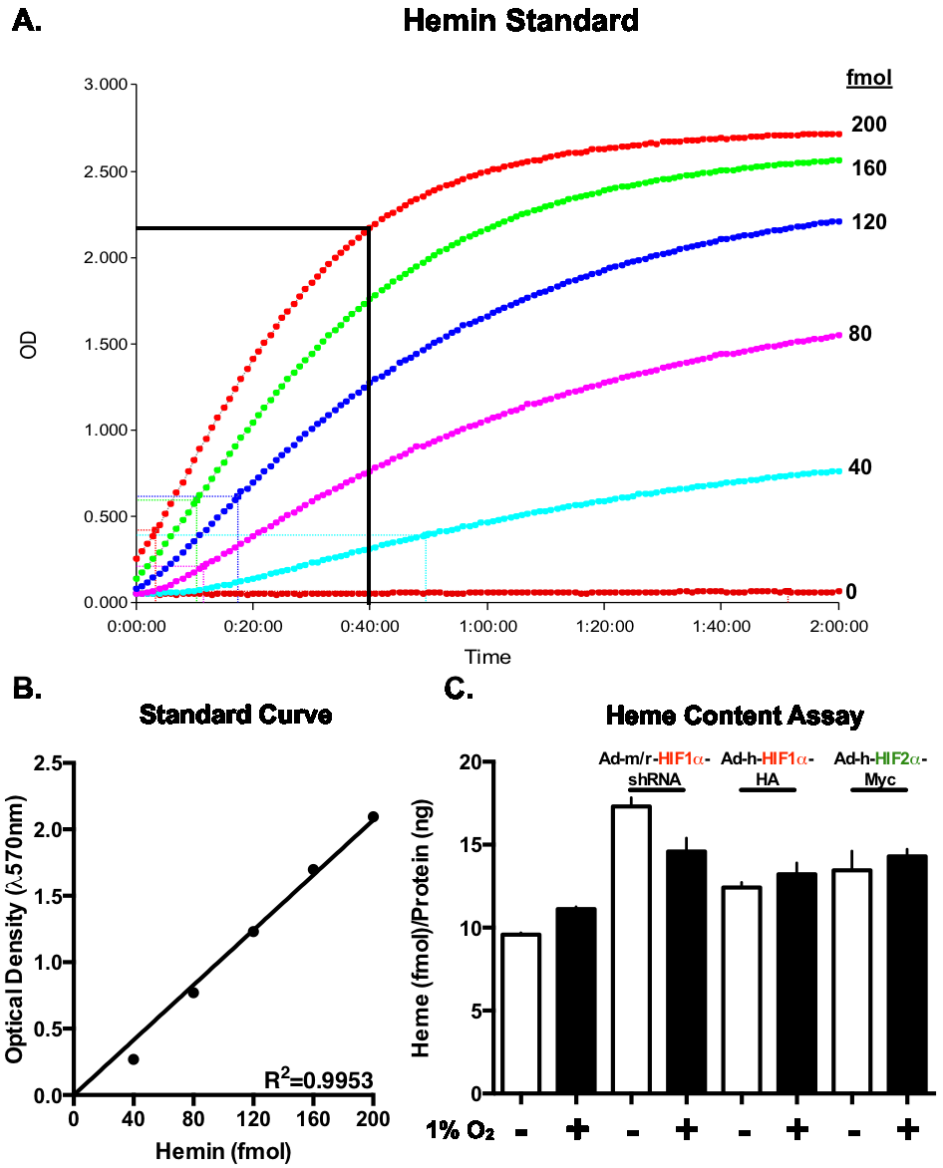

Figure 3.25. Effect of HIF1/2α Overexpression and HIF1α Knockdown on Heme Content under Hypoxia. Heme content in H9C2 myotubules exposed to either normoxia or 1% O_2 for 24h was quantified by Heme Colorimetric Assay. **(A)** Raw kinetic plotting of hemin standard reaction progression. Standard curve optical densities (OD) were derived from the phase of linear growth at time = 40 minutes. **(B)** Heme content was interpolated through linear regression from a hemin standard curve (R^2=0.9953). **(C)** Heme content in adenovirally transduced H9C2 myotubules exposed to normoxia (21% O_2) or 1% O_2 for 24h. Heme content was increased in hypoxia in non-transduced cells. HIF1α and HIF2α overexpression increased heme content relative to non-transduced cells. HIF1α knockdown resulted in the largest increase in heme content; increased heme content was attenuated in hypoxia. Error bars are representative of mean ± standard error of the mean (SEM) of 2-3 technical replicates.

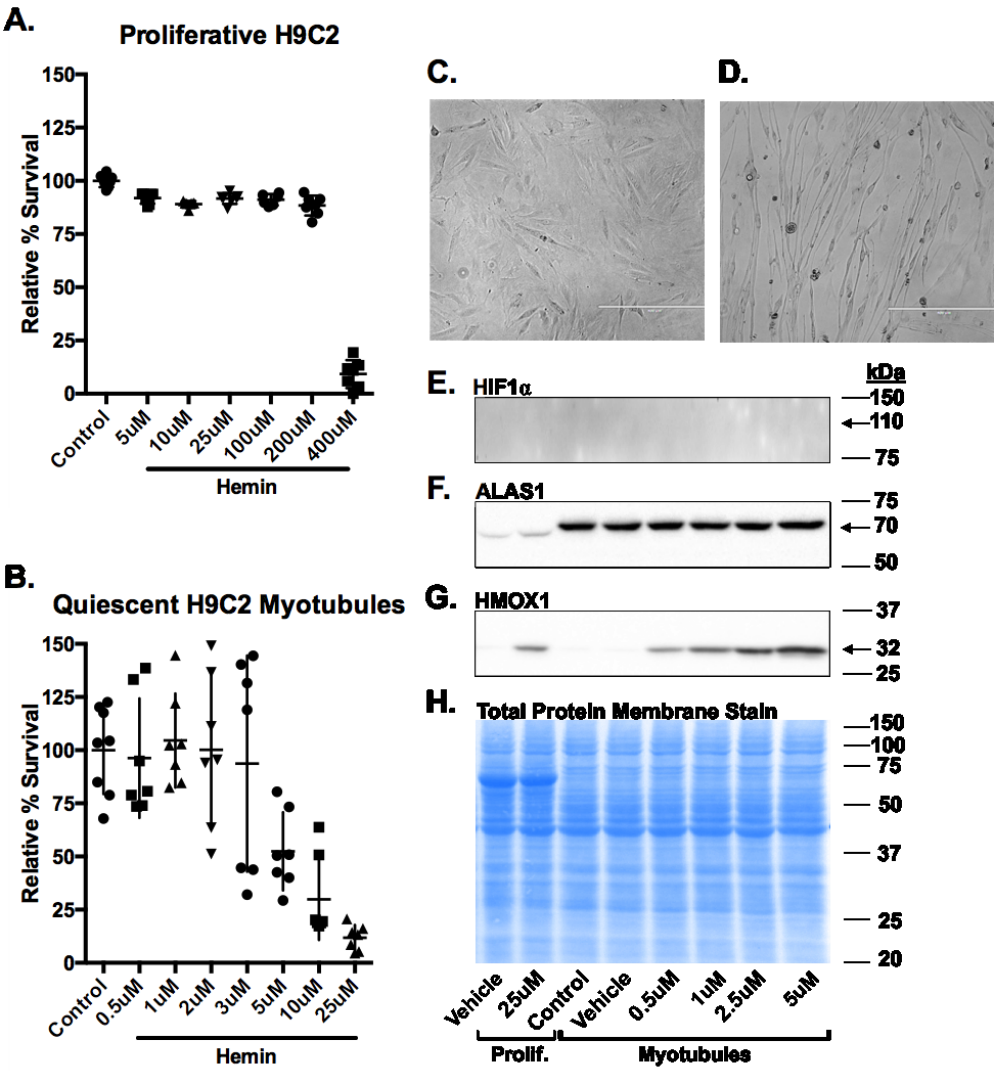

Figure-3.26. Establishing a Non-Toxic, Heme-Replete State in H9C2. PrestoBlue viability assay and dose-response of hemin in **(A, C)** Proliferative H9C2 and **(B, D)** H9C2 myotubules over 24h (N=8 biological replicates). **(A)** Proliferative H9C2 survival was markedly reduced from 200uM to 400uM hemin. **(B)** Survival of H9C2 myotubules was prominently reduced from 5uM to 25uM hemin. **(C)** Spindle-shaped, proliferative H9C2 cardiomyoblasts at 80% confluency. **(D)** Contact inhibited, quiescent H9C2 myotubules after serum-withdrawal differentiation displaying parallel alignment, increased 3-dimensional depth and elongated spindle morphology. **(E)** HIF1α expression was not affected by hemin treatment. **(F)** ALAS1 expression was elevated in quiescent myotubules in comparison to proliferating H9C2 cells. ALAS1 was not affected by hemin treatment. **(G)** HMOX1 expression demonstrated a dose-dependent induction with hemin treatment. A 25uM dose of hemin in proliferative H9C2s was comparable to a 2.5uM dose of hemin in H9C2 myotubules for HMOX1 expression. **(H)** Pierce® Memcode staining demonstrated uniform protein loading on the membrane prior to antibody probe.

Differentiated H9C2 myotubules were not as tolerant to hemin; cell viability was decreased to below 25% at 25uM hemin (Figure 3.26-B). As well, given the extended culture for myotubules in 96-well plates, there was considerable variability compared to proliferative H9C2. HIF1α was not increased in response to hemin administration (Figure 3.26-E). ALAS1 was higher in H9C2 than in proliferative cells; ALAS1 did not vary with escalating hemin concentration (Figure 3.26-F). HMOX1 expression demonstrated a dose-dependent induction with hemin treatment; a 25uM dose of hemin in proliferative H9C2s was comparable to a 2.5uM in H9C2 myotubules for HMOX1 induction (Figure 3.26-G). H9C2 myotubule differentiation was confirmed by transient myogenin (Figure 3.27; +79-fold, +460-fold after 24h serum deprivation vs subconfluence) Heme content was lower in H9C2 myotubules than in proliferative H9C2; myotubules exposed to 2.5uM hemin for 24hr raised heme content in myotubules near levels observed in proliferative H9C2 cells (Figure 3.28-C).

To determine the time-dependent induction of HMOX1 by hemin, H9C2 myotubules were treated with either vehicle or 2.5uM hemin for 4h, 24h or 72h (Figure 3.29). HMOX1 was visibly increased at 4h and peaked by 24h before attenuating at 72h (Figure 3.29-A). H9C2 myotubules were subsequently exposed to vehicle or 2.5uM hemin for 24h to investigate the protein expression of heme regulatory enzymes under heme-replete conditions (Figure 3.30). There was no observable difference in ALAS1 with hemin whereas ALAS2 was modestly increased (Figure 3.30-A, B respectively; ALAS2, +1.45-fold, +3-fold vs vehicle). HMOX1 was markedly increased (+31-fold, +880-fold vs vehicle) with 2.5uM hemin (Figure 3.30-C).

3.9 Heme Metabolism and Hypoxia Inducible Factor Protein Expression in Heme-Replete Hypoxia

Increased heme content and intracellular markers of hypoxia have been previously reported in human heart failure [93, 108]. To investigate the effect of heme-replete hypoxia on heme regulatory enzyme and hypoxia inducible factor protein expression, H9C2 myotubules were exposed to either vehicle, 2.5uM hemin, vehicle in 1% O_2, 2.5uM hemin in 1% O_2, or 2.5uM hemin in 1% O_2 with 5uM antioxidant N-acetyl cysteine (NAC) for 24h (Figure 3.31). HIF1α levels were significantly and synergistically increased in heme-replete hypoxia when compared to either hemin or

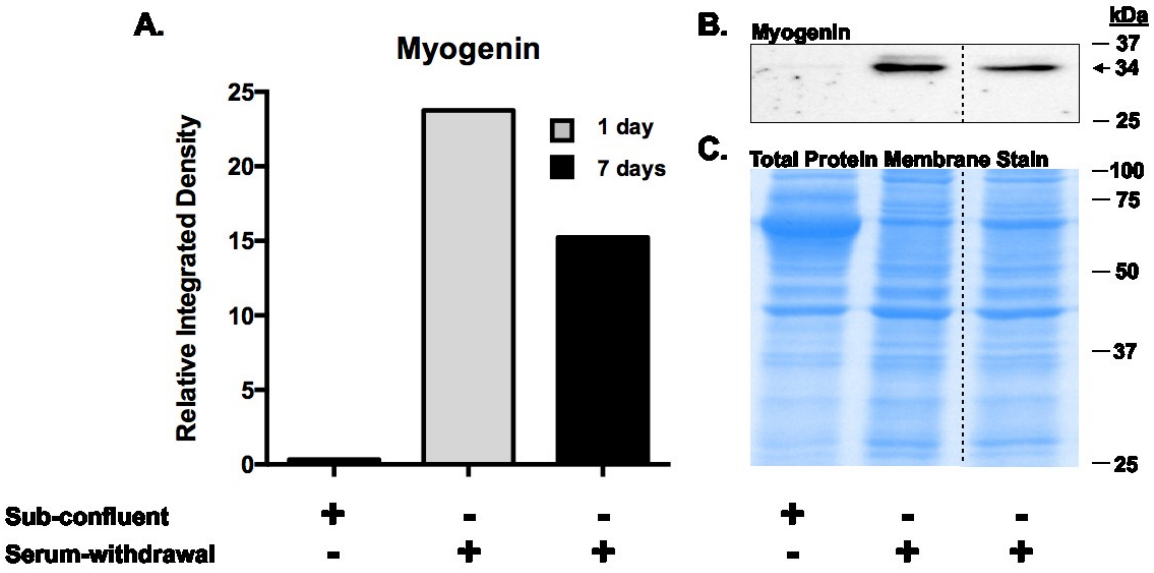

Figure 3.27. Molecular Confirmation of H9C2 Differentiation by Transient Myogenin Expression. Proliferative H9C2 were differentiated into contact-inhibited, quiescent myotubules by serum-withdrawal (1% FBS) for 1 or 7 days. **(A)** Myogenin was not detected in sub-confluent, proliferative H9C2. Myogenin expression was increased in H9C2 cells after 1 day of serum-withdrawal and attenuated after 7 days withdrawal. **(B)** Representative Myogenin-probed membrane displayed prominent Myogenin-bands at 34 kDa. **(C)** Pierce® Memcode staining demonstrated uniform protein loading on the membrane prior to antibody probe. Results are representative of 2 independent trials.

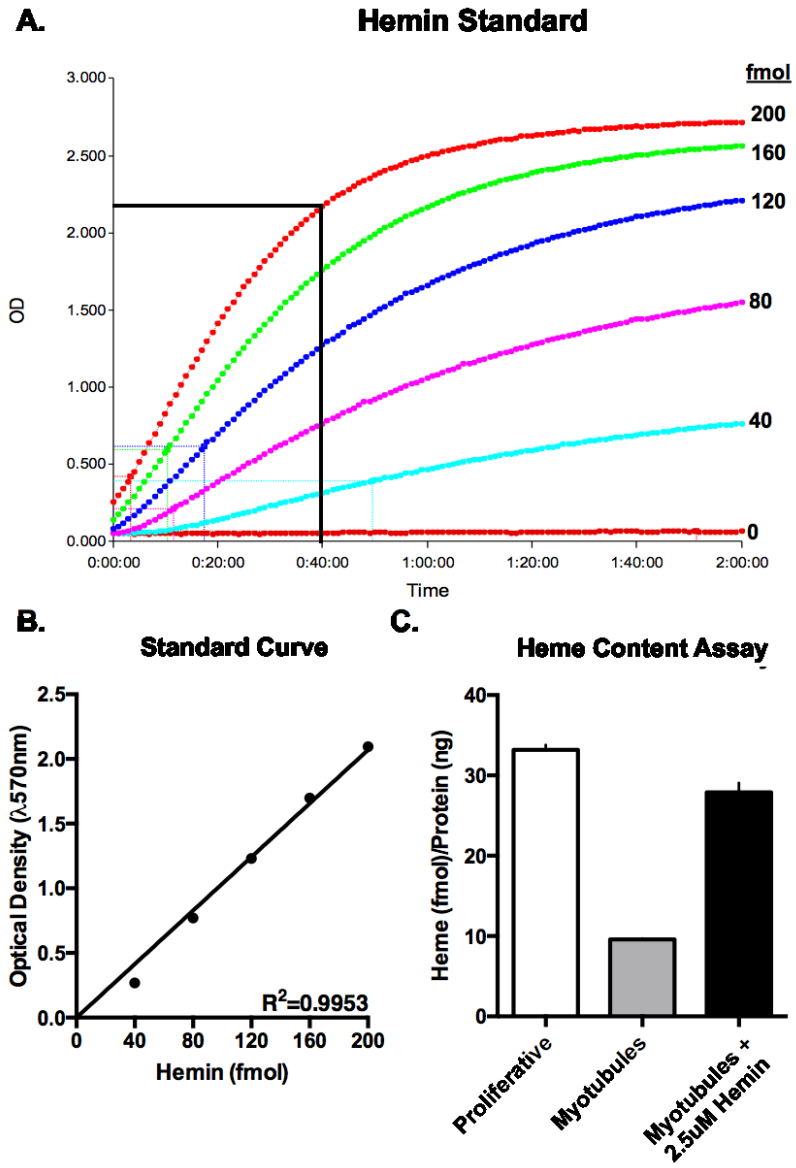

Figure 3.28. Heme Content in Proliferative H9C2, Myotubules and Heme-Replete Myotubules. (A) Raw kinetic plotting of hemin standard reaction progression. Standard curve optical densities (OD) were derived from the phase of linear growth at time = 40 minutes. **(B)** Heme content was interpolated through linear regression from a hemin standard curve (R^2=0.9953). **(C)** Heme content was lower in H9C2 myotubules than myoblasts and 2.5uM hemin for 24hr raised heme content in myotubules near levels observed in proliferative H9C2, thus a heme-replete state in myotubules is similar to proliferative H9C2s. Error bars are representative of mean ± standard error of the mean (SEM) of 3 technical replicates.

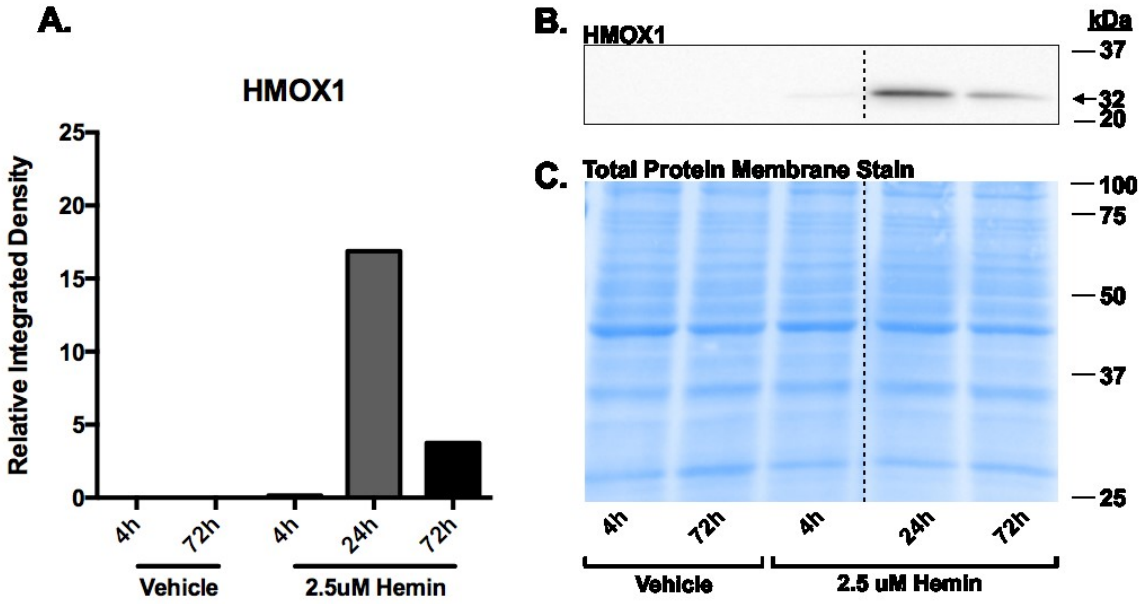

Figure 3.29. Time-Dependent Induction of HMOX1 by Hemin. H9C2 myotubules were exposed to either vehicle or 2.5uM hemin for 4h, 24h or 72h. **(A)** HMOX1 was increased at 4h and peaked at 24h, before attenuating at 72h. **(B)** Representative HMOX1-probed membrane displayed prominent HMOX1-bands at 32 kDa. **(C)** Pierce® Memcode staining demonstrated uniform protein loading on the membrane prior to antibody probe.

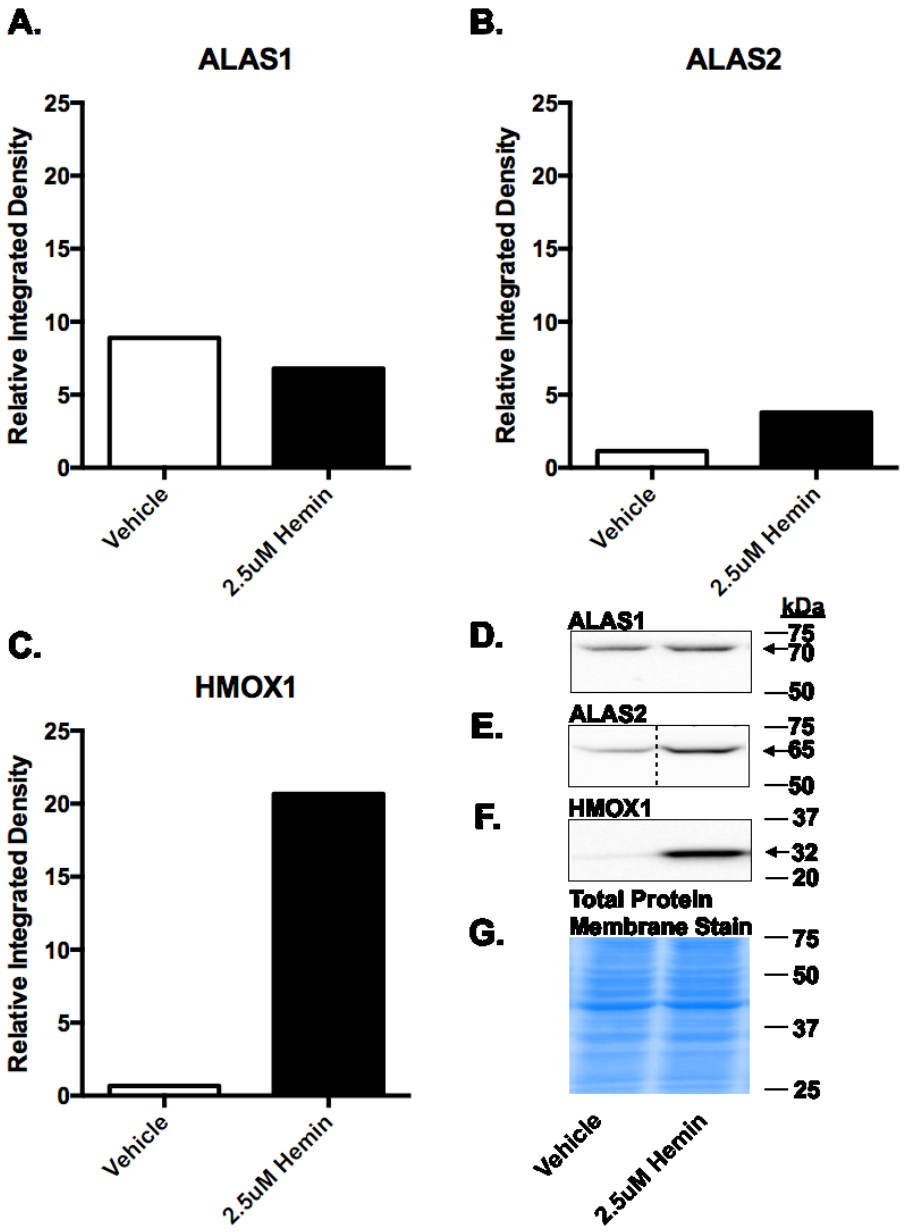

Figure 3.30. Protein Expression of Rate-Limiting Heme Metabolism Enzymes under Heme-Replete Conditions. H9C2 myotubules were exposed to vehicle or 2.5uM hemin for 24h. **(A)** ALAS1 did not vary markedly with hemin. **(B)** ALAS2 increased modestly with hemin **(C)** HMOX1 was markedly increased with hemin administration. **(D)** Representative ALAS1-probed membrane displayed specific prominent ALAS1-bands at 70 kDa. **(E)** Representative ALAS2-probed membrane displayed specific prominent ALAS2- bands at 65 kDa. **(F)** Representative HMOX1-probed membrane displayed specific prominent HMOX1-bands at 32 kDa. **(G)** Pierce® Memcode staining demonstrated uniform protein loading on the membrane prior to antibody probe. Results are representative of 2 independent trials.

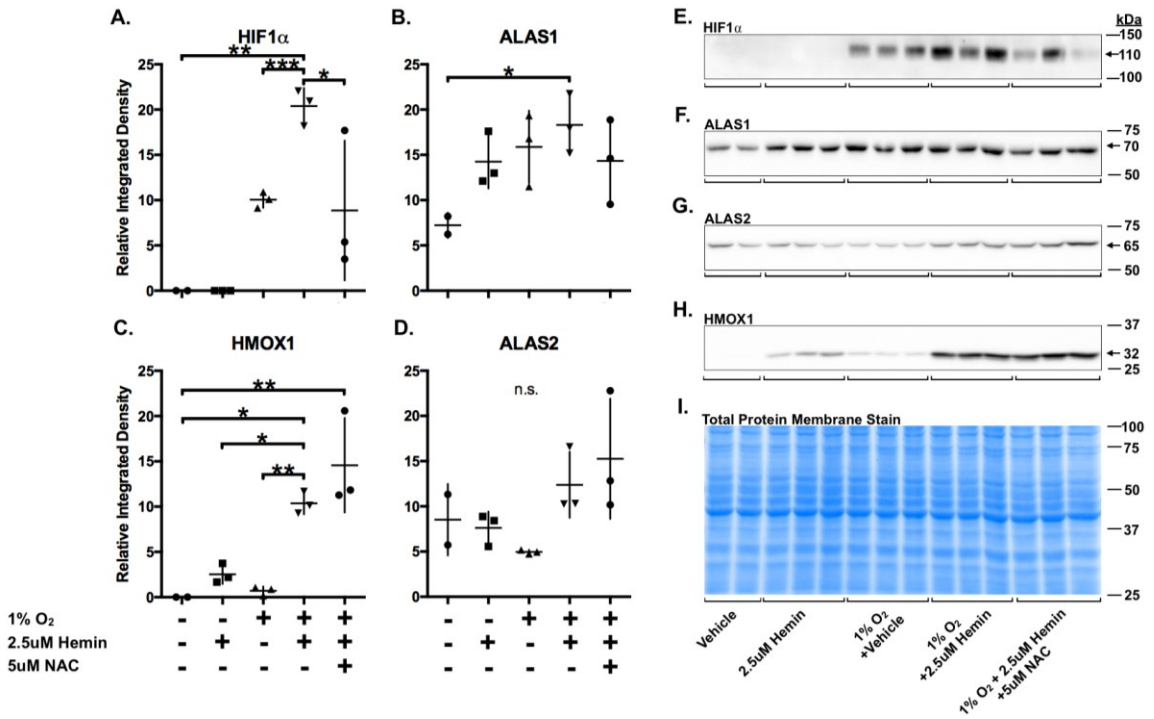

Figure 3.31. HMOX1 and HIF1α are Elevated in Heme-Replete Hypoxia. H9C2 myotubules were exposed to vehicle, 2.5uM hemin, 1% O_2 with vehicle, both hemin in 1% O_2, or hemin, 1% O_2 and 5uM N-acetyl cysteine (NAC) for 24h (N=2-3 biological replicates). **(A)** HIF1α induction in hypoxia was increased in hypoxia-and-hemin-treated cells. Induction of HIF1α was significantly attenuated with 5uM NAC. **(B)** ALAS1 was significantly increased in hypoxia-and-hemin-treated cells. **(C)** HMOX1 was significantly increased in hypoxia-and-hemin-treated cells. Synergistic HMOX1 induction in hypoxia-and-hemin-treated cells was not attenuated by 5uM NAC. **(D)** ALAS2 did not vary significantly between treatments. **(E)** Representative HIF1α-probed membrane displayed prominent HIF1α-bands at 110 kDa. **(F)** Representative ALAS1-probed membrane displayed specific prominent ALAS1-bands at 70 kDa. **(G)** Representative ALAS2-probed membrane displayed specific prominent ALAS2- bands at 65 kDa. **(H)** Representative HMOX1-probed membrane displayed specific prominent HMOX1- bands at 32 kDa. **(I)** Pierce® Memcode staining demonstrated uniform protein loading on the membrane prior to antibody probe. Results are representative of 3 independent trials.

hypoxia alone; HIF1α induction was significantly attenuated by NAC (Figure 3.31-A). ALAS1 was increased in heme-replete hypoxia (Figure 3.31-B). HMOX1 was significantly and synergistically increased in heme-replete hypoxia when compared to either hemin or hypoxia alone; unlike HIF1α, HMOX1 induction was not attenuated by NAC (Figure 3.31-C). ALAS2 did not vary significantly between treatments (Figure 3.31-D).

Synergistic HMOX1 induction in heme-replete hypoxia has been previously reported in proliferative H9C2 exposed to 5uM hemin and anoxia for 18h [109]. However, the synergistic induction was interpreted as an increase in oxidative stress. As such, we examined proliferative H9C2 exposed to either vehicle, 25uM hemin, vehicle in 1% O_2, 25uM hemin in 1% O_2, or 25uM hemin in 1% O_2 with 5uM NAC for 24h (Figure 3.32). Synergistic HMOX1 induction in heme-replete hypoxia was conserved in proliferative H9C2 (Figure 3.32-A) as identified in myotubules (Figure 3.31). To determine whether oxidative stress significantly contributed to synergistic HMOX1 induction in heme-replete hypoxia, proliferative H9C2 were incubated with ROS-sensitive CM-H_2DCFDA. CM-H_2DCFDA fluorescence was quantified by FACS. Hemin-treated and 1% O_2-treated cells demonstrated an increase in fluorescent intensity when compared to normoxic controls (Figure 3.33). Heme-replete hypoxia-treated cells did not show a marked increase in fluorescent intensity compared to either hemin or hypoxia alone. CM-H_2DCFDA intensity was drastically attenuated by 5uM NAC in heme-replete hypoxia-treated cells. To verify whether the synergistic induction of HMOX1 was unique to H9C2 cells, neonatal rat cardiomyocytes (NRCMs) were exposed to either vehicle, 2.5uM hemin, vehicle in 1% O_2, or 2.5uM hemin in 1% O_2 for 24h (Figure 3.34). In NRCMs, both hemin and hypoxia alone demonstrated significant induction of HMOX1, yet synergistic HMOX1 induction was conserved in heme-replete hypoxia.

3.10 HIF2α Overexpression Synergistically Increases HMOX1 Levels in Heme-Replete Hypoxia

To investigate the effect of HIF1α/2α overexpression and HIF1α knockdown on HMOX1 expression in heme replete normoxia, H9C2 myotubules were exposed to vehicle or 2.5uM hemin for 24h with, or without, adenoviral HIF transgene overexpression/shRNA (Figure 3.35). There was no observable difference in HIF1α

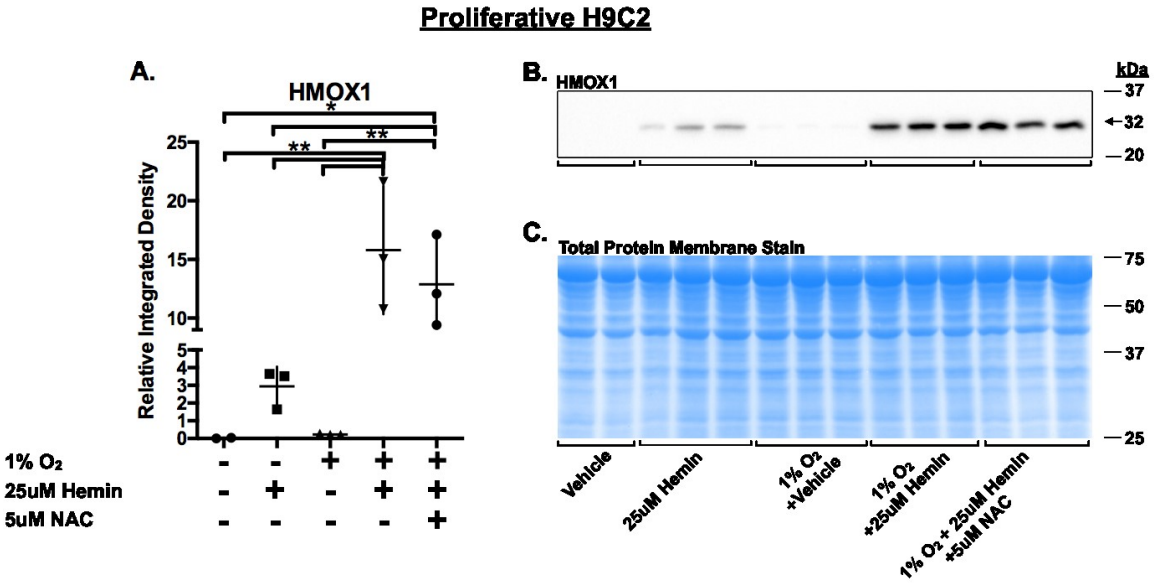

Figure 3.32. Elevation in HMOX1 Expression in Heme-Replete Hypoxia is Conserved in Proliferative H9C2. Proliferative H9C2s were exposed to vehicle, 25uM hemin, 1% O_2 with vehicle, both hemin in 1% O_2, or hemin, hypoxia and 5uM N-acetyl cysteine (NAC) for 24h (N=2-3 biological replicates). **(A)** HMOX1 was increased in hypoxia and further elevated in hemin-treated cells. HMOX1 was synergistically induced in hypoxia-and-hemin-treated cells. Synergistic induction was not significantly attenuated with 5uM NAC. **(B)** Representative HMOX1-probed membrane displayed specific prominent HMOX1- bands at 32 kDa. **(C)** Pierce® Memcode staining demonstrated uniform protein loading on the membrane prior to antibody probe. Results are representative of 3 independent trials.

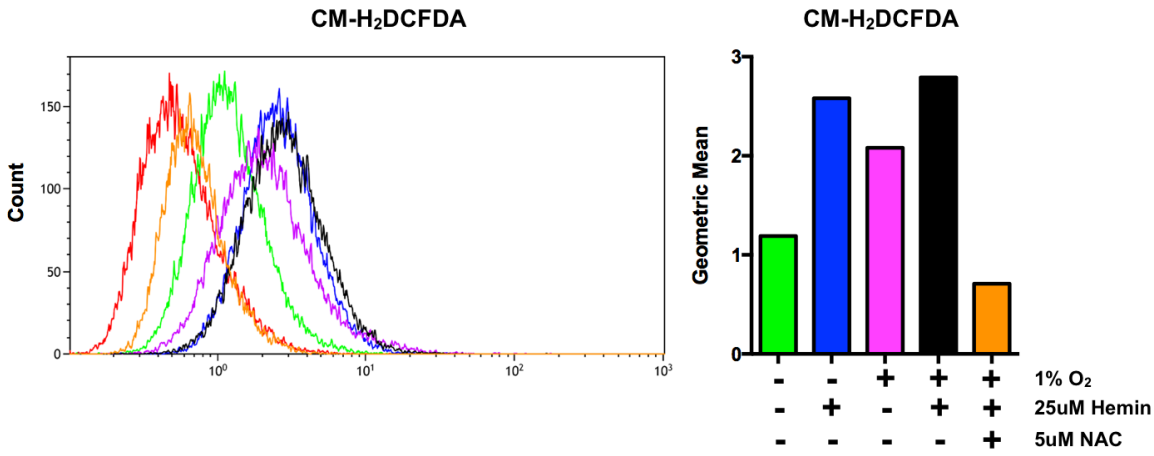

Figure 3.33. CM-H_2DCFDA Quantification of Reactive Oxygen Species (ROS) in Heme-Replete Hypoxia. FACS-derived geometric means of proliferative H9C2 cells incubated with or without 5uM CM-H_2DCFDA for 30min following 24h normoxia (21% O_2) with vehicle, normoxia with 25uM hemin, 1% O_2 with vehicle, 1% O_2 with 25uM hemin, or 1% O_2 with 25uM hemin and 5uM N-acetyl cysteine (NAC). Hemin-treated and 1% O_2-treated cells demonstrated an increase in fluorescent intensity in comparison to normoxic controls. Hemin-and-hypoxia-treated cells did not show a marked increase in fluorescent intensity compared to either hemin or hypoxia alone. CM-H_2DCFDA intensity was attenuated by 5uM NAC in hemin-and-hypoxia-treated cells.

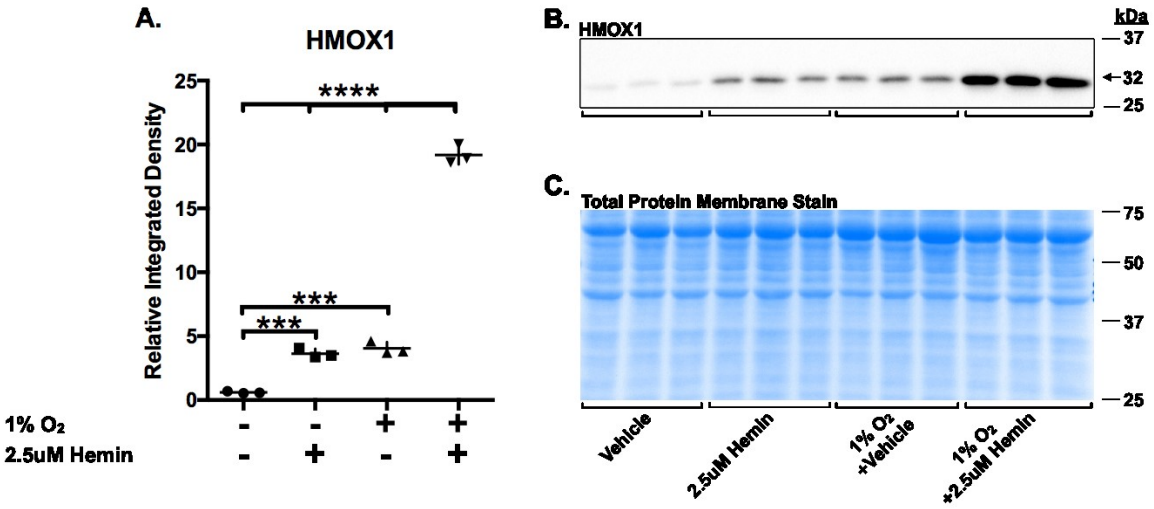

Figure 3.34. Elevation in HMOX1 Expression in Heme-Replete Hypoxia is Conserved in Neonatal Rat Cardiomyocytes. Neonatal rat cardiomyocytes (NRCMs) were exposed to vehicle, 2.5uM hemin, 1% O_2 with vehicle, or both hemin and 1% O_2, (N=3 biological replicates). **(A)** HMOX1 was increased in hypoxia and hemin-treated cells. HMOX1 was synergistically induced in hypoxia-and-hemin-treated cells. **(B)** Representative HMOX1-probed membrane displayed specific prominent HMOX1- bands at 32 kDa. **(C)** Pierce® Memcode staining demonstrated uniform protein loading on the membrane prior to antibody probe.

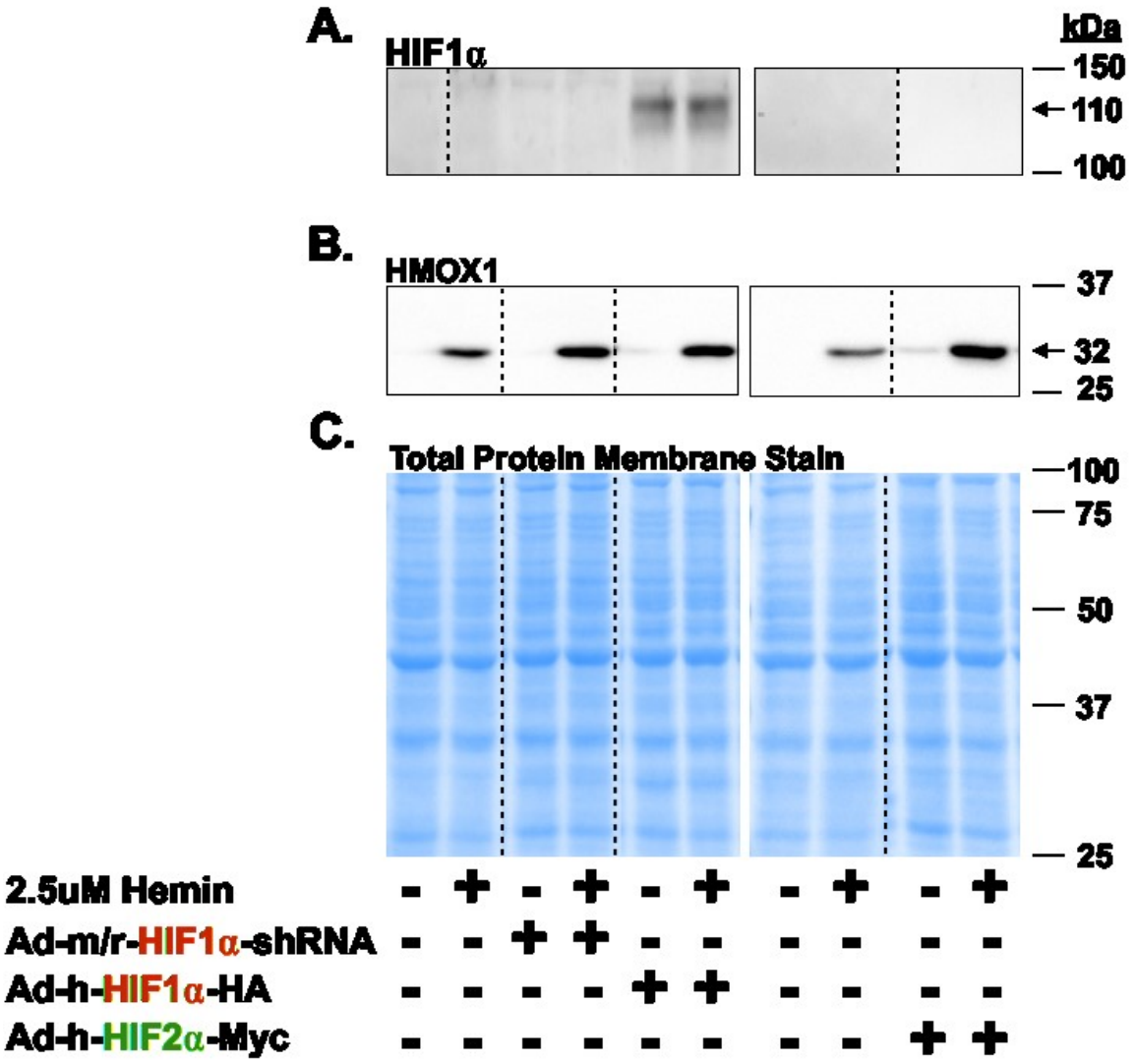

Figure 3.35. Overexpression of HIF1α Does Not Recapitulate Increased HMOX1 Expression Observed in Hypoxia. H9C2 myotubules were exposed to vehicle or 2.5uM hemin for 24h with, or without, adenoviral transduction. **(A)** HIF1α was induced with Ad-h-HIF1α-HA overexpression. **(B)** HMOX1 was increased in hemin-treated cells and with HIF2α overexpression. **(C)** Pierce® Memcode staining demonstrated uniform protein loading on the membrane prior to antibody probe. Results are representative of 2 independent trials.

levels between cells overexpressing HIF1α in vehicle or hemin in normoxia (Figure 3.35-A). HIF1α knockdown did not attenuate HMOX1 induction by hemin (Figure 3.35-B). Overexpression of HIF1α in a heme-replete state did not recapitulate the synergistic increase in HMOX1 expression observed in heme-replete hypoxia. HMOX1 was, however, increased with HIF2α overexpression and hemin (+11.3-fold, +36.5-fold vs hemin 24h).

To investigate the effect of HIF1α/2α overexpression and HIF1α knockdown on HMOX1 expression in heme-replete hypoxia, H9C2 myotubules were exposed to 2.5uM hemin or hemin and 1% O_2 for 24h with, or without adenoviral HIF transgene overexpression/shRNA (Figure 3.36). HMOX1 induction in heme-replete hypoxia may have been slightly attenuated with HIF1α knockdown (-2.4-fold, -1.5-fold vs heme-replete hypoxia). HMOX1 in heme-replete hypoxia was slightly increased with HIF1α overexpression when compared to non-transduced controls (+2.6-fold, -1.3-fold vs heme replete hypoxia). There was no observable difference in HMOX1 levels between cells overexpressing HIF1α in heme-replete hypoxia and HIF2α overexpression with hemin. HMOX1 levels were markedly increased with HIF2α overexpression in heme-replete hypoxia (+2.5-fold, +3.9-fold vs HIF1α overexpression in heme-replete hypoxia). HIF2α overexpression synergistically increased HMOX1 levels in heme-replete hypoxia (+1.6-fold, +12-fold vs non-transduced heme-replete hypoxia).

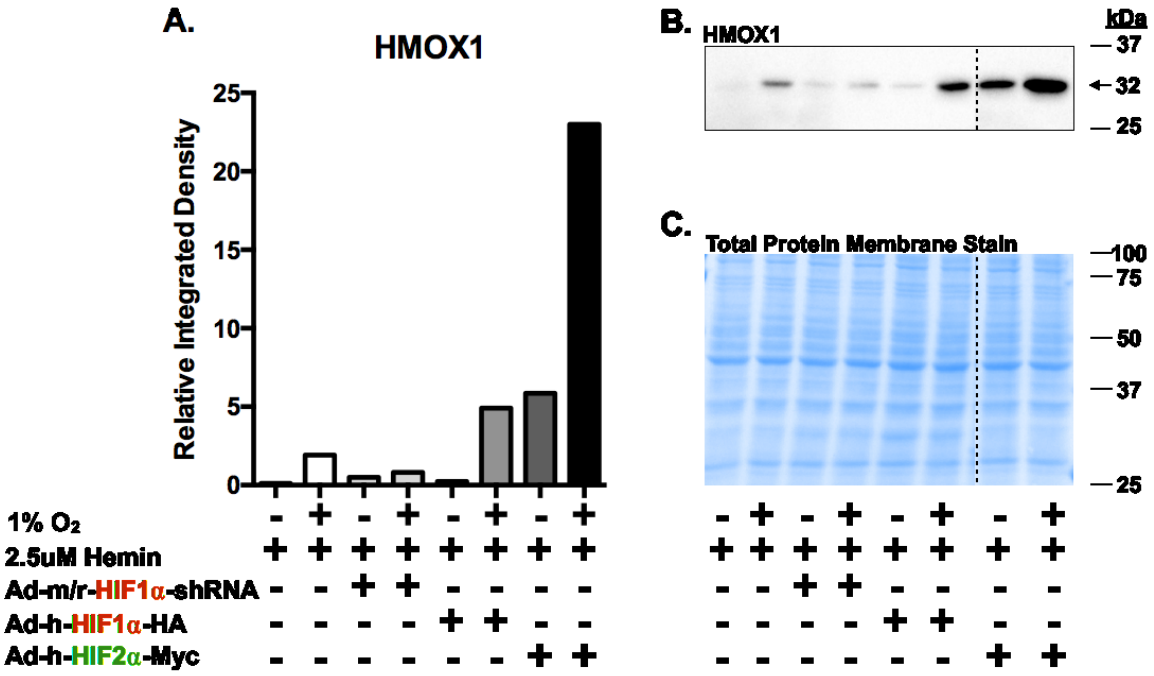

Figure-3.36. HIF2α Overexpression Synergistically Increases HMOX1 Levels in Heme-Replete Hypoxia. H9C2 myotubules were exposed to 2.5uM hemin or hemin and 1% O_2 for 24h with, or without adenoviral transduction. **(A)** HMOX1 induction in hemin-and-hypoxia treated cells was attenuated with Ad-m-HIF1α-shRNA. HMOX1 in Ad-h-HIF1α-HA-transduced hemin-and-hypoxia-treated cells was increased approximately 2-fold higher than non-transduced cells. HMOX1 was synergistically increased in hemin-and-hypoxia-treated cells transduced with Ad-h-HIF2α-Myc. **(B)** Representative HMOX1-probed membrane displayed prominent HMOX1-bands at 32 kDa. **(C)** Pierce® Memcode staining demonstrated uniform protein loading on the membrane prior to antibody probe. Results are representative of 2 independent trials.

CHAPTER 4
Discussion

4.1 Summary of Findings

Much of our understanding of clinical-hypoxia stems from models of acute, intense hypoxia that are not reflective of the degree or duration of hypoxia experienced by cardiac patients. Further, it is within these models that the basic premise of cytoprotection by HMOX1 induction by HIF1α in hypoxia is based. HIF1α is credited as the primary mediator of oxygen homeostasis in the intracellular response to hypoxia, however, little consideration has been given to the role of HIF2α in the myocardium or heme metabolism despite it containing putative heme binding motifs. Similarly, the role of ALAS enzymes in regulating heme bioavailability in the myocardium has been virtually unexplored. Here we show for the first time that heme regulatory enzymes and heme bioavailability differ in their responses to AMI and TAC-induced heart failure over time. Unexpectedly, HMOX1 protein levels were elevated only transiently in AMI and otherwise remained relatively unchanged or decreased in experimental models of heart failure, nor was there evidence of change in HMOX1 in clinical heart failure. However, HMOX1 is increased by HIF2α overexpression and HMOX1 was synergistically increased in heme-replete hypoxia in the presence of HIF2α overexpression (see summary, Table 3.).

Our research provides a series of novel findings. This is the first time that rate-limiting heme regulatory enzyme levels were investigated in AMI or TAC models throughout the progression to failure. Further, this is the first time that heme regulatory enzyme levels, HIFs *and* heme content have been simultaneously measured in the context of heart failure or hypoxia as an inter-related molecular pathway. Importantly, this is the first time that HIF2α overexpression, either directly or indirectly, has been shown to modulate HMOX1 levels. The findings presented here collectively improve our understanding of the complex relationships between heart failure, hypoxia, HIFs and heme regulatory enzymes. These findings may provide insight into the potential therapeutic targeting of the cytoprotective heme metabolism pathway or how increased heme bioavailability could act to sensitize HIF2α-related mechanisms which may also

Table 3. Summary of Clinical and Preclinical Observational Results

Species	Model/condition	Heme	ALAS1	ALAS2	HMOX1	HMOX2	HIF1α	HIF2α	Reference
Human	Heart failure	↑	NM	↑	-/-	NM	NM	NM	[89]
Human	Idiopathic heart failure	NM	↑	NM	-/-	NM	↓	-/-	Eadie *et. al.*
Human	Dilated heart failure	NM	↑	NM	-/-	NM	-/-	-/-	Eadie *et. al*
Rat	AMI	NM	NM	NM	↑	NM	↑	↑	[91]
Mouse	AMI (mRNA)	NM	↓	↓	↑	-/-	↑	-/-	Eadie *et. al*
Mouse	AMI (protein, infarct)	NM	↓	-/-	↑(early)	NM	ND	ND	Eadie *et. al*
Mouse	AMI (protein, peri-infarct)	↑(variable)	↓	↑	↑(early)	ND	ND	ND	Eadie *et. al*
Mouse	TAC (mRNA)	NM	↓	↓	↑	-/-	↑	↓	Eadie *et. al*
Mouse	TAC (protein)	↑	↓	-/-	↓	ND	ND	ND	Eadie *et. al*

-/-, no change; ALAS, delta-aminolevulinic acid synthase; AMI, acute myocardial infarction; HIF, hypoxia inducible factor; HMOX, heme oxygenase; ND, not detected; NM, not measured; TAC, transverse aortic constriction.

be a contributing factor to HMOX1 desensitization in heart failure. These findings lead to a greater basic molecular understanding of HIF2α, heme metabolism and heart failure.

4.2 Expression of Heme Regulatory Enzymes and Hypoxia Inducible Factors in Clinical Heart Failure

HMOX1 is a stress-inducible, cytoprotective enzyme and has been extensively reported to be induced by increased intracellular heme content (mediated through the inhibition of transcriptional repressor Bach1 [80], oxidative stress [92] and/or inflammation [92]). However, it has been previously reported by Khechaduri *et al.* [91] that HMOX1 protein levels remained unchanged, despite measured increases in heme content in human failing hearts. The myocardium in heart failure is in a state of chronic stress and so it is unclear why HMOX1 was not elevated either by oxidative stress, hypoxic stress or the heme-replete state. Our investigation into heme regulatory protein expression in heart failure patients, as well as in pre-clinical models revealed similar results to that of Khechaduri *et al*., in that HMOX1 protein remained unchanged in human heart failure [91]. However, in contrast to their report, we observed a significant increase in ALAS1 in human subjects, whereas they identified an increase in ALAS2, and did not measure ALAS1.

A limitation to our *in silico* analyses obtained from the open-access GEO database is that microarray datasets, despite complying to NCBI's Minimum Information About a Microarray Experiment (MIAME) submission standards [96], datasets were often missing one or more target genes of interest (i.e. ALAS2, HMOX2), so we were unable to confirm altered ALAS2 expression in our human subjects at this time. This may be the result of either a limited gene library or hybridization technique. Further, such findings are also potentially influenced by demographics, comorbidities and medical therapies. Nevertheless, our finding that ALAS1 expression is higher than control subjects adds further insight into heme metabolism and hypoxia inducible factor gene expression in the context of human heart failure. Although the extent of hypoxia within the cardiac biopsies is unclear, it is presumed – based on our understanding of molecular oxygen supply and demands within the failing heart (whether it be dilated or idiopathic heart failure) – that clinical biopsies were obtained from hearts undergoing some degree of hypoxia. It is thus unclear why HIF1α gene expression was *decreased* in end-stage

idiopathic heart failure in the left ventricle. Regulation of HIFs at the transcriptional level remains to be fully understood (i.e. what transcription factors regulate HIFs?). More detailed studies of human heart failure are required. Additionally, dedicated studies of heme metabolism and hypoxia-related factors should be measured using quantitative PCR or RNA-sequencing, proteomics and metabolomics.

The foremost limitation of investigating rate-limiting heme regulatory enzyme and HIF expression in heart failure remains that cardiac biopsies are only obtained immediately during explant for the purpose of transplant, that is in the terminal stage of heart failure when all other forms of intervention have been exhausted. This masks the sequence of molecular events that occurs during the window of therapeutic intervention between initial onset and terminal failure and makes it difficult to distinguish between causal and consequential molecular signalling.

4.3 Expression of Heme Regulatory Enzymes and Hypoxia Inducible Factors in Preclinical Heart Failure

We investigated the expression of heme metabolism enzymes and hypoxia inducible factors in experimental heart failure models over time. Considering the vast number of studies investigating the putative therapeutic benefits elicited by HMOX1 induction in myocardial injury [6-8, 92]), it was surprising that heme metabolism enzymes had never yet been measured, concurrently, throughout the progression of either model of heart failure. In AMI, we did not observe a statistically significant increase in heme bioavailability, however an increase in overall variability was observed from 3 days to 2 weeks post-AMI in comparison to sham and end-stage heart failure. It is unclear why such variability exists. Further studies will examine whether a correlation exists between heme bioavailability and cardiac function in AMI.

Most studies do not account for regional differences in the myocardium (i.e. left, right ventricles, atria or septum), particularly relevant to cardiac samples in AMI (infarct region vs. peri-infarct region). We showed distinct differences in ALAS1, ALAS2 and HMOX1 protein expression between the infarct and peri-infarct regions of left ventricle tissue (Table 3.). This may be the result of different cell compositions and roles between the two regions; the peri-infarct region consists primarily of tentatively viable, yet hypertrophying cardiomyocytes, whereas the infarct consists predominantly of infiltrating

leukocytes/macrophages, fibroblasts and myofibroblasts. The limitation of isolating the infarct by its discoloration, however, is that minor cross-contamination of molecular signalling may still occur and thus immunohistochemistry should further be used to characterize the distinct anatomical and cellular expression. For clinical translation, it becomes important to distinguish between regions when identifying the potential therapeutic window specific to either the surviving myocardium or remodelling scar wall, otherwise important molecular information can be masked either in the infarct or peri-infarct region, which have very different adaptive requirements (i.e. myelofibrosis in the scar, hypertrophy/neovascularisation in the peri-infarct, HMOX1 transience in the infarct vs the peri-infarct).

Here we are the first to identify that within the peri-infarct left ventricle tissue, rate limiting heme synthesis enzymes, ALAS1 and ALAS2, demonstrated isotype switching. ALAS1 was decreased in AMI, whereas ALAS2 was steadily increased over time. This change in ALAS2 is in agreement with the observed increase in ALAS2 protein expression reported in human failing hearts [91]. Over this same period, heme content varied wildly, but lacked statistical significance across timepoints. These results should be examined further with higher N-values or corroborated to cardiac functional parameters over time. Interestingly, despite higher gene expression in 2 and 18 week AMI, HMOX1 protein levels were only increased after the 3 day AMI before returning to near-sham levels. The increase in HMOX1 protein expression may be attributable to the previously characterized early ischemic and/or inflammatory phase [110].

Although we were unable to detect HIF1α and HIF2α in whole heart, Jürgensen *et al.* have previously characterized the temporal-spatial accumulation of both protein isoforms within the nucleus of cardiomyocytes following coronary ligation, presuming that their antibodies were appropriately selective to the isoforms [93]. HIF1α accumulation was reported along the peri-infarct border, while HIF2α accumulation occurred within the remote regions of the peri-infarct zone. Further, HIF2α levels were observed to be elevated over the entire 4week period after coronary artery ligation, wheras HIF1α accumulation is attenuated by 7 days. This continues to suggest a complementary role between the two isoforms, where HIF1α may be responsible for

mediating the cellular response to more sudden and severe hypoxia but HIF2α may in turn regulate an adaptive response in lower, more chronic hypoxia.

After TAC, we observed a significant increase in heme bioavailability. Khechaduri *et al.* demonstrated a similar increase in heme content in clinical heart failure biopsies using an iron-dependent assay to interpret heme content [91]. Using heat and acid, Khechaduri *et al.* removed the heme's iron core, which then reacted with oxalic acid for detection. However, the use of oxalic acid is limited by its crystalline properties: differences in "heme" content by this method are indirect and may be attributable to differences in crystal formation time and light refraction, independent of iron chelation. As well, their assay did not account sufficiently for other sources of iron. Distinguishing between intracellular iron-mediated molecular mechanisms and iron involved in heme metabolism is challenging considering the risk of non-heme iron contamination. We have used a superior method of heme quantification, using direct measures of the enzymatic conversion of heme to biliverdin. It remains to be fully understood whether this increase in heme content with TAC originates predominantly from heme synthesis, from hemoprotein breakdown, or from reduced HMOX1 activity. In TAC, we speculate that this may be the result of free heme release as ALAS1 levels are decreased and ALAS2 levels remain relatively unchanged. In AMI, however, isotype switching is observed and it is unknown what differences in enzymatic activity (if any) exist between ALAS1 and ALAS2.

Cardiac heme regulatory enzyme expression in TAC differed from AMI. Following TAC, both ALAS1 and ALAS2 protein expression were not in agreement with their respective mRNA expression, however this was not entirely unexpected as ALAS is also regulated by post-transcriptional modification and mRNA stability [111]. ALAS1 protein expression was significantly decreased with TAC. However, ALAS2 remained relatively unchanged. Heme content gradually increased with TAC, yet HMOX1 protein expression was decreased over time. The gradual decrease in HMOX1 in response to TAC is interesting as previous reports have shown detrimental, not therapeutic, effects of cardiac-specific HMOX1 overexpression in mice after TAC [90], in contrast to extensive studies of AMI [6, 8, 87]). The differences may be related to the duration of HMOX1 expression or the severity and type of stress in the myocardium. In AMI, after the initial

ischemia causes oxidative and hypoxic stress further injury is caused by excessive inflammation. However, in TAC there is believed to be continuous chronic oxidative stress due to metabolic contractility demands to maintain cardiac output, hypertrophy and increased angiotensin II [112]. Further, hypoxia and nutrient deprivation likely builds chronically in TAC as interstitial perivascular fibrosis accumulates [54]. These findings could indicate that the balance between therapeutic or detrimental effects of HMOX1 expression levels depend on other endogenous signalling mechanisms. This may also suggest that decreased or unchanging HMOX1 levels could be an adaptive response to myocardial injury in some contexts.

A limitation to the use of whole hearts in investigating heme regulatory enzyme and hypoxia inducible factor expression is that of its cellular makeup. As previously discussed, pathological cardiac remodeling increases the activation and infiltration of fibroblasts and macrophages respectively within the myocardium. Even in consideration to the cardiomyocytes of the whole heart, this classification includes distinct cells of the atrioventricular node, bundles of HIS, septum, and right or left ventricles-each serving a distinctly different role within the heart, and thus potentially exerting divergent heme metabolism and hypoxia inducible factor responses. Nonetheless, whole heart studies are critical to placing heme regulatory enzyme and hypoxia inducible factor expression within the context of these cell-cell interactions as well as the functional myocardium as a whole. In future studies, we will seek to minimize this by characterizing the septum, and right and left ventricles specifically to detail changes in these regions. Performing additional *in vitro* experiments on non-cardiomyocytes from the heart (specifically fibroblasts or vascular cells) would also provide added information. As well, detailed immunohistochemical analysis is required to identify the specific cells in which the changes are predominantly occurring.

4.4 HIF2α as a Novel Regulator of HMOX1 in Hypoxia

HIF1α has been extensively studied in acute, severe conditions of hypoxia. It is under these conditions that HIF1α has been shown to transactivate the HMOX1 promoter [113] to elicit protection from hypoxic and oxidative stress [114, 115], though this may not persist in chronic states [90, 116]. Interestingly, the byproduct of heme catabolism, CO has also shown to be capable of stabilizing HIF1α [117]. We sought to compare heme metabolism and hypoxia inducible factor expression in various severity and duration of hypoxia. Protein expression did not vary markedly between 24h and 72h hypoxia in 8% O_2 or 1% O_2. The degree of moderate (8% O_2) hypoxia may have posed a limitation as, relative to H9C2 myotubules, oxygen tension may not have been lowered to a level of intracellularly moderate hypoxia. This further limited our ability to investigate whether HIF2α adopted the role of primary regulator of oxygen homeostasis in chronic, moderate hypoxia. Decreasing oxygen levels to 8% O_2 from the normal culture conditions (21% O_2, 2.6-fold lower) was presumed to accomplish moderate hypoxia and further gradation studies are warranted.

To elucidate the effect of HIF1α and HIF2α overexpression and HIF1α knockdown on rate-limiting heme metabolism enzyme protein expression, H9C2 myotubules were transduced with adenoviral vectors encoding human HIF1α/2α or HIF1α shRNA. Due to a limited ability to measure HIF2α gene and protein expression and not being able to confirm knockdown of HIF2α in H9C2s, adenoviral HIF2α shRNA vectors were not able to be included in the present study. In agreement with previous reports [113], HIF1α overexpression increased HMOX1 levels in 1% O_2 and HMOX1 induction in 1% O_2 was attenuated by HIF1α knockdown. For the first time, we have shown that HIF2α overexpression increases HMOX1 levels in both normoxia and hypoxia. It remains unclear whether differences exist between HIF1α and HIF2α stabilization or rate of transcription for different target genes.

In contrast to our initial hypothesis, we did not find that ALAS or HMOX1 was regulated by HIF2α in chronic/moderate hypoxia. It is unclear why HMOX1 levels were increased after 72h at baseline. In alignment with our intitial hypothesis, we have shown that HIF2α regulates HMOX1, either directly or indirectly. Expression of either HIF1α

or HIF2α increased heme bioavailabilty to a similar degree. Surprisingly, HIF1α knockdown also resulted in further relative increase in heme bioavailabilty, both in normoxia and after 24h at 1% O_2. Considering the role of heme as an essential oxygen carrier, and HIF1α as a principle mediator of oxygen homeostasis in hypoxia, it is unclear why HIF1α knockdown increases heme bioavailability. Further experimental replication is required to confirm these results but compensation, maybe by HIF2α, could be implicated. Moving forward, additional optimization and validation of our HIF2α shRNA vector, or use of short-interfering RNA, will be of utmost priority to elucidate the mechanisms of HMOX1 regulation by HIF2α definitively.

4.5 Synergistic HMOX1 Induction in Heme-Replete Hypoxia is Independent of ROS but Amplified by HIF2α Overexpression

In heart failure a heme-replete and hypoxic state have been previously reported [91, 93]. We defined a heme-replete state as a high level of heme exposure, without overt heme-toxicity. Thus, we sought to characterize rate-limiting heme metabolism and hypoxia inducible factor protein expression in H9C2 myotubules in heme-replete hypoxia (2.5uM hemin and 1% O_2, 24h; see Table 4. for a summary report). In agreement with Foresti *et al.*, 2001 [109], we observed synergistic increase in HMOX1 levels in H9C2 cells under heme-replete hypoxia. However, administration of 5uM NAC and confirmation of ROS reduction in heme-replete hypoxia by CM-H_2DCFDA proved that HMOX1 levels were synergistically increased in heme-replete hypoxia, independent of ROS in contrast to the mechanism purported by Foresti *et al*. Synergistic increase in HMOX1 protein, independent of ROS expression was conserved across proliferative H9C2 and NRCMs. It could be hypothesized that, in low oxygen tension, abundant heme releases the transcriptional repressor Bach1 from the HMOX1 promoter region. This would provide an opportunity for transactivation by HIF1α and/or HIF2α. Thus, H9C2 myotubules were transduced with adenoviral vectors to overexpress or knockdown HIF1α or HIF2α. We find that increased transgene of HIF2α, more than HIF1α, synergistically increased HMOX1 levels in heme-replete hypoxia. This additional synergism may be the result of a HIF2α stabilization by the putative heme-regulatory motifs found in HIF2α [118]. Further experiments involving HIF2α knockdown and

Table 4. Summary of *In Vitro* Observational Results

Cell Type	Condition	Heme	ALAS1	ALAS2	HMOX1	HMOX2	HIF1α	HIF2α	Reference
H9C2 (p)	Heme-replete hypoxia	NM	NM	NM	↑	NM	↑	NM	[107]
H9C2 (p)	Heme-replete hypoxia	NM	-/-	-/-	↑	NM	ND	ND	Eadie *et. al.*
H9C2 (d)	Heme-replete hypoxia	NM	-/-	-/-	↑	NM	↑	ND	Eadie *et. al.*
H9C2 (p)	Hemin	NM	NM	NM	↑	NM	NM	NM	[119]
H9C2 (p)	Hemin	NM	-/-	NM	↑	ND	ND	ND	Eadie *et. al.*
H9C2 (d)	Hemin	NM	-/-	-/-	↑	ND	ND	ND	Eadie *et. al.*
H9C2	Hypoxia	NM	NM	NM	↑	NM	NM	NM	[120]
H9C2 (d)	Hypoxia	↑	-/-	↓	↑	ND	↑	ND	Eadie *et. al*
NRCM	Heme-replete hypoxia	NM	-/-	-/-	↑	NM	ND	ND	Eadie *et. al*
NRCM	Hypoxia	NM	NM	NM	NM	NM	↑	NM	[121]

-/-, no change; ALAS, delta-aminolevulinic acid synthase; ARCM, adult rat cardiomyocyte; d, differentiated; HIF, hypoxia inducible factor; HMOX, heme oxygenase; ND, not detected; NM, not measured; NRCM, neonatal rat cardiomyocyte; p, proliferative.

immunoprecipitated pulldown, subsequent probing for heme and the HMOX1 promoter sequence using the adenoviral HIF2α Myc tag, are required to better understand how HIF2α regulates HMOX1 levels.

4.6 Implications for Pharmacological Management of Heart Failure

The findings reported here continue to bring about new perspectives and questions regarding the pharmacological targeting of the heme metabolism pathway in heart failure, questions that have failed to be addressed adequately. Namely, when do we target heme metabolism and how might we best achieve therapeutic efficacy? It remains unclear whether the changes in heme bioavailability and the relatively unchanged expression of HMOX1 is adaptive or maladaptive. If adaptive then elevating heme bioavailability would be appropriate. However, if maladaptive then only HMOX1 based therapies would be appropriate. Yet, this could also be context dependent – for example, requiring a heme based approach for preventing heart failure in hypertension heart failure, whereas a HMOX1 strategy would be effective in ischemia induced heart failure. Still we lack sufficient context to determine the best strategy for clinical pharmacology translation at this time.

With the advent of prolyl hydroxylase inhibitors, or "HIF" stabilizers, as potential treatment options for tissue hypoxia or ischemia, our finding that HIF2α can synergistically increase HMOX1 is further implicated in the treatment of heart failure. HIF stabilizers aim to increase vascularization to hypoxic tissue and harness the pleiotropic effects of transcription factor therapy to produce multiple mRNA products (greater than 200 in the case of HIF1α). However, our finding that HIF2α is implicated in the increase of HMOX1 more prominently than HIF1α it is unclear whether HIF-stabilizers can be isotype selective and whether this is essential to their therapeutic potential.

Moving forward, it will also be important to take into consideration the existing clinical standards of care. One of the limitations to preclinical modeling of heart failure, and one that we hope to address in the future, is that not only are the patient demographics not being reflected in animal models (i.e. sex and age) but neither are the effects of standard medications. It remains unclear how medications such as: β-antagonists, angiotensin-converting enzyme inhibitors, antiplatelet agents or statins affect

heme bioavailability or heme regulatory enzyme expression, thus potentially resulting in discordance or risk of adverse side effects from therapeutic heme metabolism-targeting as we translate preclinical models to patients.

4.7 Conclusions

In conclusion, the current study characterizes heme regulatory enzyme expression comparatively throughout volume and pressure overload-induced heart failure and shows for the first time that HIF2α is a novel regulator of HMOX1. Further understanding of heme regulation with respect to HIF2α is required to optimize therapeutic targeting of the heme metabolic pathway in heart failure.

REFERENCES

[1] Ponikowski P, Anker SD, AlHabib KF, Cowie MR, Force TL, Hu S, et al. Heart failure: preventing disease and death worldwide. ESC Heart Failure. 2014;1:4-25.

[2] Mozaffarian D, Benjamin EJ, Go AS, Arnett DK, Blaha MJ, Cushman M, et al. Heart Disease and Stroke Statistics—2016 Update. A Report From the American Heart Association. 2015.

[3] Roger VL. Epidemiology of heart failure. Circulation research. 2013;113:646-59.

[4] Ma X, Sayed N, Beuve A, van den Akker F. NO and CO differentially activate soluble guanylyl cyclase via a heme pivot-bend mechanism. The EMBO journal. 2007;26:578-88.

[5] Balla G, Jacob HS, Balla J, Rosenberg M, Nath K, Apple F, et al. Ferritin: a cytoprotective antioxidant strategem of endothelium. The Journal of biological chemistry. 1992;267:18148-53.

[6] Liu X, Simpson JA, Brunt KR, Ward CA, Hall SR, Kinobe RT, et al. Preemptive heme oxygenase-1 gene delivery reveals reduced mortality and preservation of left ventricular function 1 yr after acute myocardial infarction. American journal of physiology Heart and circulatory physiology. 2007;293:H48-59.

[7] Yet SF, Tian R, Layne MD, Wang ZY, Maemura K, Solovyeva M, et al. Cardiac-specific expression of heme oxygenase-1 protects against ischemia and reperfusion injury in transgenic mice. Circulation research. 2001;89:168-73.

[8] Collino M, Pini A, Mugelli N, Mastroianni R, Bani D, Fantozzi R, et al. Beneficial effect of prolonged heme oxygenase 1 activation in a rat model of chronic heart failure. Disease models & mechanisms. 2013;6:1012-20.

[9] Ponikowski P, Voors AA, Anker SD, Bueno H, Cleland JG, Coats AJ, et al. 2016 ESC Guidelines for the diagnosis and treatment of acute and chronic heart failure: The Task Force for the diagnosis and treatment of acute and chronic heart failure of the European Society of Cardiology (ESC). Developed with the special contribution of the Heart Failure Association (HFA) of the ESC. European journal of heart failure. 2016;18:891-975.

[10] Mann DL, Bristow MR. Mechanisms and models in heart failure: the biomechanical model and beyond. Circulation. 2005;111:2837-49.

[11] Voelkel NF, Quaife RA, Leinwand LA, Barst RJ, McGoon MD, Meldrum DR, et al. Right ventricular function and failure: report of a National Heart, Lung, and Blood Institute working group on cellular and molecular mechanisms of right heart failure. Circulation. 2006;114:1883-91.

[12] Drazner MH. The progression of hypertensive heart disease. Circulation. 2011;123:327-34.

[13] Scallan J, Huxley VH, Korthuis RJ. Capillary Fluid Exchange: Regulation, Functions, and Pathology. San Rafael CA: 2010 by Morgan & Claypool Life Sciences.; 2010.

[14] Kee K, Naughton MT. Heart failure and the lung. Circulation journal : official journal of the Japanese Circulation Society. 2010;74:2507-16.

[15] Clark AL, Cleland JG. Causes and treatment of oedema in patients with heart failure. Nature reviews Cardiology. 2013;10:156-70.

[16] Sabbah HN, Sharov VG, Lesch M, Goldstein S. Progression of heart failure: a role for interstitial fibrosis. Molecular and cellular biochemistry. 1995;147:29-34.

[17] Cho S, Atwood JE. Peripheral edema. The American journal of medicine. 2002;113:580-6.

[18] Mosterd A, Hoes AW. Clinical epidemiology of heart failure. Heart. 2007;93:1137-46.

[19] Thygesen K, Alpert JS, Jaffe AS, Simoons ML, Chaitman BR, White HD, et al. Third universal definition of myocardial infarction. J Am Coll Cardiol. 2012;60:1581-98.

[20] Inoue T, Ide T, Yamato M, Yoshida M, Tsutsumi T, Andou M, et al. Time-dependent changes of myocardial and systemic oxidative stress are dissociated after myocardial infarction. Free radical research. 2009;43:37-46.

[21] Neri M, Fineschi V, Di Paolo M, Pomara C, Riezzo I, Turillazzi E, et al. Cardiac oxidative stress and inflammatory cytokines response after myocardial infarction. Current vascular pharmacology. 2015;13:26-36.

[22] Nian M, Lee P, Khaper N, Liu P. Inflammatory cytokines and postmyocardial infarction remodeling. Circulation research. 2004;94:1543-53.

[23] Muntean DM, Sturza A, Danila MD, Borza C, Duicu OM, Mornos C. The Role of Mitochondrial Reactive Oxygen Species in Cardiovascular Injury and Protective Strategies. Oxidative medicine and cellular longevity. 2016;2016:8254942.

[24] Sutton MG, Sharpe N. Left ventricular remodeling after myocardial infarction: pathophysiology and therapy. Circulation. 2000;101:2981-8.

[25] Talman V, Ruskoaho H. Cardiac fibrosis in myocardial infarction-from repair and remodeling to regeneration. Cell and tissue research. 2016.

[26] Eadie AL, Simpson JA, Brunt KR. "Fibroblast" pharmacotherapy - Advancing the next generation of therapeutics for clinical cardiology. Journal of molecular and cellular cardiology. 2016;94:176-9.

[27] Hill JA, Karimi M, Kutschke W, Davisson RL, Zimmerman K, Wang Z, et al. Cardiac hypertrophy is not a required compensatory response to short-term pressure overload. Circulation. 2000;101:2863-9.

[28] van Deel ED, Lu Z, Xu X, Zhu G, Hu X, Oury TD, et al. Extracellular superoxide dismutase protects the heart against oxidative stress and hypertrophy after myocardial infarction. Free radical biology & medicine. 2008;44:1305-13.

[29] Hilfiker-Kleiner D, Landmesser U, Drexler H. Molecular Mechanisms in Heart FailureFocus on Cardiac Hypertrophy, Inflammation, Angiogenesis, and Apoptosis. Journal of the American College of Cardiology. 2006;48:A56-A66.

[30] Sutendra G, Dromparis P, Paulin R, Zervopoulos S, Haromy A, Nagendran J, et al. A metabolic remodeling in right ventricular hypertrophy is associated with decreased angiogenesis and a transition from a compensated to a decompensated state in pulmonary hypertension. Journal of molecular medicine (Berlin, Germany). 2013;91:1315-27.

[31] Swynghedauw B. Molecular mechanisms of myocardial remodeling. Physiological reviews. 1999;79:215-62.

[32] Ito BR. Gradual onset of myocardial ischemia results in reduced myocardial infarction. Association with reduced contractile function and metabolic downregulation. Circulation. 1995;91:2058-70.

[33] Fukuoka Y, Nakano A, Tama N, Hasegawa K, Ikeda H, Morishita T, et al. Impaired myocardial microcirculation in the flow-glucose metabolism mismatch regions in revascularized acute myocardial infarction. Journal of nuclear cardiology : official publication of the American Society of Nuclear Cardiology. 2016.

[34] Leung AA, Nerenberg K, Daskalopoulou SS, McBrien K, Zarnke KB, Dasgupta K, et al. Hypertension Canada's 2016 Canadian Hypertension Education Program Guidelines for Blood Pressure Measurement, Diagnosis, Assessment of Risk, Prevention, and Treatment of Hypertension. The Canadian journal of cardiology. 2016;32:569-88.

[35] Peterson KL. Pressure overload hypertrophy and congestive heart failure. Where is the "Achilles' heel"? J Am Coll Cardiol. 2002;39:672-5.

[36] Jackson G, Gibbs CR, Davies MK, Lip GYH. Pathophysiology. BMJ : British Medical Journal. 2000;320:167-70.

[37] Sterpetti AV, Cucina A, D'Angelo LS, Cardillo B, Cavallaro A. Shear stress modulates the proliferation rate, protein synthesis, and mitogenic activity of arterial smooth muscle cells. Surgery. 1993;113:691-9.

[38] Moosavi SM, Johns EJ. Effect of renal perfusion pressure on renal function, renin release and renin and angiotensinogen gene expression in rats. The Journal of physiology. 1999;520 Pt 1:261-9.

[39] Ashley EA, Niebauer J. Cardiology Explained. London: Remedica.; 2004.

[40] Liu Z, Chen JM, Huang H, Kuznicki M, Zheng S, Sun W, et al. The protective effect of trimetazidine on myocardial ischemia/reperfusion injury through activating AMPK and ERK signaling pathway. Metabolism: clinical and experimental. 2016;65:122-30.

[41] Patten RD, Hall-Porter MR. Small animal models of heart failure: development of novel therapies, past and present. Circulation Heart failure. 2009;2:138-44.

[42] Pei H, Song X, Peng C, Tan Y, Li Y, Li X, et al. TNF-alpha inhibitor protects against myocardial ischemia/reperfusion injury via Notch1-mediated suppression of oxidative/nitrative stress. Free radical biology & medicine. 2015;82:114-21.

[43] Carretero OA, Oparil S. Essential hypertension. Part I: definition and etiology. Circulation. 2000;101:329-35.

[44] Hasenfuss G. Animal models of human cardiovascular disease, heart failure and hypertrophy. Cardiovascular research. 1998;39:60-76.

[45] Molina EJ, Gupta D, Palma J, Torres D, Gaughan JP, Houser S, et al. Novel experimental model of pressure overload hypertrophy in rats. The Journal of surgical research. 2009;153:287-94.

[46] Franchini KG, Torsoni AS, Soares PH, Saad MJ. Early activation of the multicomponent signaling complex associated with focal adhesion kinase induced by pressure overload in the rat heart. Circulation research. 2000;87:558-65.

[47] Seymour AM, Giles L, Ball V, Miller JJ, Clarke K, Carr CA, et al. In vivo assessment of cardiac metabolism and function in the abdominal aortic banding model of compensated cardiac hypertrophy. Cardiovascular research. 2015;106:249-60.

[48] Tarnavski O. Mouse surgical models in cardiovascular research. Methods in molecular biology (Clifton, NJ). 2009;573:115-37.

[49] Maulik SK, Kumar S. Oxidative stress and cardiac hypertrophy: a review. Toxicology mechanisms and methods. 2012;22:359-66.

[50] Giordano FJ. Oxygen, oxidative stress, hypoxia, and heart failure. The Journal of clinical investigation. 2005;115:500-8.

[51] Hamanaka RB, Chandel NS. Mitochondrial reactive oxygen species regulate hypoxic signaling. Current opinion in cell biology. 2009;21:894-9.

[52] Nikinmaa M. What is hypoxia? Acta physiologica (Oxford, England). 2013;209:1-4.

[53] Iemitsu M, Miyauchi T, Maeda S, Sakai S, Kobayashi T, Fujii N, et al. Physiological and pathological cardiac hypertrophy induce different molecular phenotypes in the rat. American journal of physiology Regulatory, integrative and comparative physiology. 2001;281:R2029-36.

[54] Piek A, de Boer RA, Sillje HH. The fibrosis-cell death axis in heart failure. Heart failure reviews. 2016;21:199-211.

[55] Otterbein LE, Foresti R, Motterlini R. Heme Oxygenase-1 and Carbon Monoxide in the Heart: The Balancing Act Between Danger Signaling and Pro-Survival. Circulation research. 2016;118:1940-59.

[56] Semenza GL. Hypoxia-inducible factor 1 and cardiovascular disease. Annual review of physiology. 2014;76:39-56.

[57] Dashkevich A, Hagl C, Beyersdorf F, Nykanen AI, Lemstrom KB. VEGF Pathways in the Lymphatics of Healthy and Diseased Heart. Microcirculation (New York, NY : 1994). 2016;23:5-14.

[58] Sanchis-Gomar F, Garcia-Gimenez JL, Pareja-Galeano H, Romagnoli M, Perez-Quilis C, Lippi G. Erythropoietin and the heart: physiological effects and the therapeutic perspective. International journal of cardiology. 2014;171:116-25.

[59] Yang ZZ, Zou AP. Transcriptional regulation of heme oxygenases by HIF-1alpha in renal medullary interstitial cells. American journal of physiology Renal physiology. 2001;281:F900-8.

[60] Lee JW, Bae SH, Jeong JW, Kim SH, Kim KW. Hypoxia-inducible factor (HIF-1)alpha: its protein stability and biological functions. Experimental & molecular medicine. 2004;36:1-12.

[61] Loboda A, Jozkowicz A, Dulak J. HIF-1 and HIF-2 transcription factors--similar but not identical. Molecules and cells. 2010;29:435-42.

[62] Yuan Y, Hilliard G, Ferguson T, Millhorn DE. Cobalt inhibits the interaction between hypoxia-inducible factor-alpha and von Hippel-Lindau protein by direct binding to hypoxia-inducible factor-alpha. The Journal of biological chemistry. 2003;278:15911-6.

[63] Huang BW, Miyazawa M, Tsuji Y. Distinct regulatory mechanisms of the human ferritin gene by hypoxia and hypoxia mimetic cobalt chloride at the transcriptional and post-transcriptional levels. Cellular signalling. 2014;26:2702-9.

[64] Shafighi M, Olariu R, Fathi AR, Djafarzadeh S, Jakob SM, Banic A, et al. Dimethyloxalylglycine stabilizes HIF-1alpha in cultured human endothelial cells and increases random-pattern skin flap survival in vivo. Plastic and reconstructive surgery. 2011;128:415-22.

[65] Liu Q, Davidoff O, Niss K, Haase VH. Hypoxia-inducible factor regulates hepcidin via erythropoietin-induced erythropoiesis. The Journal of clinical investigation. 2012;122:4635-44.

[66] Sanchez M, Galy B, Muckenthaler MU, Hentze MW. Iron-regulatory proteins limit hypoxia-inducible factor-2alpha expression in iron deficiency. Nature structural & molecular biology. 2007;14:420-6.

[67] Piccinelli P, Samuelsson T. Evolution of the iron-responsive element. Rna. 2007;13:952-66.

[68] Semenza GL. HIF-1, O(2), and the 3 PHDs: how animal cells signal hypoxia to the nucleus. Cell. 2001;107:1-3.

[69] Thomson AM, Rogers JT, Leedman PJ. Iron-regulatory proteins, iron-responsive elements and ferritin mRNA translation. The international journal of biochemistry & cell biology. 1999;31:1139-52.

[70] Theil EC. Regulation of ferritin and transferrin receptor mRNAs. The Journal of biological chemistry. 1990;265:4771-4.

[71] Dandekar T, Stripecke R, Gray NK, Goossen B, Constable A, Johansson HE, et al. Identification of a novel iron-responsive element in murine and human erythroid delta-aminolevulinic acid synthase mRNA. The EMBO journal. 1991;10:1903-9.

[72] Mastrogiannaki M, Matak P, Keith B, Simon MC, Vaulont S, Peyssonnaux C. HIF-2α, but not HIF-1α, promotes iron absorption in mice. The Journal of clinical investigation. 2009;119:1159-66.

[73] Zhang L, Guarente L. Heme binds to a short sequence that serves a regulatory function in diverse proteins. The EMBO journal. 1995;14:313-20.

[74] Aisen P, Enns C, Wessling-Resnick M. Chemistry and biology of eukaryotic iron metabolism. The international journal of biochemistry & cell biology. 2001;33:940-59.

[75] Kumar S, Bandyopadhyay U. Free heme toxicity and its detoxification systems in human. Toxicology letters. 2005;157:175-88.

[76] Ajioka RS, Phillips JD, Kushner JP. Biosynthesis of heme in mammals. Biochimica et biophysica acta. 2006;1763:723-36.

[77] Granick S. The induction in vitro of the synthesis of delta-aminolevulinic acid synthetase in chemical porphyria: a response to certain drugs, sex hormones, and foreign chemicals. The Journal of biological chemistry. 1966;241:1359-75.

[78] Fuchs O, Ponka P. The role of iron supply in the regulation of 5-aminolevulinate synthase mRNA levels in murine erythroleukemia cells. Neoplasma. 1996;43:31-6.

[79] Tenhunen R, Marver HS, Schmid R. The enzymatic conversion of heme to bilirubin by microsomal heme oxygenase. Proceedings of the National Academy of Sciences of the United States of America. 1968;61:748-55.

[80] Sun J, Hoshino H, Takaku K, Nakajima O, Muto A, Suzuki H, et al. Hemoprotein Bach1 regulates enhancer availability of heme oxygenase-1 gene. The EMBO journal. 2002;21:5216-24.

[81] Nath KA, Balla G, Vercellotti GM, Balla J, Jacob HS, Levitt MD, et al. Induction of heme oxygenase is a rapid, protective response in rhabdomyolysis in the rat. The Journal of clinical investigation. 1992;90:267-70.

[82] Ryter SW, Choi AM. Targeting heme oxygenase-1 and carbon monoxide for therapeutic modulation of inflammation. Translational research : the journal of laboratory and clinical medicine. 2016;167:7-34.

[83] Baranano DE, Rao M, Ferris CD, Snyder SH. Biliverdin reductase: a major physiologic cytoprotectant. Proceedings of the National Academy of Sciences of the United States of America. 2002;99:16093-8.

[84] Otterbein LE, Bach FH, Alam J, Soares M, Tao Lu H, Wysk M, et al. Carbon monoxide has anti-inflammatory effects involving the mitogen-activated protein kinase pathway. Nature medicine. 2000;6:422-8.

[85] Sadrzadeh SM, Graf E, Panter SS, Hallaway PE, Eaton JW. Hemoglobin. A biologic fenton reagent. The Journal of biological chemistry. 1984;259:14354-6.

[86] Asano T, Komatsu M, Yamaguchi-Iwai Y, Ishikawa F, Mizushima N, Iwai K. Distinct mechanisms of ferritin delivery to lysosomes in iron-depleted and iron-replete cells. Molecular and cellular biology. 2011;31:2040-52.

[87] Liu X, Pachori AS, Ward CA, Davis JP, Gnecchi M, Kong D, et al. Heme oxygenase-1 (HO-1) inhibits postmyocardial infarct remodeling and restores ventricular function. FASEB journal : official publication of the Federation of American Societies for Experimental Biology. 2006;20:207-16.

[88] Sabaawy HE, Zhang F, Nguyen X, ElHosseiny A, Nasjletti A, Schwartzman M, et al. Human heme oxygenase-1 gene transfer lowers blood pressure and promotes growth in spontaneously hypertensive rats. Hypertension (Dallas, Tex : 1979). 2001;38:210-5.

[89] Jais A, Einwallner E, Sharif O, Gossens K, Lu TT, Soyal SM, et al. Heme oxygenase-1 drives metaflammation and insulin resistance in mouse and man. Cell. 2014;158:25-40.

[90] Allwood MA, Kinobe RT, Ballantyne L, Romanova N, Melo LG, Ward CA, et al. Heme oxygenase-1 overexpression exacerbates heart failure with aging and pressure overload but is protective against isoproterenol-induced cardiomyopathy in mice.

Cardiovascular pathology : the official journal of the Society for Cardiovascular Pathology. 2014;23:231-7.

[91] Khechaduri A, Bayeva M, Chang HC, Ardehali H. Heme levels are increased in human failing hearts. J Am Coll Cardiol. 2013;61:1884-93.

[92] Ryter SW, Alam J, Choi AM. Heme oxygenase-1/carbon monoxide: from basic science to therapeutic applications. Physiological reviews. 2006;86:583-650.

[93] Jurgensen JS, Rosenberger C, Wiesener MS, Warnecke C, Horstrup JH, Grafe M, et al. Persistent induction of HIF-1alpha and -2alpha in cardiomyocytes and stromal cells of ischemic myocardium. FASEB journal : official publication of the Federation of American Societies for Experimental Biology. 2004;18:1415-7.

[94] Edgar R, Domrachev M, Lash AE. Gene Expression Omnibus: NCBI gene expression and hybridization array data repository. Nucleic acids research. 2002;30:207-10.

[95] Barrett T, Wilhite SE, Ledoux P, Evangelista C, Kim IF, Tomashevsky M, et al. NCBI GEO: archive for functional genomics data sets--update. Nucleic acids research. 2013;41:D991-5.

[96] Brazma A, Hingamp P, Quackenbush J, Sherlock G, Spellman P, Stoeckert C, et al. Minimum information about a microarray experiment (MIAME)-toward standards for microarray data. Nature genetics. 2001;29:365-71.

[97] Barth AS, Kuner R, Buness A, Ruschhaupt M, Merk S, Zwermann L, et al. Identification of a common gene expression signature in dilated cardiomyopathy across independent microarray studies. J Am Coll Cardiol. 2006;48:1610-7.

[98] Michael LH, Entman ML, Hartley CJ, Youker KA, Zhu J, Hall SR, et al. Myocardial ischemia and reperfusion: a murine model. The American journal of physiology. 1995;269:H2147-54.

[99] Rockman HA, Ross RS, Harris AN, Knowlton KU, Steinhelper ME, Field LJ, et al. Segregation of atrial-specific and inducible expression of an atrial natriuretic factor transgene in an in vivo murine model of cardiac hypertrophy. Proceedings of the National Academy of Sciences of the United States of America. 1991;88:8277-81.

[100] Pagano M, Naviglio S, Spina A, Chiosi E, Castoria G, Romano M, et al. Differentiation of H9c2 cardiomyoblasts: The role of adenylate cyclase system. Journal of cellular physiology. 2004;198:408-16.

[101] Varia MA, Calkins-Adams DP, Rinker LH, Kennedy AS, Novotny DB, Fowler WC, Jr., et al. Pimonidazole: a novel hypoxia marker for complementary study of tumor hypoxia and cell proliferation in cervical carcinoma. Gynecologic oncology. 1998;71:270-7.

[102] Wang J, Zhang G, Li Q, Jiang H, Liu C, Amatore C, et al. In vivo self-bio-imaging of tumors through in situ biosynthesized fluorescent gold nanoclusters. Scientific reports. 2013;3:1157.

[103] Manca C, Ghirarduzzi A, Baccarini S, Barilli AL, Bernardini B, Bigoli M, et al. [Effects of chronic administration of nifedipine on echo-Doppler parameters of left ventricular filling in hypertensive patients]. Cardiologia (Rome, Italy). 1990;35:149-56.

[104] Lange C, Turrero Garcia M, Decimo I, Bifari F, Eelen G, Quaegebeur A, et al. Relief of hypoxia by angiogenesis promotes neural stem cell differentiation by targeting glycolysis. The EMBO journal. 2016;35:924-41.

[105] Chen J, Kang JG, Keyvanfar K, Young NS, Hwang PM. Long-term adaptation to hypoxia preserves hematopoietic stem cell function. Experimental hematology. 2016.

[106] Mansor LS, Mehta K, Aksentijevic D, Carr CA, Lund T, Cole MA, et al. Increased oxidative metabolism following hypoxia in the type 2 diabetic heart, despite normal hypoxia signalling and metabolic adaptation. The Journal of physiology. 2016;594:307-20.

[107] Morgan BJ, Adrian R, Wang ZY, Bates ML, Dopp JM. Chronic intermittent hypoxia alters ventilatory and metabolic responses to acute hypoxia in rats. Journal of applied physiology (Bethesda, Md : 1985). 2016;120:1186-95.

[108] Sawicki KT, Shang M, Wu R, Chang HC, Khechaduri A, Sato T, et al. Increased Heme Levels in the Heart Lead to Exacerbated Ischemic Injury. Journal of the American Heart Association. 2015;4:e002272.

[109] Foresti R, Goatly H, Green CJ, Motterlini R. Role of heme oxygenase-1 in hypoxia-reoxygenation: requirement of substrate heme to promote cardioprotection. American journal of physiology Heart and circulatory physiology. 2001;281:H1976-84.

[110] Frangogiannis NG. Regulation of the inflammatory response in cardiac repair. Circulation research. 2012;110:159-73.

[111] Hamilton JW, Bement WJ, Sinclair PR, Sinclair JF, Alcedo JA, Wetterhahn KE. Heme regulates hepatic 5-aminolevulinate synthase mRNA expression by decreasing mRNA half-life and not by altering its rate of transcription. Archives of biochemistry and biophysics. 1991;289:387-92.

[112] Zablocki D, Sadoshima J. Angiotensin II and oxidative stress in the failing heart. Antioxidants & Redox Signalling. 2013; 19(10): 1095-1109.

[113] Lee PJ, Jiang BH, Chin BY, Iyer NV, Alam J, Semenza GL, et al. Hypoxia-inducible factor-1 mediates transcriptional activation of the heme oxygenase-1 gene in response to hypoxia. The Journal of biological chemistry. 1997;272:5375-81.

[114] Ockaili R, Natarajan R, Salloum F, Fisher BJ, Jones D, Fowler AA, 3rd, et al. HIF-1 activation attenuates postischemic myocardial injury: role for heme oxygenase-1 in modulating microvascular chemokine generation. American journal of physiology Heart and circulatory physiology. 2005;289:H542-8.

[115] Hinkel R, Lange P, Petersen B, Gottlieb E, Ng JK, Finger S, et al. Heme Oxygenase-1 Gene Therapy Provides Cardioprotection Via Control of Post-Ischemic Inflammation: An Experimental Study in a Pre-Clinical Pig Model. J Am Coll Cardiol. 2015;66:154-65.

[116] Wang S, Shao X, Li X, Su X, Huo Y, Yang C. HIF-1alpha may provide only short-term protection against ischemia-reperfusion injury in Sprague-Dawley myocardial cultures. Molecular and clinical oncology. 2016;4:579-83.

[117] Choi YK, Kim CK, Lee H, Jeoung D, Ha KS, Kwon YG, et al. Carbon monoxide promotes VEGF expression by increasing HIF-1alpha protein level via two distinct mechanisms, translational activation and stabilization of HIF-1alpha protein. The Journal of biological chemistry. 2010;285:32116-25.

[118] Yang J, Kim KD, Lucas A, Drahos KE, Santos CS, Mury SP, et al. A novel heme-regulatory motif mediates heme-dependent degradation of the circadian factor period 2. Molecular and cellular biology. 2008;28:4697-711.

[119] Naughton P, Foresti R, Bains SK, Hoque M, Green CJ, Motterlini R. Induction of heme oxygenase 1 by nitrosative stress. A role for nitroxyl anion. The Journal of biological chemistry. 2002;277:40666-74.

[120] Chen D, Jin Z, Zhang J, Jiang L, Chen K, He X, et al. HO-1 Protects against Hypoxia/Reoxygenation-Induced Mitochondrial Dysfunction in H9c2 Cardiomyocytes. PLoS ONE. 2016;11.

[121] Wang X, Ma S, Qi G. Effect of hypoxia-inducible factor 1-alpha on hypoxia/reoxygenation-induced apoptosis in primary neonatal rat cardiomyocytes. Biochemical and biophysical research communications. 2012;417:1227-34.